Communications of the

LUNAR AND PLANETARY LABORATORY

Communications Nos. 105–111

Volume 7   Part 1

THE UNIVERSITY OF ARIZONA

Communications of the

LUNAR AND PLANETARY
LABORATORY

Communications Nos. 105–111

Volume 7   Part 1

THE UNIVERSITY OF ARIZONA

1967

Communications of the Lunar and Planetary Laboratory

These *Communications* contain the shorter publications and reports by the staff of the Lunar and Planetary Laboratory. They may be either original contributions, reprints of articles published in professional journals, preliminary reports, or announcements. Tabular material too bulky or specialized for regular journals is included if future use of such material appears to warrant it. The *Communications* are issued as separate numbers, but they are paged and indexed by volumes.

The *Communications* are mailed to observatories and to laboratories known to be engaged in planetary, interplanetary or geophysical research in exchange for their reports and publications. The University of Arizona Press can supply at cost copies to other libraries and interested persons.

The University of Arizona   GERARD P. KUIPER, *Director*
Tucson, Arizona   *Lunar and Planetary Laboratory*

TABLE OF CONTENTS

by Thomas Gehrels

February 27, 1967   N 69 - 18302

ABSTRACT

Comparison of the wavelength dependence of interstellar polarization with that observed in reflection nebulae appears to rule out metallic and purely graphitic grains for the general interstellar medium. The observations on reflection nebulae are best explained with composite grains that have an absorptive nucleus of diameter 0.05 μ and an icy shell of diameter 0.3 μ. The visual albedo of the grains is near 0.5 and the asymmetry factor 0.6. Because of this asymmetry, reflection nebulae generally are not observable if the star is in front of the nebula. NGC 7023 has 4×10^{-10} grains/cm^3 and the visual optical depth within the nebula is only 0.2.

1. Introduction

MARTEL (1958) made extensive observations of the polarization of reflection nebulae, and she has given a detailed bibliography. Vanýsek and Svatoš (1964) and Roark (1966) have added new photometric studies. Elvius and Hall (1966) reported polarimetric as well as photometric observations. They found the amount of polarization in three reflection nebulae to increase, linearly and fairly steeply, with increasing wavelength. Their conclusion is used in this paper in a combination with the generally observed wavelength dependence of interstellar polarization.

Section II describes the observational results, including those of Elvius and Hall. The Mie calculations of Herman and Browning are described in Sec. III, and they are compared with the observations in Sec. IV. The Mie theory is for spherical particles, but recent experiments (Powell et al. 1966) indicate that the optical character of polydisperse, randomly aligned particles is not a sensitive function of particle shape. Most of the calculations in this paper are for single sizes, but a test case of size distributions is in Sec. V. The variation of the refractive index with wavelength has not been taken into account; the effect does not appear large enough to affect the conclusions of this paper. NGC 7023 is considered in Secs. VI and VII with the assumption of a uniform spherical reflection nebula with HD 200775 at its center, and an approximate knowledge (±20%) of the distance is needed. The optical depth within NGC 7023 is found from the

scattering efficiency of the grains and from the observed brightness ratio of nebula and illuminating star; the interstellar extinction is thereby taken into account. In Sec. VIII we return to the interstellar grains in general, with a discussion of grain parameters and radiation pressure. This paper is primarily a reconnaissance of observational requirements and of techniques of interpretation, to be followed by improved work on reflection nebulae and interstellar polarization.

2. Observations

Table I reproduces the result of Paper II (Gehrels 1960a) in this series. The wavelength dependence of the interstellar polarization w: · compared with calculations by Mrs. E. v. P. Smith for perpendicular incidence on long cylinders; the resulting particle diameters are in Table I. The work on the interstellar polarization since then (for instance, see Coyne and Gehrels 1966) has confirmed these conclusions; there are differences from star to star but the general conclusion is well summarized in Table I. The observations on the wavelength dependence on reflection nebulae have been reported (Gehrels 1960b; also see Greenberg 1967), but the detailed comparison with the Mie theory is in this paper.

TABLE I. Particle diameters μ obtained from fitting the theory to observations of interstellar polarization and reddening.

Refractive index m	Diameter 2a, from interstellar polarization	reddening
1.25	0.49	0.70
1.25–0.10i	0.31	...
1.50	0.28	0.35
1.50–0.10i	0.20	0.32
1.50–0.25i	0.16	...
1.41–1.41i	0.05	0.07

TABLE II. Observations in NGC 7023.

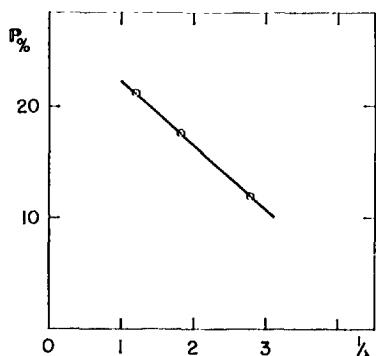| Object	Date UT Aug. 1959	1/λ	P (%)	θ (deg)
E-38"	1	1.82	8.5±0.9	150
		2.78	4.0	143
NE-38"	8 2 7 2 7	1.20	20.5	130
		1.82	16.0	134
		2.78	10.1	123
N-38"	6 8 3 4 3 4	1.20	21.6	86
		1.82	19.2	87
		2.78	13.6	91
Central star	2	1.82	0.92±0.07	89
		2.78	0.85	84

FIG. 1. Percentage polarization of the average of two regions in NGC 7023 as a function of the reciprocal of the wavelength (in microns).

Table II gives a few measurements in reflection nebula NGC 7023 [central star HD 200775, BD +67°1283, $\alpha(1959) = 21^h01^m4$, $\delta(1959) = 68°00'$] made with the McDonald 82 in. in August 1959. The three filters are ultraviolet, green, and red, U', G', and R' of Table I of Gehrels and Teska (1960). The integration times are of the order of 1 min. The diaphragm is 22″58 in diameter. The regions are all at 38″ ($\pm2″$ p.e.) from HD 200775 in directions east, northeast, and north. At 38″ from the central star NGC 7023 probably does not show emission, other than the reflected emissions of HD 200775 (Greenstein and Aller 1947, p. 142). The skies are measured at about 2′6 due east or west of the central star. At this distance the sky settings are not entirely out of the nebula but the readings presumably are close to those of sky without stars; because of some obscuration, the spots could be chosen to be free of background stars.

The choice at the telescope is difficult to make. Because of nebular background, one overcorrects if the spot for the sky-background readings is chosen too close; however, because of background stars penetrating the dark nebula, one also overcorrects if the spot is too far.

The work on reflection nebulae and sky is time consuming, and measurements of various nights (6 and 8 August, for instance) are combined.

The directions of the position angles of the northeast and north regions (Table II) are perpendicular to the direction of HD 200775. It is therefore probable that this is the illuminating star, and that the material of the nebula is not appreciably aligned. The east region appears to be anomalous in percentage polarization and it is not further discussed in this paper.

Elvius and Hall (1966) observed colors and polarization of several spots in NGC 7023, as well as in the Merope Nebula and in NGC 2068. They used the Perkins telescope, in 1962–64, with focal-plane diaphragms of 29″ and 42″. The filter system is approximately that of U, B, and V. There is only one region of NGC 7023 in common with "northeast" in Table II, and Elvius and Hall found amounts of polarization

that are about 0.7 times the amounts in Table II. The discrepancy is partially understood in terms of the corrections for sky light: it makes a large difference in the amount of light if the skies are measured farther out than the above-mentioned 2′6. Corrections for scattered light from the central star also are a problem. For the measurements of Table II, the 82-in. mirror was washed (thanks to Mr. Marlyn Krebs), and special baffling inside the photometer was installed; approximate checks of the absence of scattered light were made, but not in great detail and it is possible that a small effect was overlooked.

The remarkable conclusion of Elvius and Hall is that the wavelength dependence of most regions in NGC 7023, the Merope Nebula, and NGC 2068 is approximately the same. I also found this in some (unpublished) measurements on NGC 2068.

Figure 1 shows the average of the polarizations for "north" and "northeast" in Table II. The observations of Elvius and Hall give approximately the same wavelength dependence for several spots in three reflection nebulae; the effect of their smaller amount, observed northeast of HD 200775, is discussed in Sec. V. In any case, some smoothing over regional differences and observational errors is included by taking the average of two regions, and the fitting of the Mie theory will, therefore, be made to the line in Fig. 1.

3. Mie Calculations

For the interpretations below, the tables of LaMer (1943) are used. In addition, especially for absorbing particles, new calculations were made with the IBM 7072 of the Numerical Analysis Laboratory at the University of Arizona. The Mie program is that of Dr. B. M. Herman and Maj. Genl. (ret.) S. R. Browning, to whom I am greatly indebted. Details of the Mie calculations have been published (viz., Herman and Battan 1963).

Table III gives an approximate identification of refractive indices, most of which were taken from van de Hulst (1957, Table 26).

Figures 2 and 3 show a sample of the present calculations. The format is that of van de Hulst (1957, pp. 152–153), who gives plots for spheres with refractive index $m = 1.33$, 1.50, 1.55, and 2, and for

TABLE III. Identification of refractive indices, for aerosols at wavelength 0.5 μ.

Substance	Refr. index
Ices	1.3
Impure ices	1.3 −0.05i
Glasses	1.5
Impure glasses	1.5 −0.05i
Carbon	1.6 −0.7i
Metallic, generally	1.4 −1.4i
Nickel and zinc	1.5 −3i
Copper	1.1 −2i
Sodium	0.06–2i
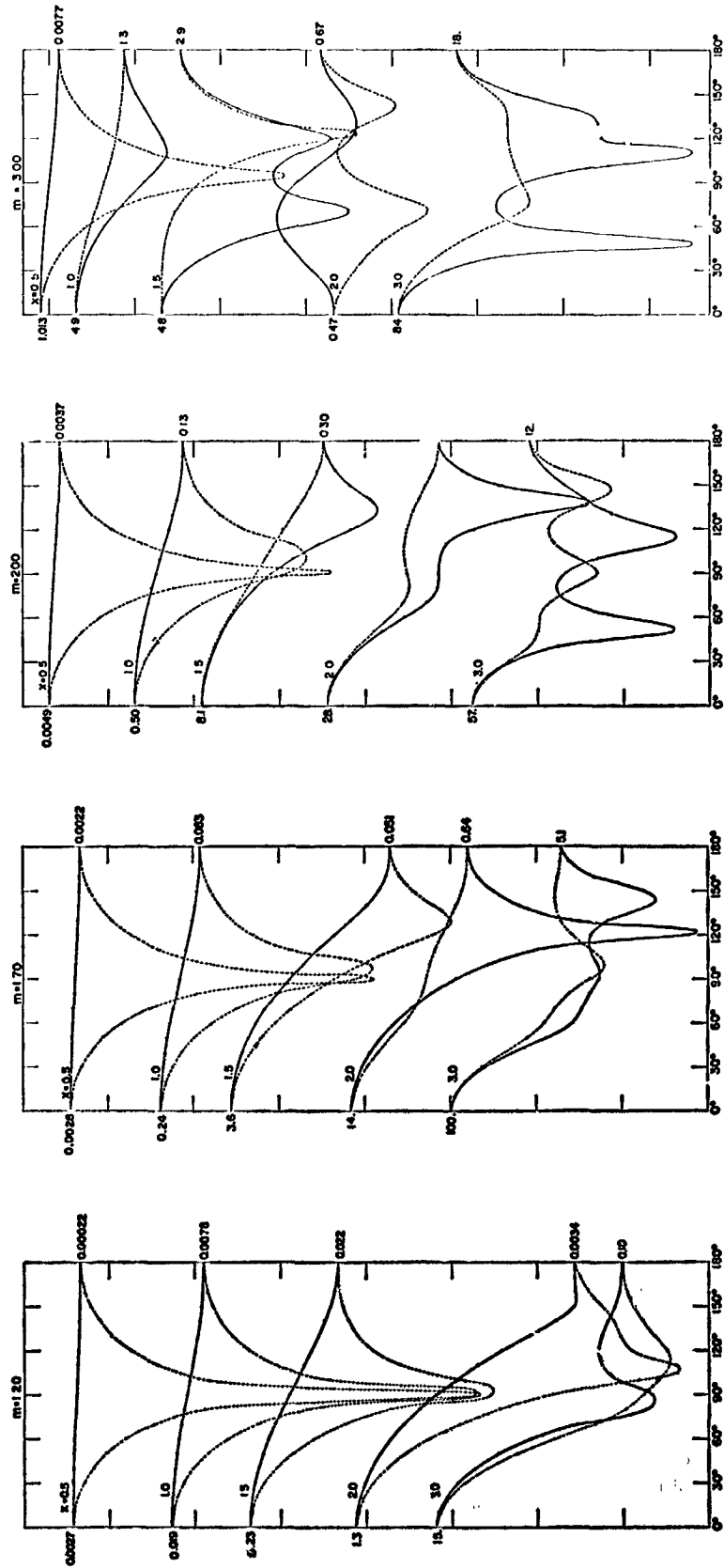
FIG. 2. Intensity parameters i_1 (solid line) and i_2 (dotted) as a function of the scattering angle (see Sec. III), for nonabsorbing homogeneous spheres of refractive index m. The values at scattering angles 0° and 180° are labeled, but the ordinate scales are logarithmic. With respect to the plane through light source–particle–observer, i_1 is perpendicular and i_2 is parallel.
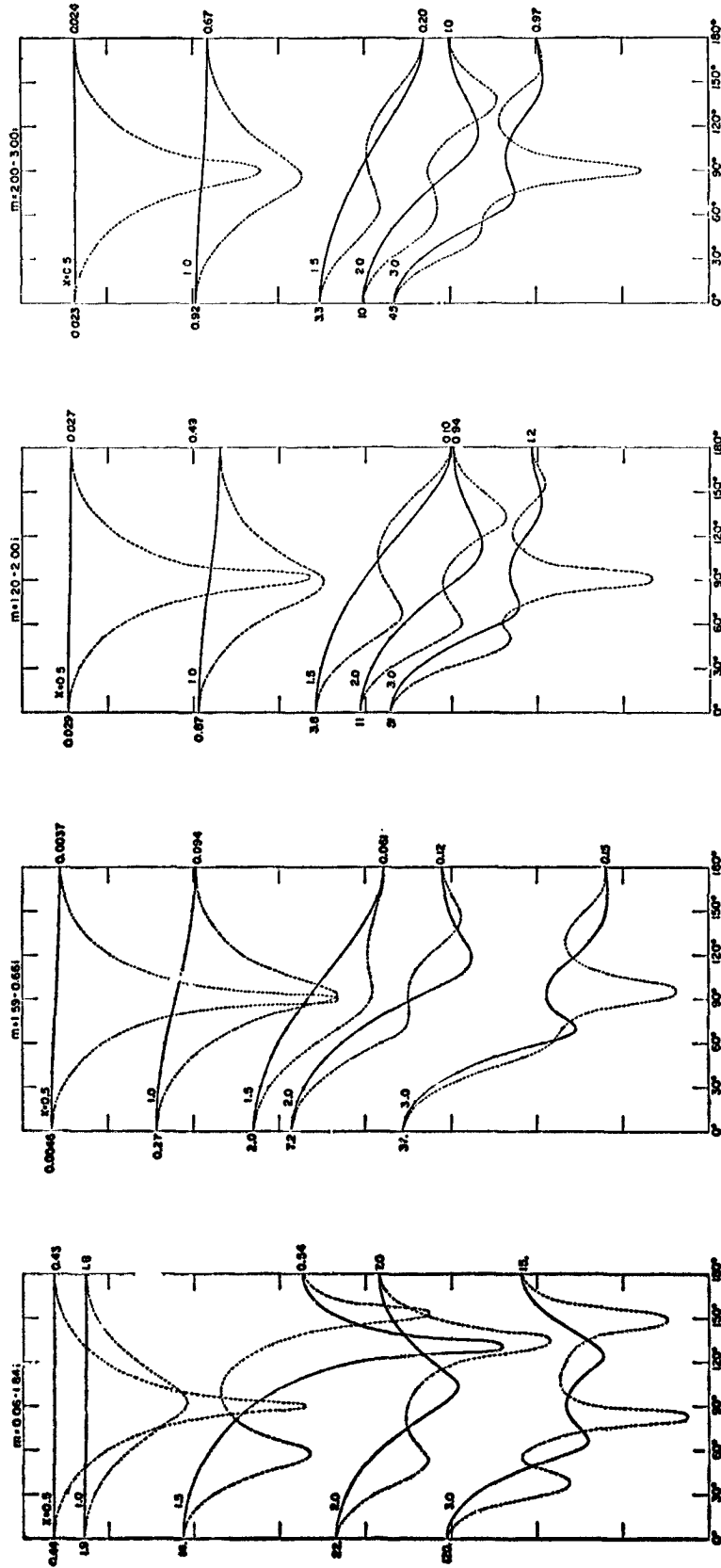
THOMAS GEHRELS

FIG. 3. As in Fig. 1, but for absorbing homogeneous spheres.

TABLE IV. Computed polarizations and particle diameters μ for star *at the center* of nebula; scattering angles 20-160°.

| Refr. index | $2\pi a/\lambda$ | $P\%$ | Particle diameter at $1/\lambda=$ | | |
			1.20	1.82	2.78
1.20	1.5	+36.9			
	2.0	+25.4	0.59	0.43	0.33
	3.0	+11.4			
1.33	1.8	+25.2			
	2.0	+18.3	.50	.35	.25
	2.5	+10.0			
1.44	1.5	+31.9			
	1.8	+18.6	.47	.31	.22
	2.0	+11.2			
1.55	1.5	+27.6			
	1.8	+10.5	.42	.29	.20
	2.0	− 0.9			
1.70	1.0	+40.1			
	1.5	+18.2	.38	.26	.19
	2.0	− 1.9			
1.33-0.15i	1.5	+34.1			
	2.0	+20.2	.51	.38	.31
	3.0	+ 9.8			
1.33-0.30i	1.5	+33.5			
	2.0	+21.2	.53	.41	.36
	3.0	+12.8			
1.33-0.60i	1.5	+32.7			
	2.0	+23.2	.61	.59	...
	3.0	+18.7			
1.57-0.15i	1.0	+40.5			
	1.5	+27.1	.44	.31	.22
	2.0	+ 9.1			
1.57-0.30i	1.0	+40.4			
	1.5	+27.5	.46	.32	0.23
	2.0	+12.0			
1.59-0.66i	1.0	+40.0			
	1.5	+27.3	0.48	0.34	...
	2.0	+16.7			
0.06-1.84i	1.5	+18.1			
	2.0	+31.7	...	...	...
	3.0	+32.9			

cylinders with $m=1.50$. The parameter $x=2\pi a/\lambda$, where a is the particle radius and λ is the wavelength of the light. In this paper the *scattering angle* is used, which is the supplement of the phase angle (used in the tables of LaMer). For nonpolarized incident light of unit intensity, the intensity (in erg cm^{-2} sec^{-1}, for instance) of a single particle observed at distance r is (van de Hulst 1957, p. 129)

$$(I_1+I_2)=(i_1+i_2)\lambda^2/8\pi^2r^2, \qquad (1)$$

where I_1 and I_2 are the scattered intensities in two orthogonal directions and i_1 and i_2 are the computed and plotted quantities. I am indebted to Mrs. Tricia Coffeen for plotting Figs. 2 and 3. We also have graphs for $m=1.70-4.00i$ and $m=3.00-4.50i$, which are almost identical to those of $m=2.00-3.00i$, graphs for $m=0.56-3.01i$ are also quite similar.

Figure 4 shows a cross section of an idealized spherical nebula with the illuminating star at its center. The discussions of this paper are for uniform space density of the particles in NGC 7023.

In Tables IV-X the weighted mean polarizations are calculated from the values of i_1 and i_2 over a range of scattering angles. The weights depend: on R^{-2},

where R is the distance from the illuminating star; on V, which is the volume of the segment that has, on the average, a certain scattering angle; and on the scattering efficiency of each particle into a given direction. Conveniently,

$$R^{-2}\times V\cong \text{const} \qquad (2)$$

(demonstrated in Table XII of Sec. VI), so that the weighting is only with (i_1+i_2). From i_1 and i_2, tabulated at 10° intervals in the Herman and Browning program, one calculates

$$P=100(\Sigma i_1-\Sigma i_2)/(\Sigma i_1+\Sigma i_2), \qquad (3)$$

where the summations in Table IV, for instance, are over the 20-160° range. A plus sign for P in Tables IV-IX indicates that the electric vector maximum is perpendicular to the direction of the illuminating star (as is generally observed in NGC 7023; see Sec. II); a minus sign is for radial direction.

4. Interpretations

In Table IV the illuminating star is at the center of a uniform spherical nebula. At the values of refractive index m and of $x=2\pi a/\lambda$, the percentage polarization P is calculated (Sec. III). The computed P values are plotted as a function of x and the observed polarizations of Fig. 1 (21.1% at $1/\lambda=1.20$, 17.6% at 1.82, and 11.9% polarization at $1/\lambda=2.78$) are then used to find the values of $2a$. For none of the refractive indices in Table IV is $2a$ constant; in other words, the observed wavelength dependence of polarization is not reproduced by the calculations.
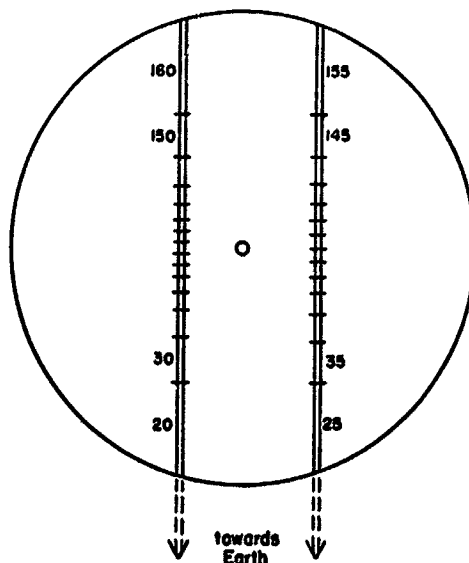

FIG. 4. Cross section through a spherical reflection nebula that has the illuminating star at its center. Volume segments are labeled with their mean scattering angle. On *the left*, for Secs. IV and V; *on the right*, for Sec. VI.

TABLE V. Computed polarizations for star *in front* of nebula; scattering angles 120-160°.

Refr. index	$2\pi a/\lambda$	$P\%$
	1.2	+32.5
	1.5	+41.0
	1.8	+70.8
1.33	2.0	+ 8.3
	2.4	− 4.1
	2.5	+ 2.1
	3.0	+50.8
	3.6	−31.0
	1.2	+34.6
	1.5	+47.9
	1.8	+50.8
1.44	2.0	−33.2
	2.4	−14.8
	2.5	− 7.7
	3.0	−16.0
	3.6	−39.1
	1.0	+30.3
1.33-0.15i	1.5	+42.7
	2.0	−30.6
	3.0	+81.0
	1.0	+30.3
1.33-0.30i	1.5	+38.5
	2.0	−31.3
	3.0	+28.5
	1.0	+29.6
1.33-0.60i	1.5	+24.0
	2.0	− 9.9
	3.0	− 0.4
	1.0	+32.6
1.57-0.15i	1.5	+65.5
	2.0	−53.4
	3.0	−48.0
	1.0	+32.6
1.57-0.30i	1.5	+49.5
	2.0	−46.9
	3.0	−43.5
	1.0	+31.4
1.59-0.66i	1.5	+41.9
	2.0	−10.9
	3.0	−25.0

In Table V the illuminating star is placed in front of the nebula. The computed wavelength dependence now is even steeper than that in Table IV. The abrupt change from positive to negative polarization can be seen in Figs. 2 and 3. The computed wavelength dependence is very irregular near scattering angle 140°. The filters used for the observations in NGC 7023 are narrow enough so that such strong variations from positive to negative polarization, and vice versa, would have been detected. It is possible that a very wide dispersion of diameters and refractive indices would average out the steep variations; but the computed wavelength dependence of polarization would still be much too steep in the neighborhood of $x=1.5$. In any case, very wide dispersions are unlikely since they would "wash out" the marked shape of Fig. 1 and of the interstellar polarization dispersion.

In Table VI the illuminating star is behind the nebula. The three columns of $2a$ now generally are similar; the observed wavelength dependence is reproduced by the Mie calculations. Next, a comparison is made, for various refractive indices, with the results of interstellar polarization and reddening (Table I).

The best consistency appears for values of

$$2a \cong 0.3 \, \mu \qquad (4)$$

and

$$(1.2 - \epsilon i) < m < (1.6 - \epsilon i) \qquad (5)$$

with

$$0.1 < \epsilon < 0.4. \qquad (6)$$

The calculations for m without imaginary component in Table VI have not been carried out for refractive indices greater than 2.0 because the (approximate) linearity of P as a function of x breaks down. The wavelength dependence of polarization near $x=1.2$ would be much steeper than is observed.

Table VII supplements Tables IV and VI with modifications of the range of scattering angles. The strong forward scattering at 10°, which is relatively little polarized, tends to dilute the polarizations. It is seen that 10-50° is too extreme; at no value of x do the calculations give the high observed polarizations (20%). To the contrary, the range 30-80° gives the wavelength dependence too steep. A range slightly different from 20-60° (for instance 10-70°) is acceptable, and the interpretations made with Table VI appear unchanged.

TABLE VI. Computed polarizations and particle diameters μ for star *behind* nebula; scattering angles 20-60°.

Refr. index	$2\pi a/\lambda$	$P\%$	Particle diameter at $1/\lambda =$		
			1.20	1.82	2.78
	1.5	+22.0			
1.20	2.0	17.7	0.42	0.36	0.32
	3.0	10.5			
	1.5	19.9			
1.33	2.0	13.8	.36	.29	.25
	3.0	3.9			
	1.0	23.6			
1.44	1.5	17.7	.32	.26	.22
	2.0	10.5			
	1.0	22.9			
1.55	1.5	14.9	.30	.23	.19
	1.8	9.0			
	0.5	25.7			
	1.0	21.9			
1.70	1.5	10.1	.26	.21	.17
	2.0	7.2			
	0.5	25.6			
2.00	1.0	19.0	.22	.17	.14
	1.5	1.1			
	1.5	20.0			
1.33-0.15i	2.0	16.0	.36	.32	.30
	3.0	8.9			
	1.5	20.5			
1.33-0.30i	2.0	17.8	.37	.35	.35
	3.0	.1			
	1.5	22.2			
1.33-0.60i	2.0	21.2	.53	.54	.55
	3.0	17.9			
	1.0	22.6			
1.57-0.15i	1.5	15.2	.29	.24	.21
	2.0	11.0			
	1.0	22.6			
1.57-0.30i	1.5	16.4	.29	.25	.23
	2.0	13.2			
	1.5	19.1			
1.59-0.66i	2.0	17.7	0.26	0.34	0.39
	3.0	+13.7			

TABLE VII. Computed polarizations and particle diameters μ for various ranges of the scattering angle.

Scattering angles	Refractive index	$2\pi a/\lambda$	$P\%$	Particle diameter at $1/\lambda=$ 1.20	1.82	2.78
10-160°	1.33	1.8	+20.0			
		2.0	14.3	0.47	0.33	0.24
		2.5	7.5			
	1.44	1.5	26.4			
		1.8	14.8	.44	.31	.22
		2.0	8.8			
10- 50	1.33-0.15i	0.5	15.9			
		1.0	14.5	...	...	.18
		1.5	12.1			
	1.33-0.30i	0.5	15.9			
		1.0	14.6	...	.06	.18
		1.5	12.4			
	1.33	0.5	15.8			
		1.0	14.6	...	...	.17
		1.5	12.1			
30- 80	1.33-0.15i	1.5	34.2			
		2.0	25.4	.60	.43	.34
		3.0	11.7			
10- 60	1.33-0 15i	1.0	21.1			
		1.5	15.6	.27	.24	.23
		2.0	12.1			
	1.33-0.30i	1.0	19.2			
		1.5	16.0	.17	.22	.26
		2.0	13.3			
	1.20	1.0	19.9			
		1.5	17.2	.21	.25	.26
		2.0	13.5			
	1.70	0.5	20.8			
		1.0	17.4	.1?	.16	.15
		1.5	8.0			
10- 80	1.33-0.15i	1.5	21.8			
		2.0	14.8	.40	.32	.27
		3.0	5.7			
	1.33-0.30i	1.5	22.0			
		2.0	16.1	0.41	0.33	0.29
		3.0	+ 7.8			

The range of 10-80° appears less likely; the wavelength dependence again is becoming too steep.

The principal conclusion is that purely absorptive grains in the general interstellar medium are ruled out. Qualitatively one could already see in Fig. 3 the steep increase in polarization to occur, for scattering angles 20-60°, at $x\simeq2$; in Fig. 1 it occurs at $1/\lambda\simeq2.5$; it follows that $2a\simeq0.25\,\mu$. The wavelength dependence of three reflection nebulae was found approximately the same. On the assumption that these three are typical interstellar clouds, one brings in the comparison with the "interstellar" results of Table I, and the above 0.25 μ for absorptive grains is then ruled out. Absorptive grains as condensation nuclei for the general interstellar particles are considered next.

Table VIII gives some calculations for concentric shells. The refractive indices and the diameters (in microns) are listed in the first column with subscripts c for the core and s for the shell. The value of $1/\lambda$ (in reciprocal microns) for which the calculations are made is in the second column. The three cases of star/nebula geometry of Tables IV, V, and VI are in the next three columns: scattering angles 20-160°, 120-160°, and 20-60°, respectively.

The first model in Table VIII is a graphite grain with 0.08 μ diameter, having an ice coating to 0.224 μ; this particle was suggested by Wickramasinghe (1963) as providing a fair fit to the observed interstellar reddening. Since the wavelength dependence of Fig. 1 is not quite reproduced, the outside diameter is enlarged (second model) and impurities are added to the ice (third model). The last model in Table VIII has a small metallic core and a shell of ice, as proposed by Whitney (1965) to explain the 4430 Å band. It is seen in Table VIII that the observations of Fig. 1 can indeed be reproduced with the coated grains of the proper outside dimension ($2a\simeq0.3\,\mu$). Straight averaging of $P(\lambda$; 20-60°) of the first and last models reproduces Fig. 1 precisely.

The high imaginary component of expression (6), needed for the best fit to Fig. 1, is rather alarming. What type of material in interstellar space could yield homogeneous grains with such a refractive index? "Dirty ices" as proposed by Oort and van de Hulst (1946) have $m=1.3-0.05i$ (in visual light). Here may be an argument in support of the composite grains (I am indebted to Dr. Greenberg for pointing this out).

5. Size Distributions

Table IX has computations of the percentage polarization for two size distributions, and also for a single size, of homogeneous grains with refractive index 1.40-0.21i. The three computed columns are for scattering angles 20-160°, 120-160°, and 20-60°, respectively. The Oort-van de Hulst size distribution is used, for example in the first case: with relative weight, by number of particles, of 0.48 for particle diameter 0.16 μ,

TABLE VIII. Computed polarizations for coated particles.

Grain specifications; core and shell	For $1/\lambda$	Percentage polarization having star at center	in front	behind
$m_c=1.63-0.82i$	0.91	+42.3	+27.9	+25.9
$m_s=1.33$	1.11	+42.1	+28.5	+25.4
$2a_c=0.08; 2a_s=0.224$	1.43	+41.4	+29.8	+24.4
	2.00	+37.3	+35.2	+21.3
	3.33	+14.3	+27.5	+11.8
$m_c=1.63-0.82i$	0.91	+36.7	+37.7	+20.8
$m_s=1.33$	1.11	+27.3	+60.4	+16.8
$2a_c=0.08; 2a_s=0.50$	1.43	+12.8	- 8.3	+12.0
	2.00	+ 5.1	+35.3	+ 3.8
	3.33	- 1.2	+56.9	- 2.2
$m_c=1.63-0.82i$	0.91	+35.9	+39.2	+20.7
$m_s=1.33-0.13i$	1.11	+27.2	+65.2	+17.6
$2a_c=0.08; 2a_s=0.50$	1.43	+15.5	- 6.6	+14.3
	2.00	+ 8.3	+29.6	+ 7.5
	3.33	+ 2.2	+49.6	+ 1.7
$m_c=1.40-1.40i$	0.91	-43.7	+32.1	+23.2
$m_s=1.33-0.13i$	1.11	+36.5	+38.1	+21.0
$2a_c=0.02; 2a_s=0.40$	1.43	+25.6	+69.5	+17.2
	2.00	+12.5	+28.5	+12.3
	3.33	+ 4.5	+77.3	+ 3.2

TABLE IX. Computed polarizations for various size distributions.

Specifications $m=1.40-0.21i$	For $1/\lambda$	Percentage polarization having star		
		at center	in front	behind
	0.80	+42.3	+30.6	+27.3
Distribution about	1.20	33.5	+34.1	19.6
$2a=0.3\ \mu$	1.85	20.6	+33.8	14.6
	2.78	11.8	+28.6	9.6
	0.80	42.4	+27.6	26.1
Distribution about	1.20	42.0	+28.8	25.1
$2a=0.16\mu$	1.85	39.2	+32.1	22.4
	2.78	26.7	+33.0	18.1
	0.80	41.9	+29.1	24.9
No size-distr.;	1.20	38.8	+34.6	21.9
$2a=0.32\mu$	1.85	21.1	− 9.0	16.0
	2.78	+10.0	+82.7	+ 9.3

0.30 for 0.24 μ, 0.15 for 0.32 μ, 0.05 for 0.40 μ, and 0.02 for 0.48 μ. The second case has the same distribution but all particle diameters are smaller by a factor 2. This case, incidentally, gives less polarization dispersion than that of Fig. 1. The last case is for the single size of diameter 0.32 μ.

It is seen from the comparison in Table IX that the conclusions in the previous section, made for an "infinitely narrow" size distribution, are practically unchanged when an Oort–van de Hulst distr'oution, centered on the same particle size, is considered. This should not be surprising as Oort and van de Hulst (1946, Fig. 9) have shown how steep their actual size distribution apparently becomes because of the greater scattering efficiency of the larger particles.

It is noted that while the Oort–van de Hulst distribution centers on $2a=0.6\mu$, the present calculations, and also those on the interstellar effects (Table I), are centered on half that size, $2a=0.3\mu$.

Table X shows a few of the fittings to the observations of Elvius and Hall (1966); the table has the same type of analysis as is in Tables IV–VII, but the computed polarizations are not listed again. The observations were taken from a manuscript kindly supplied by the authors at the time of the August 1965 conference (Greenberg 1967): at 4 mm N and 4 mm E, which is at 38″ from HD 200775, 12.6% polarization with a filter at 5740 Å, 9.5% at 4460 Å, and 7.4% at 3760 Å. By extrapolation and interpolation the following normal points were obtained, and used for Table X: 15.8% at $1/\lambda=1.20$, 12.1% at $1/\lambda=1.82$, and 6.7% at $1/\lambda=2.78$. It is seen that a fit can be made nearly at the same grain parameters as before, stated in expressions (4)–(6), but at slightly smaller scattering angles than before so that the star is farther behind the nebula.

6. Space Density in NGC 7023

A photometric distance determination of HD 200775 is made as follows. Mr. R. I. Mitchell (personal com-

munication) obtained the values: $V=7.43$, $B-V=+0.38$, $U-B=-0.41$:, $V-R=+0.57$, and $R-I=+0.30$ mag. With these values, and reference to the papers by Johnson (1965) and Johnson and Borgman (1963), the ratios of Table XI are obtained. A precise determination of the ratio of total to selective absorption cannot be made without far-infrared photometry, but a value of 4.2 appears consistent also with the interpolation formula

$$A_V/E_{B-V} = (0.96+0.58E_{V-I}/E_{B-V})E_{V-I}/E_{B-V}, \quad (7)$$

given by Johnson and Borgman. The spectral type of HD 200775 has been given as B2p by Hubble (1922) and by Keenan (1936), dB3ne by Greenstein and Aller

TABLE X. As for Tables IV–VII, but fitted to the observations of Elvius and Hall (1966).

Refractive index	Scattering angles	Particle diameter at $1/\lambda=$		
		1.20	1.82	2.78
2.00	20– 60°	0.27	0.21	0.16
1.55	20– 60	.38	.28	.22
1.20	20– 60	.01	.49	.40
1.57–0.66i	20– 60	.66	.59	.54
	20–160	.63	.48	.37
1.33–0.15i	20– 60	.55	.45	.38
	10– 60	.42	.35	.30
	10– 50	.14	.26	.33
	20–160	.70	.54	.43
1.33–0.30i	20– 60	.62	.52	.45
	10– 60	.41	.39	.37
	10– 50	0.19	0.27	0.32

(1947), B3 by Mendoza (1958), and B5e by Stebbins, Huffer, and Whitford (1940). The ultraviolet excess ratio in Table XI appears more consistent for B2V than for B3V, and I therefore adopt, for the purpose of excess-to-absorption conversion, B2V. The absolute magnitude for B2V is given by Blaauw (1963) as −2.5. The color excess $E_{B-V}=0.62$ mag. The distance modulus $(V-M_V)=7.3$ mag, and the distance is 0.29 kpc, or

$$r=0.9(\pm0.2 \text{ p.e.})\times10^{21} \text{ cm}. \quad (8)$$

This agrees with the distance of 0.3 kpc determined from proper motions by Lundmark (1922).

Table XII gives the fluxes intercepted and scattered towards the earth by various groups of grains. At each scattering-angle interval, the values of $\langle i_1+i_2 \rangle$ are obtained by straight averaging in the tables of LaMer (1943) for $m=1.33$ and 1.44 at $x=1.5$ and 1.8 (for $\lambda=0.56\mu$ and $2a=0.30\mu$), this result, for homogeneous particles, is in the second column. The third column is for coated particles and the averaging is in the Herman–Browning tables for mixture d (identified in Table XIII, below) at values of $1/\lambda=1.43$ and 2.00; this case, rather than that of the homogeneous particles, is pursued in the remaining columns of Table XII. The Distance and Volume columns are for the geometry of Fig. 4, based on the distance of HD 200775 of 0.29 kpc,

for one square second of arc observed at $0''.8$ from the central star (in order to fit to Martel's observation; see below). The Flux per Particle (fifth column) is

$$F = \langle(i_1+i_2)\rangle\lambda^2/8\pi^2R^2, \qquad (9)$$

where R is the distance of the particle from HD 200775 (fourth column). The nebular brightness is compared (below) with that observed on the star. The r^{-2} term in expression (1) is thereby taken into account—as well as the interstellar extinction—while the R^{-2} term normalizes the flux incident on the particle.

Incidentally, the last column of Table XII is nearly the same as the third, but for a constant factor, since the product of volume and inverse square distance is nearly a constant [expression (2)]. The essential weighting factor is $\langle i_1+i_2\rangle$; it shows the strong forward directivity of scattering by these grains. The range 20–$70°$ contributes most to the observed light; addition of the 70–$80°$ interval, for instance, would add only 6% to the light. The last column of Table XII also shows how hard, or impossible, it would be to observe a reflection nebula if the star were in front, rather than behind, the nebula: the sum over 110–$160°$ is 330 compared to 8163 for 20–$70°$. For NGC 7023, one of the brightest reflection nebulae, the nebular brightness would be about one-tenth that of the sky. (Exceptionally high space densities might make the nebula observable.)

TABLE XI. Color-excess ratios, and ratio of total to selective absorption.

Object	$\dfrac{E_{U-V}}{E_{B-V}}$	$\dfrac{E_{V-R}}{E_{B-V}}$	$\dfrac{E_{V-I}}{E_{B-V}}$	$\dfrac{A_V}{E_{B-V}}$
Cepheus	1.84	0.85	1.60	6
II Per	1.68	0.81	1.69	3.75
Orion belt	1.82	1.13	2.26	4.8
HD 200775 B3V	1.52	1.09	1.97 ⎫	4.2
HD 200775 B2V	1.73	1.08	1.92 ⎭	

It is seen in Sec. IV (Tables VI and VII) that 20–$60°$, or perhaps 15–$65°$, is the most likely range of scattering angles for observations made at $38''$ from HD 200775. In Table XII (at $0''.8$ from HD 200775) such ranges correspond to 20–$70°$. The sum in the last column of Table XII therefore is taken over 20–$70°$; it is 8.2×10^3. Martel (1958) gives the brightness, after subtraction of sky brightness, per square second of arc: it is 21.3 (±0.2) visual magnitude at $0''.8$ from HD 200775. This magnitude when compared to that of HD 200775 (7.43 mag; see above) gives a brightness rati of 2.8×10^{-6}. It follows that there are 3.4×10^{-10} grains/cm³.

The precision of the derived density is of the order of $\pm40\%$ (p.e.), determined by the uncertainty in the distance, the photometry, the composition of the

particles, and the adopted range of scattering angles. Since $R^{-2}\times V \simeq$ const, the uncertainty in the distance determination does not affect the polarimetry conclusions of Sec. IV, and it affects the density determination only in the first power, i.e., in the scale conversion of sec of arc to cm of NGC 7023. As for the particle composition, the homogeneous case of $m \simeq 1.4$ (second column of Table XII) gives 4.0×10^{-10} grains/cm³ and the case of $m = 1.4$–$0.3i$ (still $2a = 0.30\mu$) gives 3.2×10^{-10} grains/cm³.

7. Self-Extinction and Multiple Scattering

The optical depth is given by

$$\tau = \pi a^2 Q_{ext}NL, \qquad (10)$$

where the particle radius $a = 1.5\times10^{-5}$ cm; the efficiency factor for the total attenuation $Q_{ext} \simeq 1.0$ (Table XIII, below) at $1/\lambda = 1.82$; the particle density $N = 3.8\times10^{-10}$ cm^{-3} [expression (11), below]; and $L = 5.2\times10^{17}$ cm which is the path length in Fig. 4 at $0''.8$ from the star, over scattering angles 20–$70°$. It follows that the optical depth $\tau = 0.14$ (±0.06 p.e.) at $1/\lambda = 1.82$. With the efficiency factors at the other wavelengths it is found that $\tau = 0.08$ at $1/\lambda = 1.20$, and 0.23 at $1/\lambda = 2.78$.

At the August 1965 Conference (Greenberg 1967) a lively discussion occurred on this topic of the optical depth of NGC 7023. Van Houten (1961), for instance, derived an optical depth of 2, but this figure arose from his assumption that HD 200775 is reddened only by the local nebulosity and not at all between the nebula and the earth. This was a poor assumption since the nebula has a radius of only one or two parsecs, but is distant by 290 pc of interstellar space, in which an appreciable amount of the observed extinction must occur. The extinction on the way has been taken into account in this paper by considering *differential* magnitudes of the

TABLE XII. Relative fluxes at various scattering angles in NGC 7023.

Scattering angle interval	$\langle i_1+i_2\rangle$ homog.	$\langle i_1+i_2\rangle$ coated	Average distance[a] $\times10^{-17}$ cm	Flux per particle $\times10^{46}$	Volume $\times10^{-48}$ cm³	Product[b]
20– 30°	3.173	4.788	4.95	7.76	4.047	3140
30– 40	2.642	3.481	3.66	10.32	2.154	2223
40– 50	2.078	2.285	2.96	10.36	1.406	1457
50– 60	1.551	1.366	2.56	8.28	1.043	864
60– 70	1.104	0.757	2.31	5.63	0.851	479
70– 80	0.756	0.406	2.16	3.46	0.748	259
80– 90	0.503	0.227	2.10	2.04	0.703	143
90–100	0.329	0.146	2.10	1.31	0.703	92
100–110	0.217	0.106	2.16	0.90	0.748	67
110–120	0.148	0.099	2.31	0.74	0.851	63
120–130	0.108	0.097	2.56	0.59	1.043	62
130–140	0.088	0.100	2.96	0.45	1.406	63
140–150	0.080	0.107	3.66	0.32	2.154	69
150–160	0.079	0.113	4.95	0.18	4.047	73

[a] From HD 200775.
[b] Of flux per particle and volume.

TABLE XIII. Grain characteristics.[a]

Grain specifications	$1/\lambda$	$\langle\cos\theta\rangle$	Q_{ext}	Q_{sca}	Q_{pr}	Albedo
$m=1.33-0.15i$	1.06	+0.23	0.496	0.102	0.473	0.206
	1.59	.56	0.894	0.301	0.725	.337
$2a=0.30$	3.18	.90	2.034	1.047	1.092	.515
$m=1.33-0.30i$	1.06	.24	0.866	0.142	0.832	.164
	1.59	.57	1.344	0.364	1.137	.271
$2a=0.30$	3.18	.90	2.202	0.925	1.370	.420
$m=1.57-0.15i$	1.06	.26	0.670	0.269	0.600	.401
	1.59	.57	1.519	0.816	1.054	.537
$2a=0.30$	3.18	.88	3.188	2.031	1.401	.637
Mixture h	1.20	.34	0.82	0.18	0.76	.22
	1.82	.63	1.25	0.43	0.98	.34
	2.78	+0.84	1.91	0.83	1.21	0.43
$m_c=1.63-0.82i$	1.11	+0.12	0.122	0.044	0.117	0.361
$m_s=1.33$	1.43	.21	0.221	0.109	0.198	.450
$2a_c=0.08; 2a_s=0.224$	2.00	.43	0.472	.295	0.345	.625
	3.33	.74	1.246	965	0.532	.774
$m_c=1.40-1.40i$	1.11	.48	0.752	0.253	0.631	.336
$m_s=1.33-0.13i$	1.43	.71	1.090	0.444	0.775	.407
$2a_c=0.02; 2a_s=0.40$	2.00	.85	1.670	0.841	0.955	.504
	3.33	.96	2.565	1.779	1.145	.577
Average, mixture d	1.20	.33	0.50	0.18	0.44	.36
	1.82	.60	0.92	0.47	0.64	.51
	2.78	+0.83	1.60	0.95	0.81	0.59

[a] Forward directivity, $\langle\cos\theta\rangle$; efficiency factors for extinction Q_{ext} scattering Q_{sca}, and radiation pressure Q_{pr}; and the albedo, Q_{sca}/Q_{ext}.

nebula with respect to the illuminating star. Almost all of the polarization is caused at the various scattering angles within the NGC 7023 nebula and all those angles were considered in Sec. IV. On the way the scattering angle is 0°, and only "interstellar type" polarization may be added. [Actually, therefore, the interstellar polarization of the central star should have been subtracted from that of the regions before application of the Mie theory. The observed interstellar polarization (bottom lines, Table II) is, however, relatively small.] A correction for self-extinction within the nebula is taken into account as follows.

The density and polarimetry conclusions are little affected by transmission losses. The distance r [of expression (1)] has been taken into account, as well as the interstellar extinction. The distance R [of expression (9)] has been taken into account by using expression (2). A small correction remains to be made for the extinction over the distance R; this is done with a factor $e^{-rR/L}$. The correction factor is 0.88 at scattering angle 25°, 0.90 (35°), 0.92 (45°), 0.93 (55°), and 0.94 (65°). The effect on the polarimetry conclusions, determined by the internal difference of these factors, is negligible. The corrected space density is

$$N=3.8(\pm1.5 \text{ p.e.})\times10^{-10} \text{ cm}^{-3}. \quad (11)$$

The effects of multiple scattering should also be considered. From the tables of Coulson, Dave, and Sekera (1960), taking the straight average at scattering angles of 23°, 36°, and 53° with a zenith angle of 180° at the bottom of an atmosphere with zero ground albedo, we have the following polarizations: 27% at $r=0.02$, 23% at $r=0.2$ and 21% at $r=0.4$. At as much as $r=0.7$ the polarization has declined to 20% for a total decrease of only 7%. The effects of multiple scattering

do not appear to be drastic. However, these numbers are for molecular scattering and they serve only as an illustration.

Multiple scattering cannot affect the density estimates of Sec. VI, at least in a first approximation, since the light that was scattered *into* the pencil beam defined by the focal-plane diaphragm of the telescope equals that scattered *out*.

8. Grain Characteristics

Table XIII gives the forward directivity, or asymmetry parameter, evaluated with

$$\langle\cos\theta\rangle=\Sigma[(i_1+i_2)_\theta\cos\theta]/\Sigma(i_1+i_2)_\theta. \quad (12)$$

The summations are made from the Herman–Browning program (Sec. III) over scattering angles $\theta=0$, 37, 53, 66, 78, 90, 102, 114, 127, 143, and 180°. Two mixtures are chosen because they exactly reproduce Fig. 1; other mixtures are, of course, possible. "Mixture h" is for *h*omogeneous particles; it is the average of $m=1.33-0.15i$ and $1.33-0.30i$. "Mixture d" is the average of the two *d*ouble-composition cases in Table XIII. For each mixture, straight averages are taken of $\langle\cos\theta\rangle$, Q_{ext}, and Q_{sca}; they are graphically interpolated for $1/\lambda=1.20$, 1.82, and 2.78. Q_{pr} is computed as described below, and the albedo is Q_{sca}/Q_{ext}. The other subscripts in Table XIII are c for *c*ore and s for outer *s*hell.

The radiation pressure is given (van de Hulst 1957, p. 13) by $\pi a^2 \rho I_0 Q_{pr}c^{-1}$, where a is the radius, ρ is material density of the particle, I_0 is the intensity of the incident light, and c is the velocity of light. $Q_{pr}=Q_{ext}-\langle\cos\theta\rangle Q_{sca}$ is expressed in terms of the efficiency factors respectively for radiation pressure, for total attenuation, and for scattering; θ is the scattering angle.

In a dynamically steady state of the grain with respect to the illuminating star, the radiation pressure is balanced by gravitation. It is readily shown that the particles in such balance must have

$$a\rho=5.9\times10^{-5}Q_{pr}(M/M_0)^{2.3} \text{ g cm}^{-2}, \quad (13)$$

where M is the mass of the star and M_0 that of the sun. In the derivation of this "balance condition," the stellar mass–luminosity law is used; torques on the particle and self-extinction within the nebula are neglected. The grains of Table XIII will be pushed outward from a B star if $2a<100 \mu$, and from a main-sequence G star if $2a<0.5 \mu$. For purely graphite grains the diameters are 3μ and 0.02μ, respectively. These numbers are for illustration only as more complicated effects enter in.

Around the illuminating star of a reflection nebula, the radiation pressure may have removed the grains from the immediate surroundings. In Fig. 4 at the place of scattering angles 70–110° there are no scatterers. The grains at angles 120–180° do not contribute an appreciable amount of light. This could explain why

the three reflection nebulae observed by Elvius and Hall appear to have the star behind the nebula.

A tentative hypothesis for the evolution of the interstellar grains is summarized as follows.

(a) Late-type stars form absorptive grains (Wickramasinghe 1963; Whitney 1965). The peculiar intrinsic polarizations and polarization dispersions of μ Cephei, V Canum Venaticorum, etc. might be explained with such grains. Radiation pressure eventually moves the smaller ones of these grains out into the interstellar medium.

(b) Accretion in interstellar space (Oort and van de Hulst 1946) forms a dielectric shell around the condensation nucleus.

(c) Radiation pressure sustains the encounters of grains (as well as the high velocities of interstellar clouds and further compression of the clouds into globules, which in turn may play a role in the formation of new stars). The particle encounters, plus, perhaps, evaporation of molecules from the particle skin, cause the upper limitation of sizes of the Oort–van de Hulst distribution. Local conditions can vary such that small variations of the grain characteristics are observed (for instance in Orion; Coyne and Gehrels 1965).

Because of the sharp cutoff in the actual size distribution and because the scattering efficiency is greatest for the largest grains, the *apparent* size distribution is narrow. The wavelength dependence of interstellar polarization and of that of reflection nebulae are, therefore, well defined.

REFERENCES

Blaauw, A. 1963, *Basic Astronomical Data*, K. Aa. Strand, Ed. (The University of Chicago Press, Chicago), p. 401.

Coulson, K. L., Dave, J. V., and Sekera, Z. 1960, *Tables Related to Radiation Emerging from a Planetary Atmosphere with Rayleigh Scattering* (University of California Press, Berkeley and Los Angeles).
Coyne, G. V., and Gehrels, T. 1966, *Astron. J.* **71**, 355 (Paper VIII).
Elvius, A., and Hall, J. S. 1966, *Lowell Obs. Bull.* **135**; also in Greenberg (1967).
Gehrels, T. 1960a, *Astron. J.* **65**, 470 (Paper II).
——. 1960b, *Lowell Obs. Bull.* **4**, 330.
Gehrels, T., and Teska, T. M. 1960, *Publ. Astron. Soc. Pacific* **72**, 115.
Greenberg, J. M., Ed. 1967, *Proceedings of the IAU Colloquium on Interstellar Grains* (National Aeronautics and Space Administration, Washington, D. C.).
Greenstein, J. L., and Aller, L. H. 1947, *Publ. Astron. Soc. Pacific* **59**, 139.
Herman, B. M., and Battan, L. J. 1963, *Electromagnetic Scattering*, M. Kerker, Ed. (Pergamon Press, New York), p. 251.
Houten, C. J., van 1961, *Bull. Astron. Inst. Neth.* **16**, 1.
Hubble, E. 1922, *Astrophys. J.* **56**, 400.
Hulst, H. C., van de 1957, *Light Scattering by Small Particles* (John Wiley & Sons, Inc., New York).
Johnson, H. L. 1965, *Astrophys. J.* **141**, 923.
Johnson, H. L., and Borgman, J. 1963, *Bull. Astron. Inst. Neth.*, **17**, 115.
Keenan, P. C. 1936, *Astrophys. J.* **84**, 601.
LaMer, V. K. 1943, Rept. No. 1857 (Office of Scientific Research and Development, Washington, D. C.); also *Applied Mathematics Series*, No. 4 (National Bureau of Standards, Washington, D. C., 1949).
Lundmark, K. 1922, *Publ. Astron. Soc. Pacific* **34**, 40.
Martel, M.-T. 1958, *Publs. de l'Obs. de Haute-Provence* **4**, No. 20.
Mendoza, E. E. 1958, *Astrophys. J.* **128**, 212.
Oort, J. H., and Hulst, H. C., van de 1946, *Bull. Astron. Inst. Neth.* **10**, 187.
Powell, R. S., Circle, R. R., Vogel, D. C., Woodson, P. D., and Donn, B. 1966, *Melpar Techn. Pre-Print Series* (Melpar Inc., Falls Church, Virginia).
Roark, T. P. 1966, thesis, Rensselaer Polytechnic Institute, Troy, New York.
Stebbins, J., Huffer, C. M., and Whitford, A. E. 1940, *Astrophys. J.* **91**, 20.
Vanýsek, V., and Svatoš, J. 1964, *Acta Univ. Carolinae, Math. Phys.* **1**, 1.
Whitney, C. A. 1965, *Sky and Telescope* **29**, 18.
Wickramasinghe, N. C. 1963, *Monthly Notices Roy. Astron. Soc.* **126**, 99.

No. 106 WAVELENGTH DEPENDENCE OF POLARIZATION X. INTERSTELLAR POLARIZATION*

by G. V. Coyne S.J., and T. Gehrels

May 25, 1967

N 69 - 18303

ABSTRACT

A survey of O and B stars was started with the new 154-cm Catalina reflector. The equipment is described and results are given for 33 stars. Of these, seven stars show variable polarization. Striking discrepencies from the mean interstellar polarization-wavelength dependence are found near Orion. The brighter component of θ^2 Orionis, a spectroscopic binary with a 21-day period, shows variations of ±0.5% in the ultraviolet. The spectroscopic binary φ Per shows variations of about ±0.2%. Both stars have a strong wavelength dependence of the polarization position angles. A time dependence of the position angle is found for the spectroscopic binary and shell star ζ Tau.

1. Introduction

AS a continuation of a program of study of the wavelength dependence of interstellar and stellar polarization, a survey of the polarization of O and B stars as faint as $V=8.0$ near the galactic plane and well distributed in galactic longitudes was undertaken. The first results of this survey are presented in Sec. III. A subsequent paper will give further observations and a more thorough discussion of the results. In Papers II and VIII (see references) we found a mean interstellar polarization curve, with a maximum at about 5200 Å decreasing rapidly towards longer wavelengths and less rapidly towards shorter wavelengths. On the other hand, several stars show large deviations from such a mean curve (Paper VIII), indicating a large dispersion in the wavelength dependence of interstellar polarization. With the additional observations contained in the present paper, we rediscuss this mean interstellar polarization curve and the degree of dispersion in the polarization-wavelength dependence for various stars (Sec. IV).

In the course of the survey several stars were found to have variable polarization. Available observations on these stars are limited. In anticipation of further observations a preliminary discussion of these variations is presented (Sec. V).

2. The Equipment

In November 1965 the 154-cm reflector of the Lunar and Planetary Laboratory, situated at an elevation of 2510 m in the Santa Catalina Mountains north of Tucson, was first used for polarization measurements. The observations in this paper represent the first group of polarization measurements made with this telescope. The telescope has Cassegrain arrangements only, and both the $f/13$ and $f/45$ secondary mirrors are used in this program.

For a determination of instrumental effects we observed 20 stars within 51 pc and with less than 0.04% polarization over a wide range of galactic coordinates (Behr 1956). The instrumental polarizations for the seven filters from Infrared to Nickel

sulfate, described below, are respectively 0.03, 0.07, 0.11, 0.11, 0.13, 0.17, and 0.14%, and their equatorial position angles respectively 146, 144, 152, 148, 147, 150 and 153°. These amounts are known with a probable error of ±0.01%. No difference between $f/13$ and $f/45$ was found. We are indebted to J. H. Richardson of the Kitt Peak National Observatory for the care with which he aluminized the three mirrors.

Figure 1 shows the polarimetric equipment at the Catalina 154-cm telescope. The polarimeter is the same as that used previously (Gehrels and Teska 1960); the paper referred to also has a description of the calibration of polarization position angles. The polarimeter has, successively, a slide for the Lyot depolarizer, a field-viewing eyepiece, a slide for diaphragms (0.25 to 10 mm in diameter), an eyepiece for centering, a filterslide, a Wollaston prism, a Fabry field lens, and two photomultiplier tubes. Seen in Fig. 1 is the Wollaston neck and the dry-ice box for S-1 phototubes; there is a separate Wollaston neck and ice box for blue-sensitive tubes. For photometry with these boxes, the Wollaston neck is clamped in a fixed orientation, or a separate 1P21 ice-box is put on instead of the Wollaston arrangements.

The output of the phototubes is simultaneously received by two Weitbrecht integrators and recorded on the strip chart on top of the console. The recorder is currently used only for visual display and as a diary for the observer, since all data is punched on paper tape. The outputs are digitized by the voltmeter seen under the recorder. Below the digital voltmeter is a high-voltage power supply for the phototubes, and below it are the programmer, and the clock/timer. The time is displayed in binary code (1^h35^m4 is shown). To the right is the paper-tape punch with the integrator power supply on top.

Since Paper VIII, the following improvements have been made. D. L. Brumbaugh designed the clock/timer and he and V. J. Borg improved the digitization equipment, especially its speed. The integration time for objects brighter than eighth visual magnitude is ordinarily 7 sec, during which occur the readout and the punching of the Wollaston angle, object identification, time, depolarizer state, filter and star/sky identification,
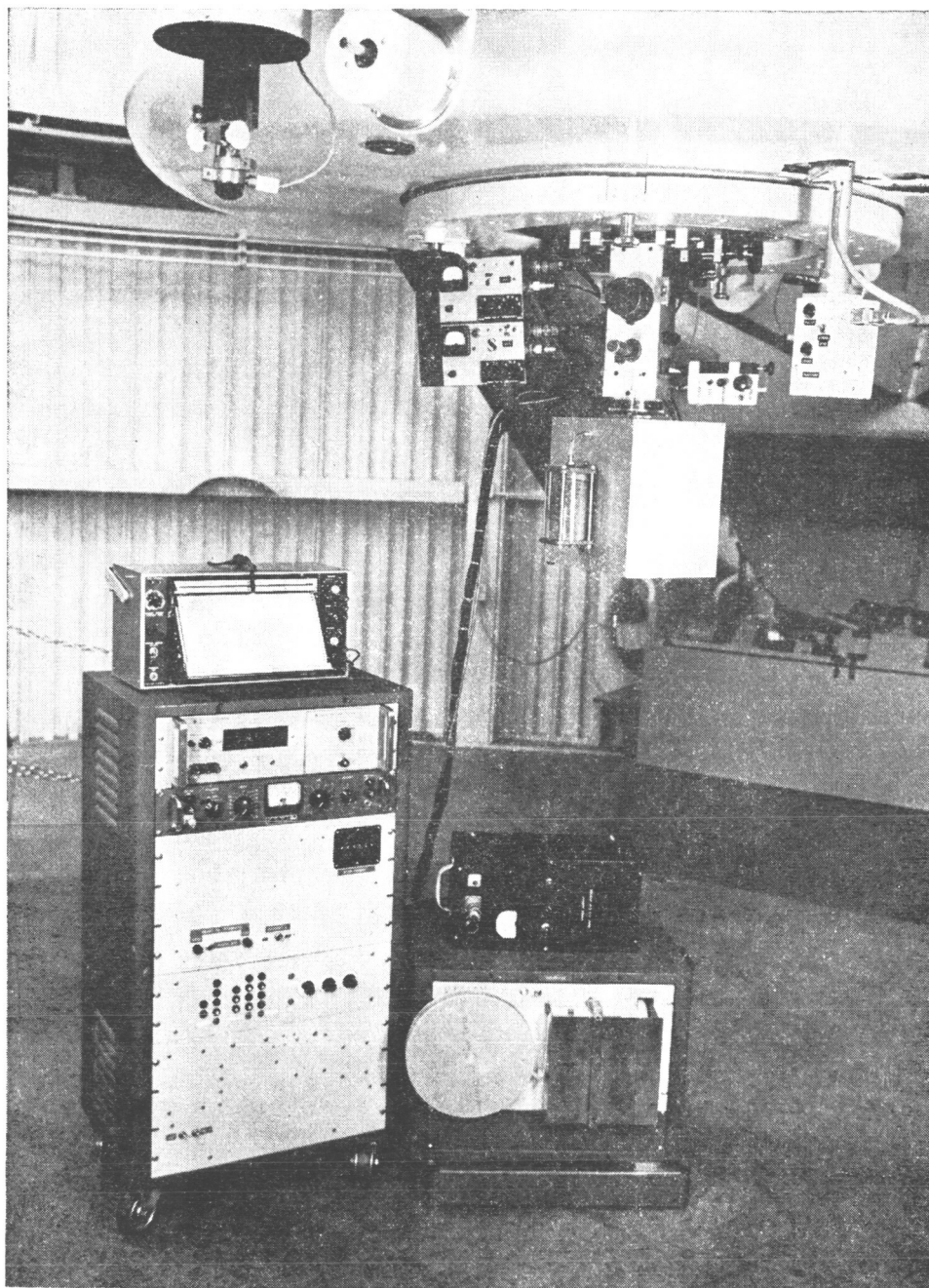
FIG. 1. Photopolarim-eter with dry-ice box and Weitbrecht integra-tors mounted on the Catalina 61-in. (154-cm) telescope. Strip-chart re-corder, digital console, paper punch, and inte-grator power supply are also shown.

After the integration, the readout and punching of the measured intensities takes 5 sec. During this latter 5 sec of readout an experienced observer has just enough time to change the Wollaston angle or the depolarizer state, and to check the centering, in order to start the next integration. E. H. Roland made the new dry-ice box for the S-1 phototubes (RCA 7102) so that the refrigeration is considerably improved. T. M. Teska selected the best blue-sensitive tubes; the EMI 6255S were replaced by 6255B, and those in turn by EMI D205R (super S-11 with quartz win-dow).

The characteristics of the filters used in this program have been given in Paper VII. The filter at $1/\lambda = 1.39$ was replaced by an orange interference filter (Baird Atomic B-5; "Peak: 6450A+50A−25A. Total width at half peak: 1032A–1290A. Peak transmission: 50–60%"). The effective wave numbers for all filter/tube combinations used in the current study were estimated anew. For white light (which approximates the reddened B stars of this paper) at 1.3 air masses they are 1.06, 1.21, 1.56, 1.93, 2.33, 2.78, 3.03 μ^{-1}, and for a reddened K star 1.05, 1.19, 1.54, 1.91, 2.29, 2.75, and 3.00 μ^{-1}. These wave numbers are uncertain by ±0.02 since the

FIG. 2. Response curves to white light through 1.3 air masses at 2200 m altitude for the various filter/tube combinations. For filter designations, characteristics and effective wave numbers see Sec. II. The response of the red system (I,R,O) has been multiplied by a factor of 40 to normalize it to the blue system (N,U,B,G).
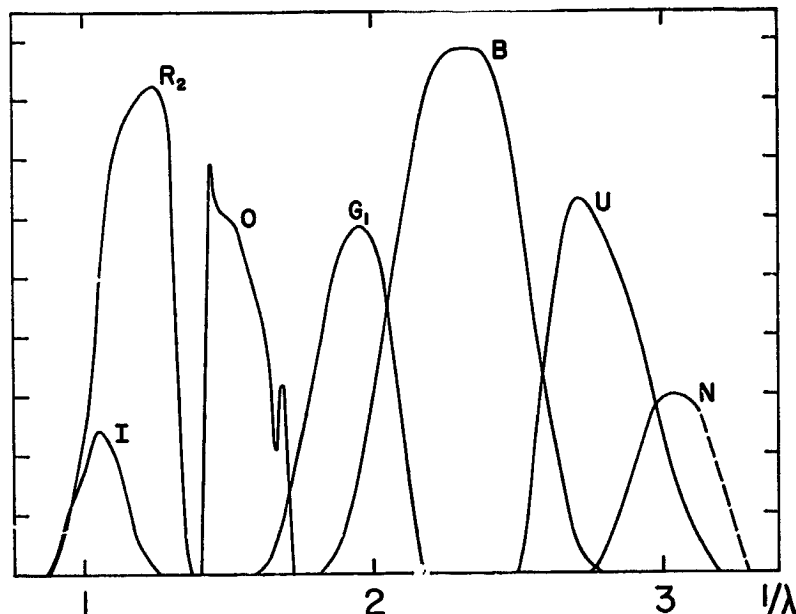
tube responses are not measured but adopted from the manufacturer's mean curve.

Figure 2 shows the response curves for the various filter/tube combinations. The letter used to designate each filter is as in Paper VII. The new interference filter described above is the O filter. In the tables to follow, these filters are designated by the effective wave numbers given above for white light and an extinction of 1.3 air masses. Only three stars with spectral type later than B occur in the tables, and these are indicated. The nearly complete absence of red leakage for the U $(1/\lambda = 2.78)$ and N $(1/\lambda = 3.03)$ filters is periodically checked, on the reddest objects. We are grateful to S. F. Pellicori for the determination of the filter and tube characteristics.

3. The Observations

Most of the observations were made between June 1966 and February 1967; a few were made earlier in 1966 or later in 1967.

The observations at each filter are made by taking measurements with and without depolarizer at each of six orientations of the Wollaston prism, the orientations being separated by intervals of 30°. On the average this routine is repeated three times giving a total of 18 pairs of measurements. For faint stars, for stars with small polarization, and especially for the filters at $1/\lambda = 1.06$ and $1/\lambda = 3.03$ a total of 24 to 30 pairs of measurements is usually made, in order to obtain the desired accuracy. Such a set, of about 18 pairs of measurements at a given filter, is defined as a single observation. A least-squares solution for the percentage polarization and position angle is run at the Numerical Analysis Laboratory of the University of

Arizona. We are indebted to D. L. Coffeen and Mrs. L. C. Hess for certain improvements in the data processing. The instrumental polarization appropriate to each orientation of the Wollaston prism is subtracted from the measured value of the polarization at that orientation. Each final value of the percentage polarization is multiplied by a factor of 1.004, the measured value for the depolarizer deficiency.

Tables I and II are a journal of observations for stars which, in the course of this program, show no variable polarization and for stars with indications of variable polarization, respectively. The polarization position angle, θ, is in the equatorial coordinate frame. The dates are given in Universal Time.

Table III gives the weighted mean percentage of polarization during the present observing period. Five stars (HD 37041, 36371, 37202, 134320, 134335) in Table III and in subsequent tables have been previously observed (Paper VIII). Only in the case of HD 36371 have we combined the previous observations with the new ones. In the cases of HD 37041 and HD 37202 there are indications of variability (discussed in Sec. V); the Paper VIII results for IID 134320 and 134335 are considered too poor to be combined with the new values. A few entries marked with a semicolon represent single observations. All other entries represent the weighted mean value of two (in some cases three) independent observations made on separate nights. In previous papers we used the inverse of the probable error as the weighting factor rather than the inverse of the probable error squared. The statistics were poor, with only six measurements per least-squares solution. This is no longer true. Hence the weights assigned here are the inverse of the squares of the probable errors obtained from each separate least-squares solution. The

average probable error of the weighted mean values is ±0.04%. This probable error is largest (±0.06%) for $1/\lambda = 1.06$ and $1/\lambda = 3.03$ and smallest (±0.02%) for $1/\lambda = 1.93$. Colons in Table III indicate probable errors greater than ±0.10%.

Table IV lists the equatorial position angles. Again we have the weighted mean values from two (in a few cases three) independent observations, with weights equal to the reciprocal of the square of the individual probable errors. These errors in position angle are proportional to the error in percentage polarization

divided by the polarization (Hall and Serkowski 1963); and weights have been assigned on this basis. The average probable error for the position angle is ±1°1. This average probable error is largest (±1°6) at $1/\lambda = 1.06$ and smallest (±0°8) at $1/\lambda = 1.93$. Single observations in Table IV are indicated by a semicolon; colons indicate probable errors greater than ±3°.

Table V presents some of the fundamental data for the stars observed in this program. This table has been constructed in the same way as Table VI of Paper VIII (see references there), with the addition of a column

TABLE I. Journal of observations. Nonvariable polarization.

HD	1/λ	Yr.Mo.Day	P% ± pe	θ		HD	1/λ	Yr.Mo.Day	P% ± pe	θ
4180	1.06	66.12.09	0.858 .032	85.33		8965	1.21	66.08.13	2.360 .061	105.46
4180	1.06	67.01.12	0.937 .043	84.82		8965	1.21	66.08.15	2.081 .050	106.21
4180	1.21	66.12.09	0.825 .020	81.69		8965	1.56	66.08.13	2.970 .071	107.31
4180	1.21	67.01.12	0.821 .022	82.06		8965	1.56	66.08.15	2.980 .051	101.51
4180	1.56	66.12.09	1.106 .032	80.88		8965	1.93	67.01.13	3.123 .033	105.17
4180	1.56	67.01.12	1.053 .023	82.64		8965	1.93	67.02.07	2.919 .029	105.10
4180	1.93	67.01.02	1.042 .019	83.79		8965	2.33	67.01.13	2.897 .027	103.49
4180	1.93	67.01.03	1.044 .016	83.45		8965	2.33	67.02.07	2.902 .020	104.54
4180	2.33	67.01.02	1.044 .018	85.87		8965	2.78	67.01.13	2.704 .035	102.44
4180	2.33	67.01.03	1.080 .019	84.81		8965	2.78	67.02.07	2.657 .023	104.14
4180	2.78	67.01.02	1.028 .019	84.38		8965	3.03	67.01.13	2.570 .062	103.77
4180	2.78	67.01.03	1.006 .018	84.31		8965	3.03	67.02.07	2.442 .086	106.90
4180	3.03	67.01.02	0.967 .037	90.73						
4180	3.03	67.01.03	1.019 .044	84.56		10898	1.06	66.10.12	2.643 .181	94.63
						10898	1.21	66.08.26	3.007 .079	95.59
4768	1.06	66.08.15	1.637 .061	83.81		10898	1.21	66.10.11	3.382 .059	93.79
4768	1.06	66.08.26	1.801 .107	97.01		10898	1.21	66.10.12	3.369 .047	92.45
4768	1.21	66.08.15	1.767 .104	82.48		10898	1.56	36.08.26	4.073 .083	94.21
4768	1.21	66.08.26	1.942 .077	71.89		10898	1.56	66.10.11	4.042 .113	94.72
4768	1.56	66.08.15	2.365 .077	79.14		10898	1.56	66.10.12	4.009 .075	93.21
4768	1.56	66.08.26	2.325 .090	82.87		10898	1.93	66.09.21	4.615 .051	93.93
4768	1.93	66.10.10	2.369 .034	82.69		10898	1.93	66.09.22	4.597 .038	94.20
4768	1.93	66.10.13	2.502 .075	81.47		10898	2.33	66.09.21	4.227 .022	95.10
4768	2.33	66.10.10	2.355 .028	81.72		10898	2.33	66.09.22	4.384 .021	93.79
4768	2.33	66.10.13	2.387 .023	80.61		10898	2.78	66.09.21	3.882 .102	94.85
4768	2.78	66.10.10	2.304 .047	81.15		10898	2.78	66.09.22	3.959 .062	94.43
4768	2.78	66.10.13	2.151 .036	79.86		10898	3.03	66.09.21	4.027 .103	95.29
4768	3.03	66.10.10	2.407 .140	78.00		10898	3.03	66.09.22	3.783 .107	93.33
4768	3.03	66.10.13	2.164 .096	78.15		10898	3.03	66.09.22	3.792 .107	93.41
7252	1.06	66.08.13	2.986 .162	107.11		15558	1.06	66.10.12	3.661 .149	121.91
7252	1.06	67.01.12	2.411 .142	97.35		15558	1.06	66.11.16	3.748 .119	121.73
7252	1.21	66.08.13	2.527 .055	101.11		15558	1.21	66.10.12	4.264 .063	121.43
7252	1.21	67.01.12	2.649 .068	96.08		15558	1.21	66.11.16	4.294 .062	121.01
7252	1.56	66.08.13	3.802 .033	96.16		15558	1.56	66.10.12	5.390 .082	119.39
7252	1.56	67.01.12	3.426 .089	96.55		15558	1.56	66.11.16	5.264 .082	119.20
7252	1.93	67.01.13	3.619 .023	97.35		15558	1.93	66.10.11	5.311 .023	120.57
7252	1.93	67.01.28	3.793 .079	98.29		15558	1.93	66.10.13	5.279 .030	119.57
7252	2.33	67.01.13	3.498 .026	98.11		15558	2.33	66.10.11	5.139 .018	121.11
7252	2.33	67.01.28	3.719 .030	98.08		15558	2.33	66.10.13	5.458 .036	118.57
7252	2.78	67.01.13	3.370 .060	97.58		15558	2.78	66.10.11	4.529 .042	119.18
7252	2.78	67.01.28	3.398 .028	97.92		15558	2.78	66.10.13	4.764 .035	118.78
7252	3.03	67.01.13	3.144 .109	98.42		15558	3.03	66.10.10	4.362 .233	121.67
7252	3.03	67.01.28	2.886 .110	101.08		15558	3.03	66.10.13	4.481 .107	114.37
7902	1.06	66.10.11	2.231 .124	94.85		17506	1.05	66.08.29	0.722 .030	118.31
7902	1.66	66.10.12	1.887 .092	96.48		17506	1.05	66.12.09	0.751 .013	118.65
7902	1.06	67.01.12	1.805 .099	95.28		17506	1.19	66.08.29	0.815 .010	119.35
7902	1.21	66.10.11	2.642 .084	98.19		17506	1.19	66.12.09	0.797 .016	115.52
7902	1.21	66.10.12	2.444 .060	95.91		17506	1.54	66.08.29	0.991 .015	113.91
7902	1.56	66.10.11	3.160 .061	94.91		17506	1.54	66.12.09	0.923 .017	110.59
7902	1.56	66.10.12	3.228 .056	95.05		17506	1.91	66.12.09	1.127 .035	112.97
7902	1.93	66.10.11	3.349 .017	96.02		17506	1.91	67.01.02	1.138 .023	115.36
7902	1.93	66.12.08	3.296 .017	95.55		17506	2.29	66.12.09	1.105 .030	111.75
7902	2.33	66.10.11	3.307 .017	96.58		17506	2.29	67.01.02	1.043 .024	111.36
7902	2.33	66.12.08	3.208 .017	95.12		17506	2.75	66.12.09	0.885 .033	112.78
7902	2.78	66.10.11	3.268 .099	93.26		17506	2.75	67.01.02	1.112 .044	119.61
7902	2.78	66.12.08	2.946 .029	96.96		17506	2.75	67.02.08	0.920 .047	111.85
7902	3.03	66.10.11	2.847 .076	93.93		17506	3.00	66.12.09	0.994 .072	116.17
7902	3.03	66.12.08	3.009 .082	97.28		17506	3.00	67.01.02	1.112 .135	119.90
						17506	3.00	67.02.08	0.764 .154	111.07
8965	1.06	66.08.13	1.955 .155	99.71						
8965	1.06	66.08.15	2.031 .110	100.71						

which lists our observed mean value of the polarization position angle. An exclamation mark (!) in this column indicates wavelength dependence of the position angle. The P_{vis} column now gives the weighted mean of the polarizations at $1/\lambda = 1.56$, 1.93 and 2.33 (colons and semicolons are given half weight). The photometric data for HD 37061 are from Lee (1966).

4. Interstellar Polarization

Table VI gives the normalized polarizations. The normalization is performed by setting the straight average of the polarizations at $1/\lambda = 1.93$ and $1/\lambda = 2.33$ equal to 100%. In this way we can both compare stars which are variously polarized to one another, and also combine the observations for various stars in order to study the more general features of interstellar polarization. Colons are used in Table VI to indicate that the probable error for the normalized polarization is $\pm 8\%$ or greater. Semicolons are for single observations.

Figures 3(a) to 3(e) give the normalized polarization curves both for the stars observed in the present study (solid curves) and for the stars of Paper VIII (dashed

TABLE I (continued)

HD	1/λ	Yr.Mo.Day	P% ± pe	θ	HD	1/λ	Yr.Mo.Day	P% ± pe	θ
25914	1.06	66.09.25	3.437 .138	138.33	32990	1.06	67.01.01	1.026 .044	85.97
25914	1.06	66.10.12	2.954 .089	137.48	32990	1.06	67.01.12	1.058 .058	88.48
25914	1.06	67.01.01	3.161 .094	137.61	32990	1.21	67.01.01	1.240 .030	86.16
25914	1.21	66.09.25	3.950 .056	137.91	32990	1.21	67.01.12	1.327 .041	86.34
25914	1.21	66.10.12	3.714 .074	137.98	32990	1.56	67.01.01	1.506 .039	83.88
25914	1.56	66.09.25	4.338 .077	139.46	32990	1.56	67.01.12	1.572 .076	85.69
25914	1.56	66.10.12	4.451 .089	137.39	32990	1.93	66.12.09	1.697 .033	78.66
25914	1.93	66.09.24	4.647 .025	141.17	32990	1.93	67.01.03	1.665 .013	85.23
25914	1.93	66.10.18	4.578 .038	139.89	32990	2.33	66.12.09	1.672 .023	84.61
25914	2.33	66.09.24	4.562 .020	141.21	32990	2.33	67.01.03	1.607 .021	85.59
25914	2.33	66.10.18	4.266 .032	139.27	32990	2.78	66.12.09	1.547 .026	83.71
25914	2.78	66.09.24	4.078 .056	139.36	32990	2.78	67.01.03	1.489 .019	86.07
25914	2.78	66.10.18	4.082 .074	140.46	32990	3.03	66.12.09	1.435 .039	83.91
25914	3.03	66.09.24	3.571 .166	138.66	32990	3.03	67.01.03	1.287 .050	85.42
25914	3.03	66.10.18	3.774 .108	138.21					
					36371	1.06	63.12.02	1.520 .031	177.64
25940	1.06	66.09.23	0.767 .038	176.23	36371	1.21	63.12.02	1.700 .058	176.47
25940	1.06	66.09.25	0.717 .046	171.14	36371	1.21	66.10.12	1.641 .023	179.92
25940	1.06	67.01.01	0.714 .029	168.65	36371	1.39	63.12.02	2.040 .040	178.59
25940	1.06	67.01.2?	0.621 .024	168.20	36371	1.39	65.09.21	1.561 .072	176.39
25940	1.21	66.05.?3	0.688 .028	174.83	36371	1.56	66.10.12	1.801 .038	181.22
25940	1.21	66.09.25	0.794 .019	170.46	36371	1.93	63.12.01	2.230 .049	173.51
25940	1.21	67.01.01	0.755 .018	167.89	36371	1.93	65.08.27	2.221 .072	179.34
25940	1.21	67.01.2?	0.700 .017	173.14	36371	2.33	63.12.01	2.090 .040	172.21
25940	1.56	66.09.23	0.759 .013	169.68	36371	2.33	65.08.27	2.197 .049	178.82
25940	1.56	66.09.25	0.879 .024	173.39	36371	2.78	63.12.01	1.830 .036	170.60
25940	1.56	67.01.01	0.928 .021	172.34	36371	2.78	65.08.13	1.690 .399	173.79
25940	1.56	67.01.2?	0.783 .023	171.41	36371	3.03	63.12.01	1.780 .081	168.90
25940	1.93	67.01.02	0.797 .027	169.38					
25940	2.33	66.09.22	0.651 .016	176.50	3706:	1.06	67.02.08	1.369 .075	62.57
25940	2.33	67.01.02	0.737 .021	170.42	37061	1.21	67.02.08	1.687 .054	57.25
25940	2.78	66.09.22	0.409 .018	176.48	37061	1.56	67.02.08	1.508 .046	63.83
25940	2.78	67.01.02	0.471 .028	171.38	37061	1.93	67.01.03	1.523 .022	66.12
25940	3.03	66.09.21	0.494 .062	171.69	37061	1.93	67.02.04	1.549 .057	65.23
25940	3.03	67.01.02	0.232 .064	178.82	37061	2.33	67.01.03	1.367 .029	70.24
					37061	2.33	67.02.04	1.454 .014	67.43
29866	1.06	66.10.12	1.528 .076	16.39	37061	2.78	67.01.03	1.201 .044	73.08
29866	1.06	67.01.12	1.616 .091	7.84	37061	2.78	67.02.04	1.293 .030	67.71
29866	1.21	66.10.12	1.482 .047	12.01	37061	3.03	67.01.03	1.096 .073	75.25
29866	1.21	67.01.12	1.544 .047	8.19	37061	3.03	67.02.04	1.478 .107	69.20
29866	1.21	67.01.26	1.522 .052	10.68					
29866	1.56	66.10.12	1.687 .036	11.00	37367	1.06	67.01.12	0.596 .108	23.69
29866	1.56	67.01.12	1.823 .056	9.00	37367	1.06	67.02.06	0.457 .071	21.17
29866	1.56	67.01.26	1.738 .051	11.08	37367	1.21	67.01.12	0.638 .030	16.00
29866	1.93	67.01.13	1.724 .012	10 26	37367	1.21	67.02.06	0.803 .045	29.22
29866	1.93	67.02.08	1.806 .013	9.09	37367	1.56	67.01.12	0.686 .075	21.61
29866	2.33	67.01.13	1.605 .011	11.12	37367	1.56	67.02.06	0.989 .060	24.74
29866	2.33	67.02.08	1.721 .082	16.51	37367	1.93	67.01.03	0.751 .065	24.34
29866	2.78	67.01.13	1.438 .032	13.68	37367	1.93	67.01.13	0.817 .011	24.60
29866	2.78	67.02.08	1.426 .023	12.29	37367	2.33	67.01.03	0.626 .019	22.22
29866	3.03	67.01.13	1.193 .051	15.75	37367	2.33	67.01.13	0.727 .061	21.68
29866	3.03	67.02.08	1.211 .067	10.84	37367	2.78	67.01.03	0.511 .020	28.64
					37367	2.78	67.01.13	0.736 .039	21.44
32481	1.06	67.02.06	1.473 .128	91.33	37367	3.03	67.01.03	0.635 .078	40.05
32481	1.21	67.02.06	1.706 .057	78.39	37367	3.03	67.01.13	0.447 .063	21.65
32481	1.56	67.02.06	2.061 .081	80.01					
32481	1.93	66.12.14	1.725 .040	77.05	40111	1.06	66.12.13	0.685 .044	177.92
32481	1.93	67.01.13	1.989 .043	81.01	40111	1.06	67.01.01	0.719 .044	161.20
32481	2.33	66.12.14	1.810 .026	77.37	40111	1.21	66.12.13	0.602 .024	180.58
32481	2.33	67.01.13	1.958 .021	81.88	40111	1.21	67.01.01	0.809 .024	161.38
32481	2.78	66.12.14	1.762 .046	72.90	40111	1.56	66.12.13	0.853 .039	180.63
32481	2.78	67.01.13	1.699 .082	82.11	40111	1.56	67.01.01	1.048 .031	163.86
32481	3.03	66.12.14	1.444 .131	83.34	40111	1.93	66.12.09	0.686 .014	170.60

curves). The average probable error for the normalized polarizations plotted in Figs. 3(a) to 3(c) is ±3.0%. Where the probable error is greater than ±8%, an open square is used; open circles represent single observations. Omitted from the figures because of unusually large uncertainties are HD 83953 of this paper and the following stars of Paper VIII: HD 24431, 134320, 134335, 193443. The irregular red variable μ Cephei (HD 206936) has also been omitted since its large amplitude variation in percentage polarization (approx 2%) will be discussed in a subsequent paper in

this series. The observation at 1/λ=3.03 for HD 134320 has not been plotted, since the probable error is ±22%. For ζ Tau (HD 37202) the combined values from Table X of Paper VIII and the present Table VI (colons and semicolons half weight) are plotted. Since θ² Orionis (HD 37041) has variable polarization only the 1964 observations are plotted.

The marked similarity of a majority of the curves is a noteworthy feature of Figs. 3(a) to 3(c), as are the departures from this "characteristic" curve. We have combined the observations for 52 of the stars in order

TABLE I (continued)

HD	1/λ	Yr.Mo.Day	P% ± pe	θ	HD	1/λ	Yr.Mo.Day	P% ± pe	θ
40111	1.93	67.01.03	0.741 .010	170.05	134335	1.05	66.03.16	0.362 .027	83.95
40111	2.33	66.12.09	0.704 .034	168.11	134335	1.05	66.06.13	0.3'3 .039	95.69
40111	2.33	67.01.03	0.680 .014	169.69	134335	1.19	66.03.16	0.508 .017	85.42
40111	2.78	66.12.09	0.512 .026	175.88	134335	1.19	66.06.13	0.578 .013	82.69
40111	2.78	67.01.03	0.273 .052	168.45	134335	1.37	66.03.16	0.489 .046	80.97
40111	3.03	66.12.09	0.253 .055	166.74	134335	1.54	66.03.16	0.550 .030	88.02
40111	3.03	67.01.03	0.533 .086	161.35	134335	1.54	66.06.13	0.624 .041	82.40
					134335	1.91	66.02.28	0.639 .079	82.28
41398	1.06	67.01.12	1.698 .110	162.79	134335	1.91	66.03.13	0.661 .014	81.10
41398	1.21	67.01.12	1.851 .068	159.42	134335	2.29	66.02.28	0.701 .073	83.23
41398	1.56	67.01.12	2.245 .071	162.80	134335	2.29	66.03.13	0.644 .072	84.18
41398	1.93	66.12.14	2.081 .025	168.46	134335	2.75	66.02.14	0.603 .082	80.70
41398	2.33	66.12.14	2.098 .020	167.71	134335	2.75	66.02.28	0.535 .044	78.97
41398	2.78	66.12.14	1.566 .029	169.89	134335	2.75	66.03.13	0.501 .058	98.32
41398	3.03	66.12.14	1.697 .019	163.79	134335	3.00	66.02.28	0.610 .075	79.61
					134335	3.00	66.03.13	0.453 .089	76.69
46484	1.06	66.12.13	0.825 .096	162.17					
46484	1.21	66.12.13	0.977 .046	174.18	179406	1.06	66.06.11	0.994 .056	177.20
46484	1.56	66.12.13	1.492 .087	181.43	179406	1.21	66.06.11	1.006 .037	181.18
46484	1.93	66.12.14	1.290 .029	175.28	179406	1.56	66.06.11	1.211 .045	178.92
46484	2.33	66.12.14	1.206 .017	177.35	179406	1.56	66.07.06	1.111 .035	184.74
46484	2.78	66.12.14	0.990 .054	178.99	179406	1.93	66.06.15	1.385 .01'	183.71
					179406	1.93	66.07.06	1.315 .057	182.46
47240	1.06	66.12.13	1.000 .072	178.24	179406	1.93	66.07.22	1.078 .057	
47240	1.06	67.01.01	0.657 .050	167.19	179406	2.33	06.06.15	1.327 .010	184.62
47240	1.06	67.02.08	0.607 .050	171.90	179406	2.33	66.06.15	1.239 .036	
47240	1.21	66.12.13	0.945 .036	173.63	179406	2.78	66.06.15	1.155 .018	183.65
47240	1.21	67.01.01	0.841 .068	170.82	179406	2.78	66.07.22	0.820 .078	
47240	1.21	67.02.08	0.753 .034	172.10	179406	3.03	66.06.15	1.147 .037	186.99
47240	1.56	66.12.13	1.078 .039	180.95	179406	3.03	66.07.22	1.065 .067	
47240	1.56	67.01.01	0.993 .040	172.90					
47240	1.56	67.02.08	1.021 .068	176.22	193237	1.06	66.08.27	0.761 .035	40.73
47240	1.93	67.02.07	0.996 .013	172.45	193237	1.06	66.10.14	0.953 .032	39.46
47240	2.33	67.02.07	1.076 .051	172.68	193237	1.21	66.08.27	0.918 .020	38.85
47240	2.78	67.02.07	0.691 .033	180.80	193237	1.21	66.10.14	1.062 .015	40.74
47240	2.78	67.02.07	0.752 .074	180.16	193237	1.56	66.08.27	1.201 .025	38.84
47240	3.03	67.02.07	0.631 .067	176.06	193237	1.56	66.10.14	1.383 .023	40.22
					193237	1.93	66.07.26	1.372 .007	38.17
83953	1.06	67.01.03	0.539 .078	175.14	193237	1.93	66.08.27	1.432 .010	35.08
83953	1.06	67.01.12	0.337 .035	174.70	193237	2.33	66.07.26	1.365 .030	38.58
83953	1.21	67.01.03	0.381 .021	172.76	193237	2.33	66.08.27	1.501 .005	35.15
83953	1.21	67.01.12	0.364 .025	172.64	193237	2.78	66.07.26	1.381 .012	38.42
83953	1.56	67.01.03	0.411 .035	177.61	193237	2.78	66.08.27	1.412 .013	37.22
83953	1.56	67.01.12	0.297 .018	177.78	193237	3.03	66.07.26	1.372 .019	40.04
83953	1.93	67.01.13	0.323 .014	183.13	193237	3.03	66.08.27	1.368 .022	39.28
83953	2.33	67.01.13	0.580 .074	167.16					
83953	2.78	67.01.13	0.114 .022		216411	1.06	66.08.15	1.588 .068	45.69
83953	3.03	67.01.13	0.105 .037		216411	1.06	66.08.22	1.389 .084	44.10
					216411	1.21	66.08.15	2.082 .046	5C.89
134320	1.05	66.03.16	0.404 .035	89.75	216411	1.21	66.08.22	2.131 .031	46.52
134320	1.05	66.06.13	0.447 .031	90.56	216411	1.56	66.08.15	2.627 .053	45.19
134320	1.19	66.03.16	0.432 .019	83.51	216411	1.56	66.08.22	2.427 .068	49.16
134320	1.19	66.06.13	0.456 .029	84.19	216411	1.93	66.07.22	2.659 .046	5C.96
134320	1.37	66.03.16	0.529 .029	86.80	216411	1.93	66.07.26	2.653 .066	48.39
134320	1.54	66.03.16	0.621 .027	86.28	216411	1.93	66.10.10	2.784 .063	48.66
134320	1.54	66.06.13	0.600 .024	85.94	216411	2.33	66.07.22	3.010 .044	51.27
134320	1.91	66.03.13	0.604 .011	82.84	216411	2.33	66.07.26	2.529 .016	49.28
134320	2.29	66.03.14	0.617 .016	88.20	216411	2.33	66.10.10	2.967 .059	49.21
134320	2.29	66.03.15	0.635 .023	93.14	216411	2.78	66.07.26	2.263 .052	49.01
134320	2.75	66.03.14	0.533 .055	90.20	216411	2.78	66.08.12	2.391 .040	47.95
134320	2.75	66.03.15	0.655 .036	86.88	216411	3.03	66.07.26	2.107 .067	51.20
134320	3.00	66.03.14	0.584 .143	78.87	216411	3.03	66.08.12	2.245 .087	51.84
134320	3.00	66.03.15	0.994 .141	86.39					

TABLE II. Journal of observations. Variable polarization.

HD	1/λ	Yr.Mo.Day	P%	± pe	θ
10516	1.06	66.08.22	0.822	.031	34.93
10516	1.06	66.08.29	0.812	.031	35.13
10516	1.06	66.12.09	0.902	.026	33.90
10516	1.06	67.01.02	0.843	.021	30.65
10516	1.21	66.08.15	0.676	.014	34.51
10516	1.21	66.08.22	0.744	025	36.52
10516	1.21	66.08.29	0.686	.019	38.23
10516	1.21	66.12.09	0.895	.021	39.11
10516	1.21	67.01.02	0.693	.016	34.47
10516	1.56	66.08.15	0.790	.093	41.85
10516	1.56	66.08.29	0.726	.019	45.46
10516	1.56	66.12.09	0.920	.017	45.02
10516	1.56	67.01.02	0.686	.018	39.94
10516	1.93	66.11.17	1.054	.011	41.98
10516	1.93	67.01.02	0.929	.019	42.59
10516	2.33	66.11.17	1.147	.007	41.33
10516	2.33	66.12.08	1.102	.019	40.79
10516	2.33	67.01.02	0.945	.015	42.11
10516	2.78	66.11.17	0.823	.012	50.13
10516	2.78	66.12.08	0.683	.018	53.67
10516	2.78	67.01.02	0.606	.021	59.54
10516	3.03	66.11.17	0.718	.017	59.81
10516	3.03	66.12.08	0.767	.044	65.75
10516	3.03	67.01.02	0.488	.035	70.36
35468	1.06	67.01.26	0.070	.012	74.21
35468	1.06	67.01.27	0.149	.068	82.89
35468	1.21	67.01.26	0.132	.006	79.49
35468	1.21	67.01.27	0.159	.014	81.30
35468	1.56	67.01.26	0.195	.008	74.58
35468	1.56	67.01.27	0.159	.010	75.74
35468	1.93	67.01.03	0.196	.015	85.23
35468	1.93	67.01.27	0.209	.011	79.10
35468	2.33	67.01.03	0.232	.022	82.69
35468	2.33	67.01.27	0.209	.009	76.36
35468	2.78	67.01.03	0.307	.022	73.07
35468	2.78	67.01.27	0.282	.014	68.80
35468	3.03	67.01.03	0.336	.033	68.41
35468	3.03	67.01.27	0.282	.014	70.39
37041	1.06	64.01.27	0.808	.067	94.01
37041	1.06	64.01.29	1.010	.081	103.98
37041	1.06	64.01.29	0.923	.049	94.17
37041	1.06	67.02.08	1.132	.043	104.22
37041	1.21	64.01.27	0.925	.067	108.47
37041	1.21	64.01.29	0.966	.058	101.41
37041	1.21	67.02.08	1.012	.025	100.11
37041	1.39	64.01.27	0.969	.054	85.39
37041	1.39	64.01.29	0.833	.063	94.41
37041	1.56	67.02.08	1.071	.043	100.84
37041	1.93	64.01.24	0.955	.067	106.10
37041	1.93	64.01.28	0.829	.031	105.42
37041	1.93	67.02.05	1.040	.010	91.30
37041	1.93	67.04.23	0.946	.027	98.06
37041	2.33	64.01.24	0.565	.018	98.69
37041	2.33	64.01.28	0.624	.040	104.38
37041	2.33	67.02.05	0.981	.006	86.78
37041	2.33	67.04.23	0.855	.019	9..91
37041	2.78	64.01.24	0.357	.045	79.11
37041	2.78	64.01.28	0.474	.094	102.26
37041	2.78	67.02.05	0.872	.015	81.90
37041	2.78	67.04.23	0.450	.064	84.58
37041	3.03	64.01.24	0.260	.030	
37041	3.03	64.01.28	0.447	.040	
37041	3.03	67.02.05	0.800	.034	79.44
37041	3.03	67.04.23	0.207	.134	78.67
37202	1.06	64.01.25	1.400	.054	30.43
37202	1.06	65.08.13	1.355	.027	
37202	1.21	64.01.25	1.260	.022	30.95
37202	1.21	65.09.21	1.056	.139	28.19
37202	1.21	67.04.22	1.276	.020	33.09
37202	1.39	64.01.25	1.210	.036	33.71
37202	1.39	65.09.21	1.213	.206	34.01
37202	1.56	67.04.22	1.368	.063	32.93
37202	1.93	64.01.26	1.437	.031	25.53
37202	1.93	64.01.28	1.512	.054	26.72
37202	1.93	66.12.09	1.517	.018	35.36
37202	2.33	64.01.26	1.522	.045	27.40
37202	2.33	64.01.28	1.542	.040	27.50
37202	2.33	66.12.09	1.684	.023	36.47
37202	2.33	67.04.22	1.536	.024	35.24
37202	2.78	64.01.26	0.952	.058	23.39
37202	2.78	64.01.28	0.997	.045	23.20
37202	2.78	65.08.13	1.080	.112	
37202	2.78	66.12.09	1.111	.015	40.62
37202	2.78	67.04.22	1.089	.050	29.36
37202	3.03	64.01.26	0.688	.081	18.16
37202	3.03	64.01.28	0.669	.063	17.24
37202	3.03	66.12.09	0.908	.052	41.63
37202	3.03	67.04.22	0.558	.025	35.00
169454	1.06	66.06.08	1.239	.032	9.23
169454	1.06	66.10.14	1.498	.045	13.92
169454	1.21	66.06.08	1.431	.025	10.34
169454	1.21	66.10.14	1.593	.028	14.05
169454	1.56	66.06.08	1.888	.025	16.33
169454	1.56	66.10.14	1.982	.047	18.13
169454	1.93	66.06.14	2.022	.029	17.04
169454	1.93	66.07.12	1.714	.021	13.58
169454	2.33	66.06.14	1.879	.015	16.90
169454	2.33	66.07.12	1.511	.020	16.41
169454	2.78	66.06.14	1.724	.040	14.45
169454	2.78	66.07.12	1.255	.104	20.30
169454	3.03	66.06.14	1.968	.087	21.92
181615	1.06	66.06.07	0.594	.033	163.19
181615	1.06	67.04.22	0.437	.023	173.85
181615	1.21	66.06.07	0.696	.010	163.06
181615	1.21	67.04.22	0.596	.014	174.84
181615	1.56	66.06.07	0.939	.021	164.82
181615	1.56	67.04.22	0.664	.020	171.17
181615	1.93	66.06.14	1.004	.026	168.20
181615	1.93	66.11.17	0.780	.015	170.70
181615	2.33	66.11.17	0.667	.038	173.63
181615	2.78	66.06.14	0.920	.015	171.79
181615	2.78	66.11.17	0.514	.019	179.15
181615	3.03	66.06.14	0.859	.034	171.03
181615	3.03	66.11.17	0.580	.040	188.56
197770	1.06	66.08.13	2.845	.109	131.35
197770	1.21	66.08.13	3.175	.038	130.65
197770	1.56	66.08.13	3.475	.039	129.71
197770	1.85	66.08.13	4.077	.044	131.04
197770	1.93	66.07.26	4.005	.011	130.17
197770	1.93	66.10.10	3.772	.016	130.02
197770	2.33	66.10.10	3.770	.013	129.18
197770	2.78	66.07.26	3.571	.027	131.80
197770	2.78	66.10.10	3.367	.019	128.55
197770	3.03	66.07.26	3.380	.035	130.02
197770	3.03	66.10.10	2.860	.089	128.36

to obtain a mean interstellar polarization curve. All stars in Figs. 3(a) to 3(e) except HD 6675, 35468, 37041, and 37202 have been used for this purpose.

In Table VII we list the results obtained by taking the weighted mean of the normalized polarizations for all stars at a given wavelength and the curve is plotted at the bottom of Fig. 3(e). The error bars there give the average probable error, which is a measure of the precision of determining polarization for a single star at the respective wavelength. It does not indicate the dispersion in interstellar polarization for various stars.

The mean curve shows the characteristic broad maximum centered at about 5200 Å with a sharper decrease at larger than at shorter wavelengths. We have also determined a separate mean interstellar polarization curve for stars with $P \geq 2\%$ and $P < 2\%$, respectively, at $1/\lambda = 1.93$. There is no significant difference between the two groups. It is to be noted,

however, that all of the stars in Figs. 3(a) to 3(d) which show marked peculiarities have polarizations less than 2%. We include among such stars the following: HD 6675, 25291, 25940, 35468, 37041, 37202, 37367, 40111.

Table VIII lists the residuals of the observed position angles from the weighted mean position angle (see Table V). In determining this mean, colons and semi-colons in Table IV are given half weight. Colons in Table VIII indicate probable errors greater than $\pm 3°$; semicolons indicate single observations. Exclamation marks (!) behind the HD number note stars for which there is an appreciable rotation of the plane of polarization with wavelength. The judgment that a star shows rotation is based both upon the probable errors and the smoothness of the variation of the residuals with wavelength.

5. Variable Polarizations

There is a growing problem in polarization studies as to whether the interstellar polarization is varying or whether all the variations which we observe are intrinsic to a star, stellar system, or circumstellar clouds. Intrinsic variations are now well established for various types of stars including the spectroscopic binary β Lyrae (Shakhovskoi 1964; Appenzeller 1965;

FIG. 3 (b). Same as for Fig. 3(a).
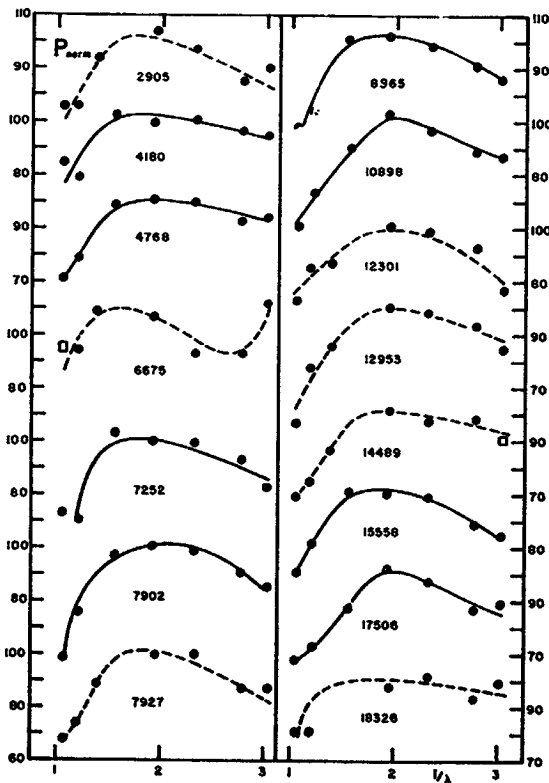
FIG. 3 (a). Normalized polarizations (see Sec. IV). Open circles are single observations; squares indicate that the probable error is greater than $\pm 8\%$. Dotted curves are for previous and solid curves for present observations.
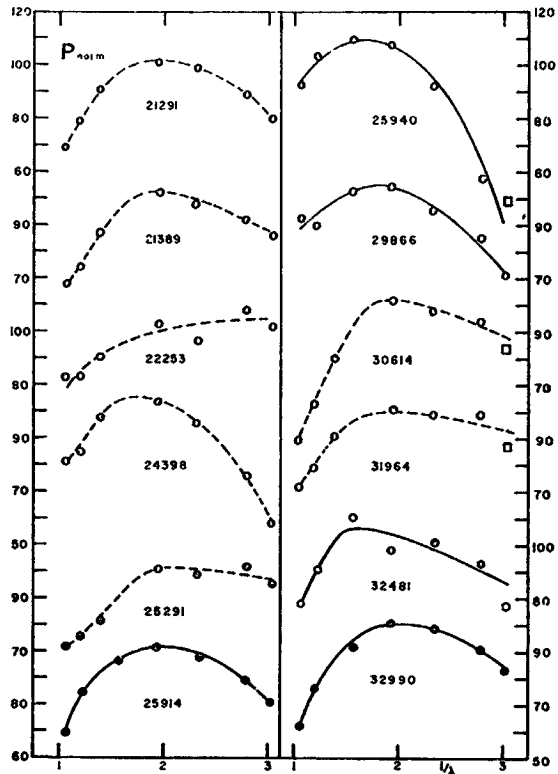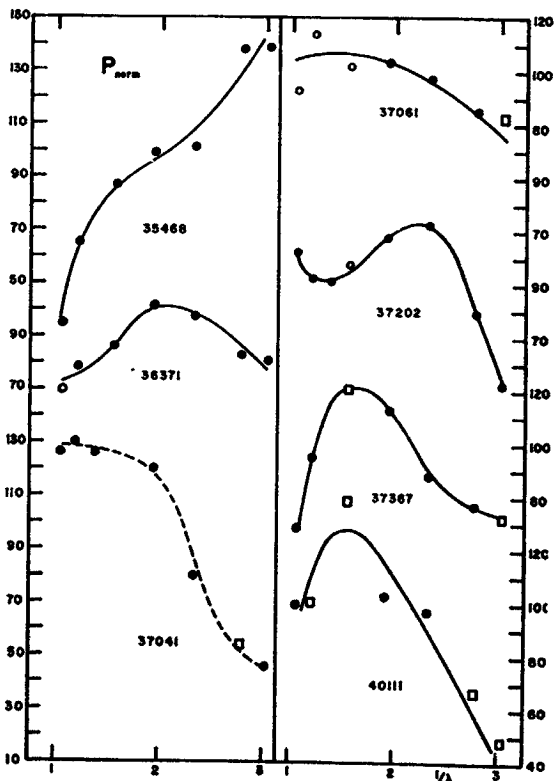
FIG. 3 (c). Same as for Fig. 3(a).
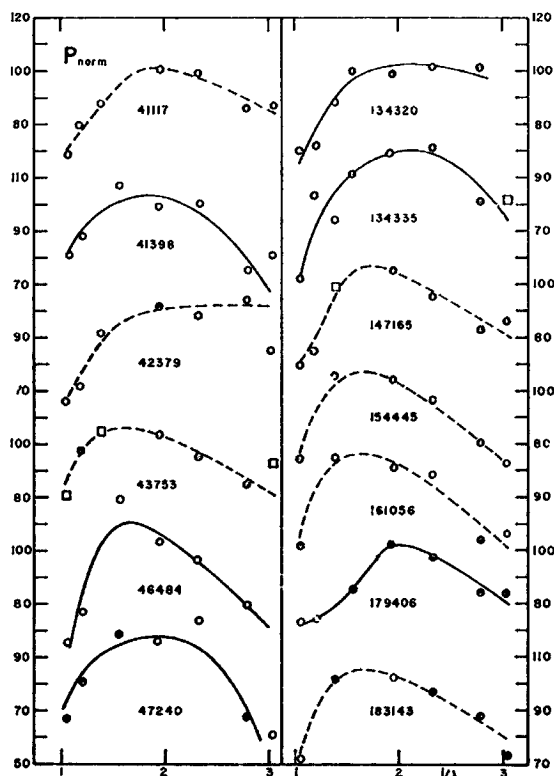
FIG. 3 (d). Same as for Fig. 3(a).
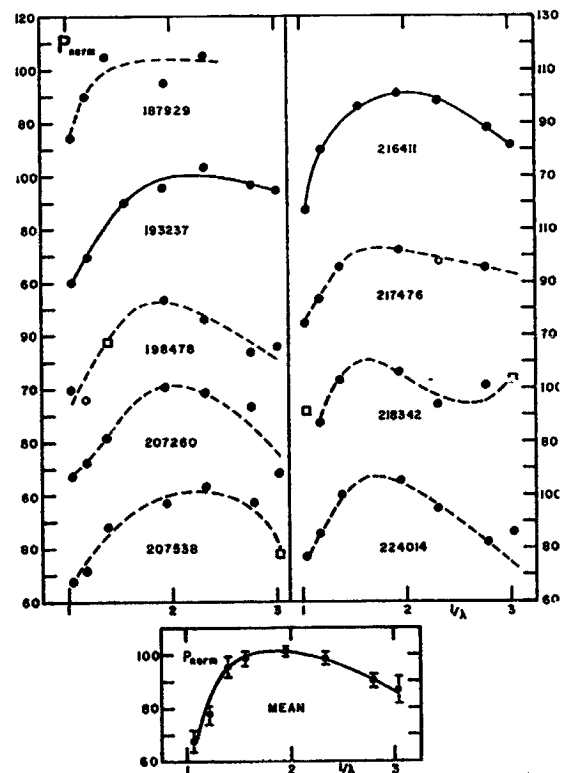
FIG. 3 (e). Same as for Fig. 3(a). Error bars on mean curve give the average probable errors.

TABLE III. Observed percentages of interstellar polarization. Weighted mean values.

HD	Percentage polarization observed at $1/\lambda =$						
	1.06	1.21	1.56	1.93	2.33	2.78	3.03
179406	0.99;	1.01;	1.15	1.38	1.32	1.14	1.13
134335[a]	0.35	0.55	0.60	0.66	0.67	0.54	0.55
134320[a]	0.43	0.44	0.61	0.60;	0.62	0.62	0.79:
193237	0.87	1.01	1.30	1.39	1.50	1.40	1.37
216411	1.51	2.12	2.55	2.67	2.61	2.34	2.16
4180	0.89	0.82	1.07	1.04	1.05	1.02	0.99
4768	1.68	1.88	2.35	2.39	2.37	2.21	2.24
7252	2.66:	2.58	3.76	3.76	3.63	3.39	3.02
7902	1.94	2.51	3.20	3.32	3.26	2.97	2.81:
8965	2.01	2.19	2.98	3.01	2.90	2.67	2.53
10898	2.72	3.27	4.04	4.60	4.31	3.94	3.87
15558	3.71	4.28	5.33	5.30	5.20	4.67	4.46
17506[a]	0.75	0.81	0.96	1.13	1.07	0.96	0.98
25914	3.15	3.86	4.39	4.63	4.48:	4.08	3.71
25940	0.68	0.77	0.81	0.80;	0.68	0.43	0.37
29866	1.56	1.52	1.73	1.76	1.61	1.43	1.20
36371	1.52;	1.65	1.80	2.23	2.14	1.81	1.78
37367	0.50	0.69	0.87:	0.82	0.64	0.56	0.52
32990	1.04	1.27	1.52	1.67	1.64	1.51	1.38
32481	1.47;	1.71;	2.06;	1.85	1.90	1.75	1.44;
41398	1.70;	1.85;	2.25;	2.08;	2.10;	1.57;	1.70;
40111	0.70	0.71	0.97	0.72	0.68	0.46	0.33
37202	...	1.28;	1.37;	1.52;	1.61	1.11	0.62
35468	0.07	0.14	0.18	0.21	0.21	0.29	0.29
46484	0.83;	0.98;	1.49;	1.29;	1.21;	0.99;	...
47240	0.70	0.84	1.03	1.00;	1.08;	0.70	0.63:
37061	1.37;	1.69;	1.51;	1.53	1.44	1.26	1.22:
37041	1.13;	1.01;	1.07;	1.03	0.97	...	...
83953	0.37	0.37	0.32	0.32;	0.58;	0.11;	0.11;

[a] These stars are K-type stars and the corresponding effective wave numbers are 1.05, 1.19, 1.54, 1.91, 2.29, 2.75, and 3.00 μ^{-1}.

TABLE IV. Observed position angles of interstellar polarization. Weighted mean values.

HD	Position angle observed at $1/\lambda =$						
	1.06	1.21	1.56	1.93	2.33	2.78	3.03
179406	177.2;	181.2;	182.3	183.7	184.6;	183.7;	187.0;
134335	90.1:	83.3	84.5	81.1	83.8	84.6:	78.2
134320	90.4	83.9	86.1	82.8;	91.2	87.4	85.3
193237	39.9	40.2	39.7	37.1	35.2	37.9	39.7
216411	45.2	47.8	46.6	49.0	49.6	48.3	51.5
4180	85.1	81.9	82.0	83.6	85.4	84.3	88.0
4768	87.5:	75.2:	80.7	82.5	81.1	80.4	78.1
7252	102.6:	99.0	96.2	97.4	98.1	97.9	99.6
7902	95.6	96.8	95.0	95.0	95.9	96.6	95.2
8965	100.4	105.9	103.5	105.1	104.2	103.6	104.8
10898	93.5	93.4	93.9	94.1	94.4	94.5	94.1
15558	121.8	121.2	119.3	120.2	120.6	118.9	115.6:
17506	118.6	118.3	112.6	114.6	111.5	115.0	116.6
25914	137.8	137.9	138.6	140.8	140.7	139.8	138.3
25940	171.2	170.9	170.4	169.4;	173.9	174.7	172.9
29866	12.6	10.2	10.5	9.7	11.2	12.8	13.9
36371	177.6;	179.6	181.1	175.9	175.2	171.0	168.9
37367	22.2	21.5:	24.0	24.6	22.2	26.1	21.7;
32990	86.9	86.2	84.3	84.3:	85.1	85.2	84.4
32481	91.3;	78.4;	80.0;	79.2	80.3	75.0:	83.3;
41398	162.8;	159.4;	162.8;	168.5;	167.7;	169.9;	163.8;
40111	169.2;	168.2:	168.8:	170.2	169.5	175.4	163.3
37202	...	33.1·	32.9;	35.4;	35.9	39.7	37.8
35468	75.2	79.9	74.9	80.0	77.4	70.2	70.0
46484	162.2;	174.2;	181.4;	175.3;	177.4;	179.0;	...
47240	173.1	177.2	172.7	172.5;	172.7;	180.7	176.1;
37061	62.6;	57.3;	63.8;	66.0	67.9	69.3	72.5
37041	104.2;	100.1;	100.8;	92.0	85.6;	82.4	79.2
83953	174.8	172.7	177.7	183.0;	167.2:	...	...

TABLE V: Various data on the stars observed in this program.

HD	Name	Galactic long	Galactic lat	Sp	V	B−V	E_{B-V}	R	Phot.	Par.	Rel.[a]	P_{vis}	θ̄	Remarks[b]
169454	−14°5039	18°	0°	B1Ia+	6.61	+0.94	1.16	3.6	0.7:	···		···	15.5	
181615	υ Sgr	22	−14	A pep	4.61	+0.10	···	3.6	···	···		···	169.0	Sp. bin. Var.
179406	20 Aql	28	− 8	B3IV	5.4	···	···	3.6				1%28	182.91	Var.?
134335	BS 5640	38	+59	gK1	5.83	+1.21	0.11	3.6	0.3:	···		0.64	83.0	
134320	46 Boo	39	+60	gK2	5.68	+1.24	0.08	3.6	0.3:	···		0.61	87.0	
193237	P Cyg	76	+ 1	Bp	4.80	+0.41	···	3.6	···	1.0	f	1.40	38.5	Shell, Nova 1600
197770	BS 7940	94	+ 9	B2IV	6.32	+0.33	0.57	4.2	0.3	···	n	···	130.1	
216411	+58°2492	108	− 2	B1Ia	7.20	+0.60	0.82	4.9	0.9	···	f	2.61	48.31	
4180	o Cas	122	−15	B2V	4.50	−0.06	0.18	5.4	0.2	···	n	1.05	84.0	
4768	+58°119	123	− 3	B5Ib	7.57	+0.38	0.48	5.4	1.4	···	f	2.37	80.7	
7252	+60°188	126	− 3	B1V	7.12	+0.09	0.35	5.5	0.6	···	f	3.68	98.4	
7902	+57°257	127	− 5	B6Ib	6.93	+0.40	0.48	5.5	1.0	···	f	3.26	95.7	
8965	+59°260	128	− 2	B0.5V	7.28	+0.02	0.30	5.6	1.0	···	f	2.96	104.0	
10898	+57°399	131	− 4	B2Ib	7.40	+0.35	0.53	5.6	1.1	···	f	4.32	94.0	
10516	φ Per	131	−11	B1III? pe	4.06	−0.04	···	5.6	···	0.06	n	···	44.41	Sp. bin. Var.
15558	+60°502	135	+ 2	O6	7.81	+0.52	0.84	5.8	0.5	···		5.28	120.0!	
17506	η Per	139	− 3	K3Ib	3.79	+1.69	0.31	5.8	0.2	0.25	n	1.05	115.3	
25914	+56°884	147	+ 3	B6Ia	7.99	+0.60	0.68	6.0	1.5	···	f	4.50	139.1	
25940	48 Per	153	− 3	B3V pe	4.04	−0.06	0.14:	6.0	0.1:	0.07	n	0.76	172.11	Var.?
29866	BS 1500	163	− 3	B7? e	6.06	+0.10	···	6.1	···	···		1.70	11.5	
36371	χ Aur	176	+ 1	B5Iab	4.77	+0.35	0.45	6.1	0.5	···		2.06	175.51	Sp. bin.
37367	BS 1924	179	− 1	B2V	5.95	···	···	6.0	···	···		0.76	23.2	Sp. bin.
32990	103 Tau	179	−10	B2V	5.41	···	···	6.0	···	···		1.61	85.3	Sp. bin.
32481	+21°754	181	−13		8.10	···	···	6.0	···	···		1.91	80.8	
41398	+28°1008	182	+ 3	B2Ib	7.46	+0.32	0.50	6.0	1.1	···	f	2.14	165.0	
40111	139 Tau	184	+ 1	B1Ib	4.83	−0.07	0.15	6.0	0.9	···		0.79	169.3	
37202	ζ Tau	186	− 6	B2IV p	3.03	−0.18	0.06:	5.9	0.2:	neg		1.53	35.81	Sp. bin. Var? Shell
35468	γ Ori	197	−16	B2III	1.63	−0.21	0.03	5.6	0.1	0.04	n	0.20	75.41	Var.?
46484	+04°1319	207	− 4	B1V	7.74	+0.36	0.62	5.2	0.4	···		1.33	174.9	
47240	BS 2432	207	+ 1	B1Ib	6.15	+0.14	0.36	5.2	1.0	···		1.04	175.6	
37061	−05°1325	209	−15	B1V	6.80	+0.27	0.53	5.2	0.3	···		1.49	66.81	
37041	θ² Ori	209	−19	O9.5V p	5.07	−0.08	0.22:	5.2	0.6	neg		1.01	89.81	Var.? Sp. bin.
83953	BS 3858	256	+22	B2 pe	4.78	−0.12	···	···	···	···		0.39	175.1	

[a] In the relative distance column, near stands for 0.1-0.3 kpc and far for 0.6-1.5 kpc.
[b] In the position angle column, an exclamation mark (!) indicates wavelength dependence of position angle.

TABLE VI. Normalized polarizations.

HD	Normalized percentage polarization at 1/λ =						
	1.06	1.21	1.56	1.93	2.33	2.78	3.03
179406	73.5;	74.4;	85.0	102.3	97.7	84.2	83.4
134335	52.0	82.9	90.4	99.1	100.9	80.3	81.8:
134320	69.8	71.6	99.3	98.5	101.5	100.7	129.1:
193237	60.0	69.9	90.0	96.4	103.6	96.6	94.8
216411	57.2	80.2	96.6	101.1	98.9	88.8	81.8
4180	84.5	78.5	102.2	99.5	100.5	96.9	94.4
4768	70.4	78.9	98.5	100.4	99.6	92.7	94.1
7252	73.3	70.9	103.4	100.1	99.9	93.4	83.1
7902	58.8	76.3	97.2	101.0	99.0	90.6	85.5
8965	67.9	74.2	100.8	101.8	98.2	90.4	85.5
10898	61.1	73.4	90.6	103.3	96.7	88.4	86.9
15558	70.7	81.5	101.4	100.9	99.1	88.9	84.9
17506	68.0	73.8	87.7	102.8	97.2	87.0	89.6
25914	69.2	84.9	96.3	101.6	98.4	89.6	81.6
25940	92.4	103.5	109.9	107.7	92.3;	57.7	49.6:
29866	92.8	90.0	102.8	104.6	95.4	84.9	71.2
36371	69.6;	75.4	82.5	102.1	97.9	82.8	81.5
37367	68.8	95.0	120.1:	112.4	87.6	77.0:	71.9:
32990	62.6	76.8	92.0	101.0	99.0	91.3	83.4
32481	78.6;	91.1;	110.0;	98.6	101.4	93.2	77.1;
41398	81.3;	88.6;	107.4;	99.6;	100.4;	74.9;	81.2;
40111	99.9	100.5;	138.4:	102.8	97.2	66.0:	47.5:
37202	···	82.8;	87.5;	97.1;	102.9	70.9	39.6
35468	34.4	64.9	86.4	98.8	101.2	137.9	138.4
46484	66.1;	78.3;	119.6;	103.4;	96.6;	79.3;	···
47240	67.9	81.4	99.8	96.1;	103.9;	67.7;	60.9;
37061	92.4;	113.8;	101.8;	103.0	97.0	85.3	82.1:
37041	113.0;	101.0;	107.0;	103.0	97.0	···	···
83953	82.2;	82.8;	71.1;	71.5;	128.5;	25.2;	23.3:

TABLE VII. Mean interstellar polarization.*

1/λ	No. of Stars	Mean Norm. Pol.	Average Prob. Error
1.06	52	68%	3%
1.21	49	78	3
1.39	27	96	3
1.56	25	99	2
1.93	52	101	2
2.33	52	98	2
2.78	51	90	3
3.03	50	87	5

* All stars of Table X in Paper VIII and of the present Table VI except HD 6675, 24431, 35468, 37041, 37202, 83953, 193443, and 206936.

Belton and Woolf 1965; Serkowski 1965; Rucinski 1966), the irregular red variable μ Cephei (Grigoryan 1959; Coyne and Gehrels 1966; Serkowski 1966), and various Mira type variables (Serkowski 1966).

Tables IX and X list the difference of our observations made during 1966-1967, with those of other observers extending from 1949 to 1965. The second column in each of these tables lists the difference between our observations at 1/λ=2.33 and those of Hall (1958); the third column lists the difference between our observations at 1/λ=1.93 and Hiltner (1956); the

TABLE VIII. Residuals of position angles.

HD*	Observed minus mean for each star at 1/λ=						
	1.06	1.21	1.56	1.93	2.33	2.78	3.03
179406!	- 6°;	- 2°;	0°	+1°	+2°;	+1;°	+ 4°;
134335	+ 7:	0	+ 1	-2	+1	+2:	- 5
134320	+ 3	- 3	- 1	-4;	+4	0	- 2
193237	+ 1	+ 2	+ 1	-1	-3	-1	+ 1
216411!	- 3	0	- 2	+1	+1	0	+ 3
4180	+ 1	- 2	- 2	0	+1	0	+ 4
4768	+ 7:	- 5:	0	+2	0	0	- 3
7252	+ 4:	+ 1	- 2	-1	0	0	+ 1
7902	0	+ 1	- 1	-1	0	+1	0
8965	- 4	+ 2	0	+1	0	0	+ 1
10898	0	- 1	0	0	0	+1	0
15558!	+ 2	+ 1	- 1	0	+1	-1	- 4:
17506	+ 3	+ 3	- 3	-1	-4	0	+ 1
25914	- 1	- 1	- 1	+2	+2	+1	- 1
25940!	- 1	- 1	- 2	-3;	+1	+3	+ 1
29866	+ 1	- 1	- 1	-2	0	+1	+ 2
36371!	+ 2;	+ 4	+ 6	0	0	-4	- 7
37367	- 1	- 2:	+ 1	+1	-1	+3	- 2;
32990	+ 2	+ 1	- 1	-1:	0	0	- 1
32481	+11;	- 2;	- 1;	-2	0	-6:	+ 3;
41398	- 2;	- 6;	- 2;	+4;	+3;	+5;	- 1;
40111	0:	- 1:	- 1:	+1	0	+6	- 6
372021	...	- 3;	- 3;	0;	0	+4	+ 2
35468!	0	+ 5	0	+5	+2	-5	- 5
46484	-13;	- 1;	+ 6;	0;	+2;	+4;	...
47240	- 2	+ 2	- 3	--3;	-3;	+5	+ 1;
370611	- 4;	-10;	- 3;	-1	+1	+2	+ 6
370411	+14;	+10;	+11;	+2	-4:	-7	-11
83953	0	- 2	+ 2	+8;	-8:	...	...

* Stars with exclamation marks (!) show appreciable wavelength dependence of position angles.

TABLE IX. Our percentage polarization minus that of other observers.

HD	Hall 1949–54	Hiltner 1949–54	Behr 1956–58	Serkowski 1960–65
179406	-0.38%	...	...	...
134335	...	...	+0.05%	...
134320	...	...	-0.03	...
193237	+0.26	+0.33%	...	...
216411	-0.06	-0.05	...	+0.02%
4180	-0.01	...	+0.29	...
4768	+0.30	+0.14	...	...
7252	+0.50	+0.05	...	+0.10
7902	(-0.93)	+0.33	...	+0.30
8965	-0.14	+0.16	...	+0.10
10898	(+0.63)	(+0.69)	...	...
15558	-0.10	+0.23	...	+0.02
17506	+0.15	...	...	...
25914	(-0.95)	-0.07	...	-0.16
25940	-0.47	...	-0.21	...
29866	-0.37	...	...	...
36371	-0.44	...	+0.20	+0.06
37367	-0.33	...	...	...
32990	+0.30	...	...	...
32481	+0.01	...	...	...
41398	-0.57	-0.14	...	...
37202	+0.27	...	...	...
40111	-0.47	-0.34	...	...
35468	-0.43	...	+0.03	...
46484	-0.17	-0.09	...	...
47240	-0.44	-0.06	...	...
37061	+0.01	...	...	...
37041	+0.28	...	...	...
83953	-0.20	...	...	...
Syst. Diff.	-0.10	+0.04	+0.06	+0.09
Mean Res.	0.28	0.17	0.14	0.11

fourth column gives the difference between the weighted means of our observations at $1/\lambda=1.93$ and $1/\lambda=2.33$ with those of Behr (1956); and the last column gives the average of the differences between our observations at $1/\lambda=1.93$, 2.33, and 2.78 with Serkowski's green, blue, and ultraviolet filters, respectively. The Serkowski observations were supplied to us directly by the author, corrections being applied in the same way as described in Sec. III of Paper VIII (see references there). At the bottom of each table the systematic difference is the straight average, and the mean residual the average of the absolute value, of the residuals exclusive of those in parentheses.

In Table X, with the exception of HD 35468 there are no significant residuals. Large residuals in Table IX for HD 7902, 10898, and 25914 may indicate variations in percentage of polarization. All three of these stars have large polarizations (greater than 3%) and they are relatively distant.

We now discuss the polarimetric observations of the B2III star, γ Orionis (HD 35468). In Table X, the residuals of the position angle in both the Hall and Behr columns are remarkably large (of the order of 50°) and similar. Our determination of θ is the result of measurements at seven independent wavelengths

made on three different nights (see Table II). The largest probable error for the combined value at a single wavelength is ±1.9°. For a total of ten other stars observed on three different nights on which we observed γ Orionis the mean absolute residual in position angle, Coyne-Hall, is ±4°. It appears that either the plane of polarization of γ Orionis has rotated or that we or Hall and Behr are in error by some 50° for γ Orionis. There also appears to be a dependence of θ on wavelength (see Table VIII) and a monotonically increasing polarization with decreasing wavelength [see Tables III and VI, and Fig. 3(c)]. Although the percentage of polarization is small with a maximum of 0.3% at $1/\lambda=3.03$, the average probable error of the combined observations from two different nights is also small, ±0.01%. The remarkable wavelength dependence of the percentage of polarization depicted in Fig. 3(c), which suggests a small mean particle size for the scatterer, as well as the indications of a rotation of the plane of polarization with wavelength and time, suggest γ Orionis as a candidate for more detailed observations, especially in the far ultraviolet.

For the spectroscopic binary and shell star, ζ Tau (HD 37202) we find no change in the percentage

TABLE X. Our position angle minus that of other observers.

HD	Hall 1949–54	Hiltner 1949–54	Behr 1956–58	Serkowski 1960–65
179406	− 1°	...	...	...
134335	...	...	+ 4°	...
134320	...	...	+ 6	...
193237	+ 9	+ 2°	...	...
216411	+ 2	+ 4	...	+ 3°
4180	0	...	+ 1	...
4768	− 2	− 4	...	...
7252	− 1	− 1	...	0
7902	− 1	0	...	0
8965	+ 1	+ 2	...	− 1
10898	− 3	− 1	...	...
15558	− 1	0	...	...
17506	− 4	...	...	...
25914	+ 1	− 3	...	...
25940	− 2	...	− 1	...
29866	+ 5	...	...	...
36371	0	...	+ 2	0
37367	+10	...	...	...
32990	− 3	...	...	...
32481	+ 6	...	...	...
41398	− 1	+ 2	...	...
40111	− 8	+ 6	...	...
37202	+13	...	...	...
35468	(+56)	...	(+46)	...
46484	+11	+11	...	...
47240	+ 1	+ 2	...	...
37061	+ 2	...	...	...
37041	−16	...	...	...
83953	− 1	...	...	...
Syst. Diff.	+ 0.7	+ 1.5	+ 2.4	+ 0.4
Mean Res.	4.0	2.9	2.8	+ 0.8

polarization between 1964 and 1967. There is, however, a change in the position angle. The mean angle for the 1964–65 observation is 26°8; for the 1967 observations it is 35°8. For both epochs there appears to be a rotation of position angle with wavelength of the order of 5° to 10°. The rotation, however, is in the opposite sense for the two epochs, such that the difference in the position angle at $1/\lambda = 3.03$ between the two epochs is 20°.

We have checked the internal consistency of the position angles for both the 1964–65 and the 1967 observations by intercomparisons of observations on other stars and planets observed on the different nights during each of the two observing runs when HD 37202 was observed. There appear to be no systematic effects.

In Table II, in addition to HD 35468 and HD 37202 for five other stars suspected of variability in polarization the individual observations are given. Four of these stars are spectroscopic binaries. HD 10516 (φ Persei) is of particular interest since its period is 127 days and the variations in the percentage polarization are of the order of 0.2%±0.02 occurring over a period of about 4 months. Furthermore, there is a rotation of the plane of polarization with wavelength of the order of 30°. Likewise HD 37041 (θ^2 Orionis), a spectroscopic binary with a period of 21 days, has a variation in the ultraviolet polarization of 0.5%±0.04 and a rotation of the plane of polarization with wavelength of the order of 20°.

REFERENCES

Appenzeller, I. 1965, *Astrophys. J.* 141, 1390.
Behr, A. 1956, *Nachr. Akad. Wiss. Göttingen*, II. *Math.-Phys. Kl.*, No. 7, 185; *Veröff. Göttingen*, No. 126.
Belton, M. J. S., and Woolf, N. J. 1965, *Astrophys. J.* 141, 145.
Coyne, G. V., and Gehrels, T. 1966, *Astron. J.* 71, 355 (Paper VIII).
Gehrels, T. 1960, *ibid.* 65, 470 (Paper II).
Gehrels, T., and Meltzer, A. S. 1966, *ibid.* 71, 111 (Paper VII).
Gehrels, T., and Teska, T. M. 1960, *Publ. Astron. Soc. Pacific* 72, 115.
Grigoryan, K. A. 1959, *Soobshch. Byuranskoi Obs.* 2¹, 43.
Hall, J. S. 1958, *Publ. U. S. Naval Obs.* 17, Part VI.
Hall, J. S., and Serkowski, K. 1963, in *Basic Astronomical Data*, Vol. 3 of *Stars and Stellar Systems*, K. Aa. Strand, Ed. (University of Chicago Press, Chicago), p. 296.
Hiltner, W. 1956, *Astrophys. J. Suppl.* 2, 389.
Lec, T. 1966, Doctoral dissertation, University of Arizona.
Rucinski, S. H. 1966, *Acta Astron.* 16, 127.
Serkowski, K. 1965, *Astrophys. J.* 142, 793.
——. 1966, *ibid.* 144, 857; also, *I.A.U. Inf. Bull. Var. Stars*, No. 141.
Shakhovskoi, N. M. 1964, *Astron. Zh.* 41, 1042 (English transl.: *Soviet Astron.—AJ* 8, 833).

No. 107 AN AUTOMATIC POLARIMETER FOR SPACE APPLICATIONS*

by S. F. Pellicori and P. R. Gray

December 22, 1966

ABSTRACT

Under a NASA contract, a compact automatic polarimeter was developed as a pilot model for lunar and planetary missions by spacecraft. The polarimeter simultaneously analyzes linearly polarized light into four intensities from which the Stokes parameters I, Q, and U can be determined. The measurements are made automatically by an electronic observation sequencer and an automatic gain selector. Five wavelength bands between 1900 A and 6000 A can be used, and each measurement is calibrated automatically. The successful operation during three high altitude balloon flights indicates that the design is sound, and that with modifications for rocket vibration it can be used in space missions. The feature of making simultaneous measurements makes it particularly useful on planetary scans with fly-by probes. Preliminary results on the wavelength dependence of the polarization of the whole lunar disk, obtained ground-based, between 2850 A and 5100 A are presented.

1. Introduction

Under a contract for the "Development and Testing of a Photopolarimeter for Space Vehicles", an automatic instrument was designed and constructed as a pilot model for scans of planetary disks on fly-by missions such as Mariner and Voyager. It would also be useful for lunar surface studies by Apollo.

The need for a small portable polarimeter for unmanned and manned space missions has been discussed.[1] The advantages of being able to do polarimetry from space vehicles are that a large range of phase angles is possible, and that individual areas of a planetary surface can be investigated.

As a means of testing the design in severe and changing environments, the polarimeter has been operated in several environmental chambers. It has also made three high altitude (35-km) nighttime and daytime balloon flights. Telemetry records show that the instrument performed nearly flawlessly on all three flights. Tests during the development and actual flights were important in testing components for the Polariscope balloon program.[1]

Between balloon flights, the instrument is used in a program in which the polarization–phase curve of the whole moon is observed during a complete lunation over a range of wavelengths 3200–6000 A.

2. Design Specifications

The design specifications for space flight hardware are closely approximated by those for balloon-borne equip-

ment. The obvious difference is that space flight equipment must be able to withstand severe vibration and shock and high vacuum. The polarimeter does withstand the parachute opening and landing shocks (~ 7 G) without damage. The limitations on weight, size, severe temperature profile, low ambient pressure, minimum number of ground commands, and low power consumption were observed as much as possible in this pilot model. Advantages of speed, simultaneity of measurements, and the redundancy available are discussed in Secs. III and VI.

The chassis was constructed mostly of magnesium, and the present model weighs a total of 17 kg. Existing electronic components were used, thus enabling the design-to-hardware-stage time to be short. In a space flight version the electronic module cans will be replaced by integrated circuit logic, thus reducing the weight and size of the instrument. The size is now 57 cm $\times$ 32 cm $\times$ 17 cm with 15-cm long telescope tubes. It is estimated that the volume could be reduced to one-third with microminiature electronics.

The temperature range over which the instrument is tested is from $+40°C$ to $-70°C$. The altitude range is from sea level to 40 km. No difficulties in the performance of the polarimeter are encountered between these environmental extremes. The ceiling pressure is not too important for problems such as outgassing and vacuum welding, which are of concern in the high vacuum of space; but it is critical for the possibility of coronal discharge from voltages greater than 200 V. In fact, many of the eight or so environmental tests during the developmental stages showed corona problems from either the high voltage supplies or the photomultiplier tubes.
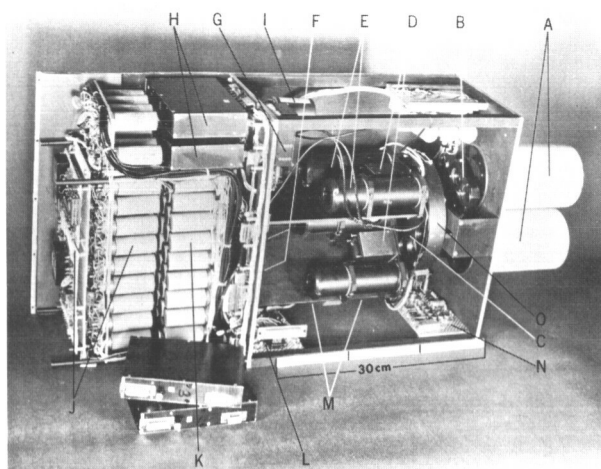
Fig. 1. Polarimeter with sides removed. A: telescopes, B: depolarizer arm, C: filter wheel, D: Wollaston prisms, E: photomultipliers (caps on PM tubes hold nickel sulfate hexahydrate crystals used for filtering), F: Fabry mirrors (not visible), G: integrator power supply, H: integrators, I: 1-/oscillator, J: gain select logic, K: sequencing logic, L: high voltage selector relays, M: high voltage power supplies (not visible), N: voltage reference supply, O: mounting for filter position indication.

To increase the versatility of the present prototype on balloon flights, it was not made completely automatic. The high voltage selection, integration time selection, and a *start* after each filter cycle are required commands from the ground.

The electronics are completely solid state; therefore, there is essentially no warm-up time, and measurements can begin as soon as the PM tubes have recovered from the initial high voltage application. The power consumption is presently 25 W, but with microminiature electronics this can be reduced to about 6 W. The battery voltages ($+12$ V and -12 V) can vary by $\pm 12\%$ without affecting the operation of the instrument. Typical precision on bright objects is better than ± 0.04 in percentage polarization.

3. Optics Section

Figure 1 shows the polarimeter, with one side removed and two integrators unplugged. The instrument is divided into the optics and the electronics sections by the vertical partition. The front face, including telescopes and filter wheel mounting, can be separated from the main body which holds the PM tubes and electronics plugs. The logic-module decks can also be separated from the main body.

The optical configuration is shown diagrammatically in Fig. 2. There are two such optical trains mounted at 45° to each other, and otherwise optically completely independent of each other. By comparing Figs. 1 and 2, the path that the light takes can be traced.

Light is collected by two $f/8$ Cassegrain-type telescopes (7.5-cm-diam primary). The mirrors are aluminized in such a way that their polarizing properties are negligible, and overcoated with a $\lambda/2$ (at 2250 Å) coating

of magnesium fluoride to protect the aluminum from the atmosphere. The glow discharge and aluminization are done normal and symmetrical to the mirror surface.

The beams pass first through the Lyot depolarizers which are used to calibrate each observation. They are constructed of two disks of birefringent magnesium fluoride crystal, cut parallel to the optical axis, the first disk having twice the retardation of the second. The two disks are aligned with the axes precisely at 45° to each other. The effect on a wide band of light is that different wavelengths in the band emerge with different polarization forms, i.e, linear, elliptical, circular, at many azimuth angles. As a result of the blending of these many polarization forms, polarized light cannot be distinguished from unpolarized light. Magnesium fluoride is used because it has higher transmission below 2500 Å than quartz. The depolarizers are automatically put into and out of the beams in a systematic sequence (Sec. IV) for each measurement. This nearly simultaneous calibration allows for possible drifts in the photometers between pairs of integrations. The intensities are kept nearly equal (except for polarization) by the use of amorphous silica equalizer disks in the beams when the depolarizer is out. This minimizes the light hysteresis which is present in some tubes (notably ASCOP 541F-08 and 05 and RCA 7102). This effect is that an appreciable time (up to 30 sec) is required for the signal to decay if light is removed from the tube, and conversely, to reach a final value if light is put onto a tube that has been dark.

Following the depolarizer, light passes through one of the five filters in the filter wheel. The filters are mounted in five pairs, each pair being identical and opposite on the filter wheel, so that the same wavelength band is observed by both telescopes simultaneously. At the end of a cycle of five filters the filter wheel signals the logical sequencer to *hold* (Sec. IV). Readout of positions is accomplished by the closing of glass magnetic-reed switches by magnets mounted on the moving depolarizer arm and filter wheel. The filter wheel and depolarizer arm are moved by pulsed stepping motors.

To satisfy the lack of acceptable filters for the 2000–3000 Å region, a set of narrow band filters was developed. The filters are described elsewhere[2], and meet the requirements of good rejection outside the passband, stability to low temperatures, low pressure, and uv radiation, and high transmission with bandwidths of 225–250 Å. After passing through identical filters, each light beam comes to a focus at its respective focal plane diaphragm, which is also the entrance end of the prism cells (see Fig. 2). The field of each telescope can be made as large as 1°3 diam in order to include the lunar disk and allowing for errors in guiding.

The entrance window of each Wollaston prism is a plano-convex fused silica lens which has the function of making the primary mirror appear to be infinitely distant. Through the use of this lens the large angles that rays from the edge of the primary mirror have (up to 5°) are accommodated. This allows the use of a smaller prism and a small prism interface angle without excessive reflection loss and without approaching inter-
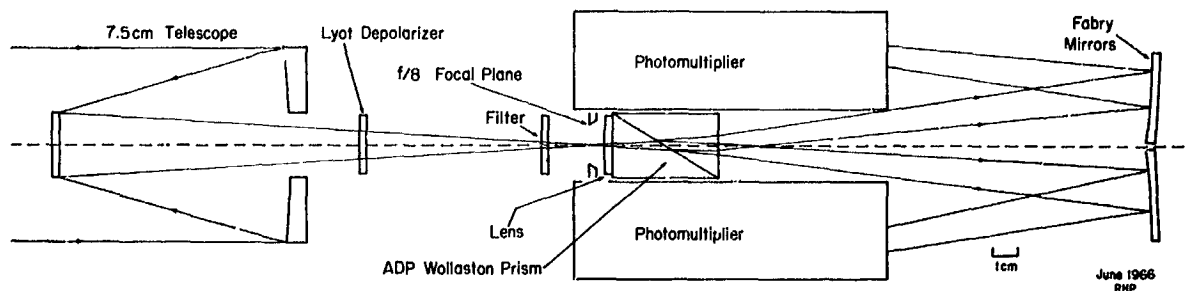
Fig. 2. Optical train of polarimeter.

nal reflection. This lens, and a plano exit window of fused silica, protect the prism from the atmosphere.

The Wollaston prism is constructed of crystalline ammonium dihydrogen phosphate (ADP). ADP is used because it has high transmission in the uv (40% at 2000 Å for 43 mm thickness[3]), but especially because of its high birefringence (0.054 at 2537 Å).[4] The crystal is water soluble and soft, and a technique of polishing surfaces flat was, therefore, developed by E. J. Plamondon and R. L. Waland of the Lunar and Planetary Laboratory Optical Shop. Preliminary polishing is done on paper toweling with a 50% mixture of Cr_2O_3 and cornstarch using Dow Corning 200 Silicone Fluid with a 5-cS viscosity as the lubricant. Paper has less drag than the usual honeycomb foundation, so it has a smaller tendency to pull out chips of ADP. Final polishing is done with a honeycomb foundation on the normal pitch lap. The above polishing materials are used with a circular stroke. The flatness normally obtainable is 1 λ over a surface, but with longer polishing times ¼ λ flatness can be obtained.

ADP is susceptible to fracture from thermal shocks. However, after more than a dozen environmental tests and four actual flights, there has been no fracture of such a prism due to careful mounting. Our prisms are mounted in aluminum cells with the entrance face mechanically held perpendicular to the incident beam and the exit face located and held in contact with the ADP by four springs on the back end of the cell. The prism halves are mounted in the cell in a semikinematic manner, and are held against small pads of silicone rubber by pressure from the springs. For optical coupling we use a thin film of Dow Corning 200 Silicone Fluid which has high transmission[3] and the proper refractive index[5] for our optical materials.

The Wollaston prism analyzes the incoming light into two orthogonally and completely linearly polarized beams, and deviates them so they strike the Fabry mirrors. The purpose of the Fabry mirrors is to image the primary mirror on the cathode of the associated photomultiplier and thus eliminate the motion of the image on the cathode as the guiding in the diaphragm varies. Investigations made in the laboratory showed that the sensitivity of the cathodes of some types of tubes can vary as much as 20% from one area to the next.

The photomultipliers originally used for the balloon flights had CsTe cathodes (solar blind) with response

from 2900 Å to below 2000 Å. At first EMR-541F were flown, and later the less expensive RCA C-31005. Recently, CsSb (S-13) cathodes (EMI 9526B) were substituted in order to extend the wavelength region to 6000 Å to 1900 Å total. The tubes have 17% quantum efficiency (cf. 9% for the CsTe), but they have appreciable dark current for faint objects unless cooled.

The Silastic potting of the cathode electrode on the first tubes failed, causing corona in an environmental test. This was repaired with silicone rubber. Considerable experience has been gained in potting the RCA and EMI photomultipliers for the balloon environment while at the same time not adding appreciable leakage current between the high voltage and the signal electrodes. High voltage corona problems are more critical for balloon altitudes (pressure ~4 mb) than for the space environment.

Because individual tubes of a specific type can vary greatly in cathode sensitivity and multiplier gain unless specially selected, the four tubes are matched to each other in total response to unpolarized light of a chosen wavelength by adjusting their multiplier gains. This is done to make the tubes give comparable output levels except, of course, for appreciably polarized light.

The optical configuration for each telescope is identical as mentioned previously, but one prism is at 45° to the other. The reason for this is to provide simultaneous observations of the components of the Stokes parameters for linearly polarized light. This allows a solution for the magnitude and azimuth of the polarization vector at a given wavelength with one observation. This feature fills the need for fast measurements such as would be necessary on a planetary scan with a fly-by probe. Another advantage is that the need to rotate large assemblies (the Wollaston and all of the optical train following it) is avoided; thus, the questionable reliability of precisely moving such an assembly in the space environment is eliminated. In addition, simultaneous photometry at the given wavelength can be obtained.

4. Electronics Section

The polarimeter electronic system consists of four photomultiplier tubes, four current integrators, two programmable high voltage power supplies, an automatic sequencer, and an automatic gain selector (plus

corresponds to a function, e.g., *set gain*, *integrate*, *read*, etc. When the clock is triggered into a state by a pulse from a 1-c/s oscillator, the function corresponding to that state is initiated, and further pulses are prevented from triggering the clock until the function is completed. A pulse is then gated to the counter and it goes on to the next state, starting the next function.

The sequence begins in the *home* state of the counter with the depolarizer out of the beam and the filter wheel in its starting position. A start command from the ground gates a pulse to the counter, causing it to go to the *set gain* state. The gain selector makes a series of trial integrations, each 1 sec long, on the light signal entering the telescopes. The first trial integration is made with the integrator gain at its least sensitive value. The resulting integrator outputs are compared with a fixed reference; if they are less than this reference, the value of gain is too low to give an on-scale readout, and the integrators are set to the next, more sensitive, gain value and another trial integration is made. This process is repeated until one of the nine gain values yields an output voltage at least as large as the fixed reference, but not large enough to cause any of the integrator outputs to be off-scale. This value of gain is selected, and a *gain is set* signal is sent to the counter.

When the gain is set another pulse is gated to the counter, causing it to go to the third state. This causes the first integration to be carried out. A second counter, driven by the precise 1-c/s clock, times the integration - either 7 sec, 15 sec, or 31 sec as selected from the ground. For spacecraft use, command requirements could be simplified with a scheme of not using fixed integration times but integrating until one of the four integrators reaches full scale, and then terminates the integration.

When this operation is complete, another pulse is gated to the counter, and the *read cycle* begins. This is a 15-sec interval during which the data are held at the outputs of the integrators so they can be recorded on the ground three times (Sec. V).

After the read cycle, two pulses are gated to the counter. The first puts the counter in the *depolarizer in* state, causing the depolarizer to be put into the light path, and the next pulse—1 sec later—moves the counter to the second integration. This is carried out exactly like the first integration, and at the same gain, and a second read cycle follows it. The eighth and last counter state, following the second read cycle, causes the depolarizer to be put out of the beam and the filter wheel to be advanced. The complete set of two integrations at one filter occupies about 1 min of time for 7-sec integration times with the 15-sec readout times. The next pulse from the clock puts the counter back in the *home* state.

The counter will not stop in the home state until five complete cycles have been made, one on each filter position, and the filter wheel is back in its initial position. At this point the observer has the option of examining his data before proceeding, or signaling the sequencer to make another cycle through the filters.

If repeated measurements are desired, the filter wheel can be held at any one filter on command from the ground.

Primary developmental problems were the previously mentioned corona discharge and noise triggering of monostable and bistable logic circuits. The noise problems arose chiefly from the operation of relays and stepping motors from the same power source as the logic circuitry, and from cross-coupling of low rise time pulses in long multiwire cables. These difficulties were eliminated by using two sets of batteries (one for relays and digimotors, the other for logic), and by adding signal conditioning circuits at various points in the system.

5. Data Recording

For the balloon flights, data are continuously telemetered, decoded, and recorded by the NCAR system. The data are printed out in thirty columns of three digits each by a Frieden Flexowriter. Important data are repeated three times in the thirty columns.

For use on the ground, a system was designed to record the important data automatically on signal from the polarimeter. Ten voltages are recorded in digital form: integrator gain, filter position, depolarizer state, four integrator outputs, two high voltage supply outputs, the reference voltage, and the time of the measurement.

The data recording system consists of a ten-channel data commutator, a digital voltmeter, a digital decoder, a digital clock, and a digital printer.

During the *read* time after each integration, a signal is sent by the polarimeter in order to cycle the data commutator. This connects sequentially each of the analog data voltages to the digital voltmeter, which converts them to a digitally coded number. Each of the digits in the number is represented by a four-bit digital word. The data appear in binary-coded—decimal (BCD) form at the voltmeter output.

The BCD output is converted to a ten-line code which is accepted by the digital printer. The conversion is done by a diode-transistor logic unit which consists of a diode decoding matrix and ten current amplifiers for each digit.

The digital clock consists of a torsional pendulum oscillator which drives a counter. It gives five BCD output digits of time in units from tenths of minutes to tens of hours in factors of ten.

In operation, the digital voltmeter gives a *print* command to the printer after sampling each input voltages. The voltage is recorded and the commutator advances. After recording the ten channels, the commutator returns to its initial position and waits for the next *record* signal from the polarimeter. Data outputs are on a scale of 0 V to 10 V. Four digits are recorded for ground based work with an accuracy of one in the fourth digit.

6. Calibrations and Data Reduction

During aluminization, efforts are made to minimize the amount of polarization by reflection from the

Table I. Wavelength Dependence of the Polarization of the Whole Moon[a]

$1/\lambda$	$P(\%) \pm$ p.e.[b] at 40°[c]	$P(\%) \pm$ p.e. at 63°8	$P(\%) \pm$ p.e. at 88°8
3.04	4.580 ± 0.013	11.203 ± 0.006	17.016 ± 0.025
2.79	4.112 ± 0.006	10.325 ± 0.002	15.176 ± 0.024
2.62	4.007 ± 0.030	9.599 ± 0.024	14.427 ± 0.015
2 33	3.087 ± 0.008	7.721 ± 0.0t0	11.272 ± 0.051
1.95	2.842 ± 0.004	6.701 ± 0.006	9.067 ± 0.021

[a] Preliminary values, September to October 1966. See Fig. 4.
[b] Probable error. See Sec. VII.
[c] Angle at center of moon subtended by sun and observer.

telescope mirrors (Sec. III). To determine how effective the efforts are, two tests of instrumental polarization are made. For visual wavelengths, stars of negligible polarization are observed. For uv wavelengths, measurements are made at normal incidence on an aluminum screen which has been blasted by fine sand dust and is illuminated by an arc source (having small, if any, polarizatiou.). The screen provides uniform illumination of the primaries, and depolarizes the light from the lamp. Any residual polarization of the combination is eliminated by making measurements at one orientation and then rotating the screen and lamp 90° for a second set of measurements. The residual polarization of the mirrors is on the order of 0.1%.

Measurements of a source of 100% linearly polarized light are made to determine how effective the depolarizers are as calibrators for each measurement. The residual polarization with the 9-mm thick magnesium fluoride depolarizers acting on 100% polarized light is 0.15%. These corrections are applied to the measurements.

The equations for the solution of linear polarization result from combinations of the four measured intensities in the Stokes parameters I, Q, and U which define polarization[6]

$$P_{0,90} = \frac{I_0 - (I_{0d}/I_{90d}) I_{90}}{I_0 + (I_{0d}/I_{90d}) I_{90}}$$

and

$$P_{45,135} = \frac{I_{45} - (I_{45d}/I_{135d}) I_{135}}{I_{45} + (I_{45d}/I_{135d}) I_{135}},$$

where the subscripts refer to t'ie angles between the transmission axes of the Wollaston beams and the sides of the polarimeter (which are perpendicular to the equator when an equatorial mounting is used). The d indicates depolarized intensities. The multiplying ratios normalize for transmission differences between depolarizer in and out.

The above quantities are substituted into equations of the form $P = P_{0,90} \cos2\alpha$ and $P = P_{45,135} \cos2(\alpha + 45)$, where α is the uncalibrated position angle of the electric vector. The resultant P_R is determined by a least squares solution of $P_R = (P^2_{0,90} + P^2_{45,135})^{1/2}$.

The Stokes parameter S_V which is used to analyze elliptically polarized light is not measured. It could be

determined by inserting a quarter-wave retarder into the beam from the $P_{45,135}$ telescope and measuring $I_{45,\pi/2}$ and $I_{135,\pi/2}$ in addition to the above intensities.

An advantage of the design of the polarimeter is that if any one of the four PM tubes or integrators would become defective, the other three would still give information suitable for solving for the polarization. This redundancy lends reliability to the instrument and increases the chance for success on a space mission. Equations for the solution using only three components of the incident intensity are easily derived.

7. Preliminary Results and Future Plans

Table I lists preliminary results on the moon obtained at three phase angles. (Phase angle is the angle at the center of the moon subtended by the sun and the observer.) These data are part of a large set made over a range of phase angles[7] (extending from first to last quarter). Positive phase angles occur from full through last quarter. Probable errors are from the main residual of the least squares solution assuming a normal distribution of the residuals. In Fig. 4, the wavelength dependence of the polarization of the whole lunar disk between 2860 Å and 5100 Å is presented. The point at 2860 Å is uncertain because the gondola stabilization failed. Points at these phase angles obtained by Lyot[8] are plotted for comparison.

More extensive work is in progress, and the results will be reported elsewhere.[7] Future plans include the use of narrower filters to investigate some of the detail shown in Fig. 4, extension of the wavelength range of the instrument to the ir, and some observations of terrestrial features from aircraft.
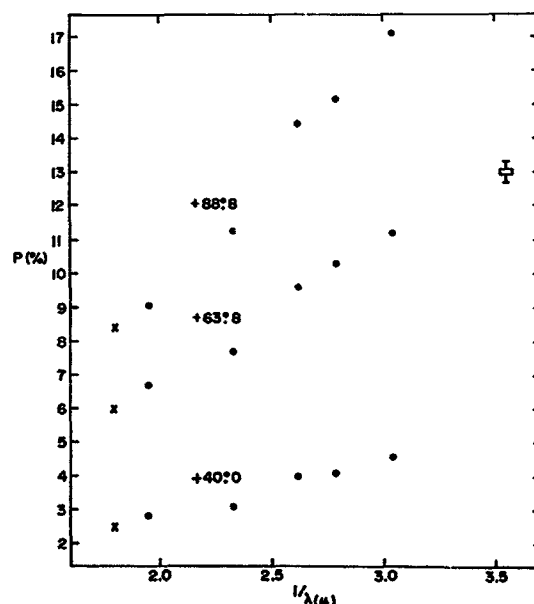
Fig. 1. Preliminary data obtained with the automatic polarimeter on the ground and from a high altitude balloon. Filled circles: ground based data at phase angles indicated. Rectangle: balloon point at −56°8 phase angle. Crosses: points obtained by Lyot (1929) at the above phase angles.

We are indebted to T. Gehrels for his encouragemc t
and guidance. The close assistance of T. M. Teska on
many matters was indispensable; he is responsible for
the design of the integrators. L. C. Hess did most of the
wiring; D. E. Hall and S. Sutton provided technical
assistance. E. E. Harber set up a program of rigid
environmental testing, and helped prepare the system
for the first two flights. D. L. Brumbaugh (who
designed the digital clock) and G. V. Coyne assisted
with the third flight. E. H. Roland devised the
mounting technique for the prisms. And lastly, we
acknowledge the assistance and patience of Ruth and
Judy during some long days and nights. The project
is supported by the National Aeronautics and Space
Administration (NASr-138).

REFERENCES

1. T. Gehrels and T. M. Teska, Appl. Opt. 2, 67 (1963).

2. S. F. Pellicori, C. A. Johnson, and F. T. King, Appl. Opt. 5, 1916 (1966).

3. S. F. Pellicori, Appl. Opt. 3, 361 (1964).

4. T. M. Teska, personal communication.

5. S. F. Pellicori, E. H. Roland, and T. M. Teska, Rev. Sci. Instr. 36, 611 (1965).

6. M. Born and E. Wolf, *Principles of Optics* (Pergamon Press Ltd., Oxford, 1965), p. 545.

7. G. V. Coyne and S. F. Pellicori, Astron. J., to be published (1967).

8. B. Lyot, NASA Tech. Transl. TTF-187 (1964), originally in Ann. Obs. Meudon 8 (1929).

No. 108   POLARIMETRY FROM HIGH-ALTITUDE BALLONS

by G. V. Coyne and T. Gehrels

February 8, 1968

ABSTRACT

The ballooning is for an extension of the groundbased polarimetry of planetary atmospheres and interstellar matter to wavelengths shorter than 3000 Å. Some of the largest available balloons are used to carry telescopes to an altitude of 36 km, which is above a sufficient fraction of the terrestrial ozone to allow polarimetry with ±0.03% precision at 2850 and 2250 Å. The development of and operations with two gondolas are described, one gondola has two 7.5 cm telescopes and the other has a 71-cm telescope.

1. Introduction

A new discipline is being developed with precise polarimetry over the widest possible range of wavelengths; the observations are compared with the Rayleigh-Chandrasekhar theory of multiple molecular scattering and with the Mie theory of light scattering by small particles. From such a comparison it is possible in certain cases to derive the optical thickness of a planetary atmosphere and to determine the sizes and refractive indices of aerosols and interstellar grains.

Since 1959 we have made polarimetric observations of a variety of objects, ranging from minor planets to extragalactic nebulae (some results are shown by Gehrels and Teska 1963). Various telescopes were used at Indiana University, the McDonald Observatory, the Kitt Peak National Observatory, and recently the 154-cm telescope in the Santa Catalina Mountains near Tucson (Coyne and Gehrels 1967).

The Polariscope programs now consist of balloon-borne as well as ground-based photometry and polarimetry in order to extend the wavelength range to 2850 and 2250 Angstroms. The possibility of using balloons above the ozone in the earth's atmo-sphere has been discussed (Gehrels and Teska 1963; Gehrels 1967). The following sections describe the equipment and flights in the ballooning.

2. Instrumentation

At the start of this new program of photometry and polarimetry at 2250 and 2850 Angstroms, preparations were needed of new materials for analyzers, depolarizers, and filters (Pellicori, Johnson, and King 1966). The required precision in most polarimetry problems is about ±0.03% polarization (±0.0006 astronomical magnitudes), which we obtain with groundbased telescopes and during the balloon flights. Development was needed of special techniques and equipment such as a suitable magnetometer compass and a noise-free telemetry system (Brumbaugh, unpublished), the radio-frequency link (Frecker 1966), the stable platform (Frecker 1968), and optical testing instruments (Pellicori, Roland, and Teska 1965). We have adhered to a rigorous testing schedule, with crane suspension as high as 200 feet, and with many sessions in environmental chambers for individual packages and also for the completed gondola.

The design, construction, and testing is being

done entirely "in house," that is all the work is done by a crew at the University of Arizona. During the balloon flights it is invaluable to have the people that developed the equipment also in charge of the operations. Troubles that occurred during the nights of balloon operations were readily spotted and cured by the operators because of their intimate knowledge of the components, assembly, and performance during the tests. The "in house" principle is to be compared with that of primarily having contracted equipment and services.

There are three distinct polarimetric systems in the Polariscope programs. The first of these is the groundbased equipment (shown in Fig. 1 of Communications No. /06, Coyne and Gehrels 1967). The second is a prototype polarimeter being developed for use on space probes to Mars and Venus (Pellicori and Gray 1967). The third is the polarimeter designed for use with 'he 71-cm balloon telescope.

Figure 1 shows che optical diagram of the space prototype polarimeter. The Cassegrain telescope of 7.5 cm in aperture is followed by a depolarizer that can alternately be inserted in and removed from the beam, followed by a filter wheel. The light is next split by a Wollaston prism into two beams with orthogonal vibrations. Each of the beams brings the 7.5-cm primary mirror into focus on the face of a photomultiplier tube. The tubes are EMI 9256B, made partially 'solar-blind' with 3mm $NiSO_4 \cdot 6H_2O$. The outputs of the phototubes are integrated, processed digitally and sent by a radio-frequency telemetry link to a ground station, which belongs to the National Center for Atmospheric Research. The polar'meter consists of two such optical trains fixed a.   to one another about the optical axis. Thus a pair of observations — one with the depolarizer in the beam and one with it out — offers a simultaneous

solution for the amount and position angle of polarization. With this arrangement, brightness, color, and polarization measurements can be made quickly during a planetary fly-by.

Figure 2 shows this polarimeter mounted on its balloon gondola. In addition to the polarimeter the yoke is seen that allows motion in elevation and in azimuth. At the bottom left is the battery pack; the ballast hopper is under the polarimeter, and the telemetry/command package is at the bottom right.

In Fig. 3 is seen the optical diagram of the 71-cm balloon telescope. On the outside is a finding telescope with a vidicon television system and also a star tracker for pointing the ensemble on the object chosen for observation. At the focus of the star tracker is a beam splitter that consists of a sharp pyramid with four polished sides. Four 1P28 photomultipliers sense the balance of the light on the four pyramid sides and they send correction signals to the gyros.

The main telescope has a diameter of 71 cm, it has an f/2 primary mirror of fused silica. The centering of the image can be checked with another vidicon, and after that check the viewing mirror is removed. The light then goes through a Lyot depolarizer, a filter wheel, a focal-plane diaphragm, a Wollaston prism, and the field mirrors form an image of the primary mirror on the Ascop 541F photomultiplier cathodes. The Wollaston prism and phototubes rotate, and measurements are made at 30° increments of the Wollaston angle.

Figure 4 shows the Polariscope telescope mounted in the gondola. Its major components are the 71-cm telescope, the polarimeter, two television cameras for star acquisition, a radio command receiver, two magnetometer compasses, a television and telemetry transmitter, three-axis servo-stabiliza-
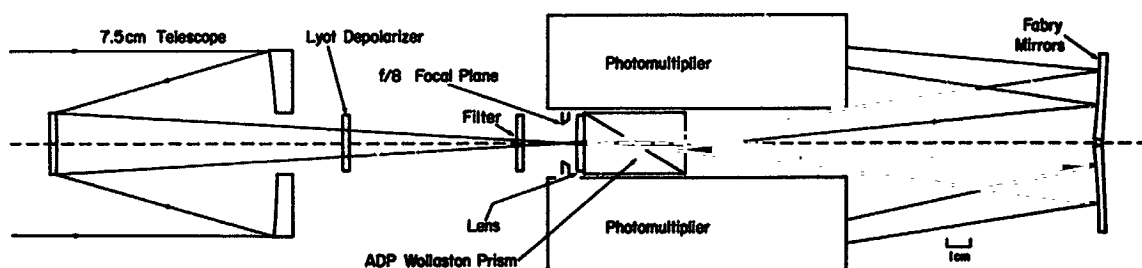
Fig. 1   Optical diagram of space-prototype polarimeter.
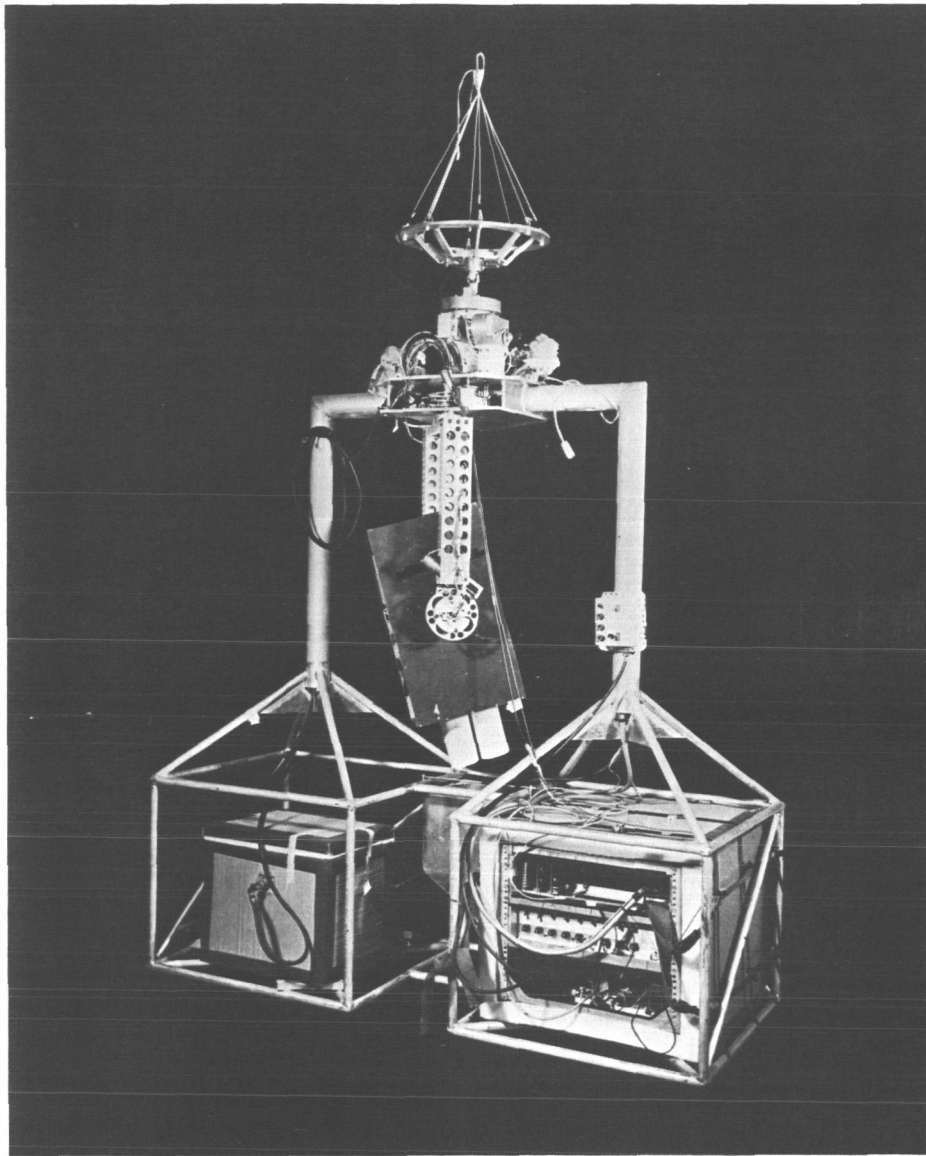
Fig. 2   Space-prototype polarimeter mounted in its balloon gondola.

tion system, and a light-weight gondola of thin alumi-um tubing to contain all of these. Power is supplied by 60 kg of silverzinc batteries in order to provide ±12 volts and 28 volts for 15 hrs. operating time. There are two ground stations (Fig. 5) to control the gondola/telescope system and to receive and record the telemetry data; one ground station is at the launch site and the other is placed in a van up to 900 km downwind.

The television system is slow scan: 500 lines, one frame per second. Vidicons were selected rather than image orthicons because of their smaller size,

lower operating voltage, and their simplicity of in-flight adjustments. The outboard television has two lenses on a turret giving a 14° and a 4° field. The second television looks through the 71-cm telescope and has a field of 13 minutes of arc.

The gondola, complete with 181 kg ballast but not including the parachute, weighs 730 kg. The telescope weighs 125 kg and it is stabilized to ±6 seconds of arc in elevation and cross-elevation.

3. Observations

The 71-cm telescope has flown 3 times success-
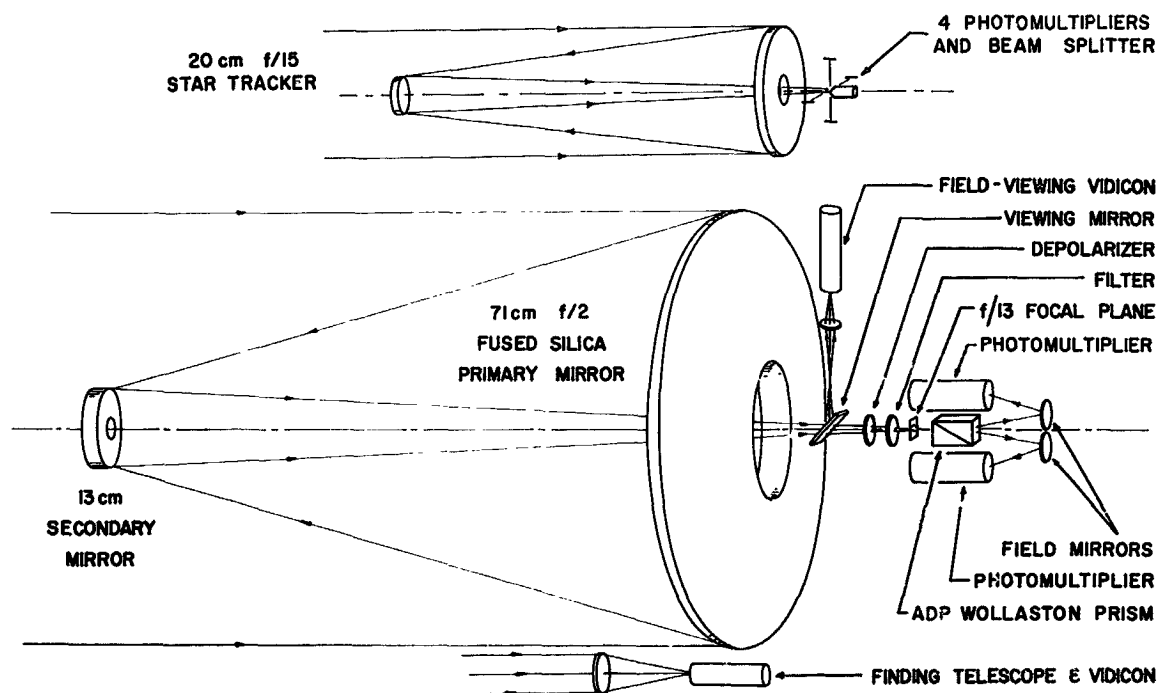
Fig. 3   Optical diagram of 71-cm balloon telescope.

fully, launched from Palestine, Texas, in May, 1966, and from Page, Arizona, in March, 1967, and in January, 1968. The launch, tracking and recovery is done by the National Center for Atmospheric Research. The balloon is made of polyethylene, 0.9 mil thick and 3×10^5 m³ in volume. The smaller system has flown 3 times for engineering tests at 36 km altitude with successful operation of the polarimeter but without azimuth stabilization.

We expect to fly the Polariscope 71-cm telescope once or twice per year. So far we have obtained new results on the interstellar polarization with measurements at 2250 and 2850 Angstroms on Zeta Ophiuchi, Kappa Cassiopeia and Gamma Orionis. Such measurements are made on stars in various directions in the galactic plane in order to determine the size and composition of particles in various interstellar clouds. The position angles of the interstellar polarization also are important as indicators of the direction of the galactic magnetic fields. With groundbased telescopes we found a peculiar dependence of the position ar.gle upon wavelength. The effect is as yet unexplained but it is undoubtedly connected with spiral structure and galactic magnetic fields, and it is important to observe the effect over the widest possible range of wavelengths.

During the March 1967 flight, precise measurements were obtained of the polarization of Mars at 2250 and 2850 Angstroms. A preliminary study of the results gives the surface pressure on Mars at 10 mbars. A surface pressure as low as 10 mbars had been found spectroscopically, and also in an occultation experiment, while polarimetric measures made by Dollfus have indicated a much higher pressure. With the wide range of wavelengths, made possible by the ballooning, the polarimetric result appears to be no longer anomalous. And the polarimetric determination is important because the technique and the detection capability differ from those in spectroscopy. We are making a detailed study of the brightness and polarization over the full range of wavelengths of observation (0.2 – 2.6 microns), with an analysis of the aerosols as well as of the molecular component of the Martian atmosphere.

During the balloon flights with both systems, preliminary, but essential, measurements were made of the sky brightness at 2250 and 2850 Angstroms, as well as reconnaissances for future work on Venus, Jupiter, the Moon and various types of stars.

The small polarimeter has also been useful on the ground for observations of the whole Moon; because of its short focal length, the whole lunar

Fig. 4 Balloon telescope mounted in its gondola and suspended from a launch truck of the National Center for Atmospheric Research (NCAR) at Page, Arizona, March 1967.

Fig. 5 A Polariscope Ground Station. The oscilloscope serves as a television screen, below which are the toggle switches for the command system, and under that is a binary clock-timer. The middle panel has quick-look indicators and recorders, and the panel on the right has special command switches operated by a separate observer. At the top, a papertape punch is shown; a magnetic tape recorder is also used.

image is accepted within the focal-plane diaphragm (Coyne and Pellicori 1968).

REFERENCES

Coyne, G. V., and Gehrels, T. 1967. *Ast. J.* **72**, 887.

Coyne, G. V., and Pellicori, S. F. 1968, *Ast., J.* **73**, to be published.

Frecker, J. E. 1966, *C. Q. Magazine* **22**, 43.

————. 1968, *Comm. LPL.* **7**, 39.

Gehrels, T. 1967, *Appl. Opt.* **6**, 231.

Gehrels, T., and Teska, T. M. 1963, *Appl. Opt.,* **2**, 67.

Pellicori, S. F., and Gray, P. R. 1967, *Appl. Opt.,* **6**, 1121.

Pellicori, S. F., Johnson, C. A., and King, F. T. 1966, *Appl. Opt.,* **5**, 1916.

Pellicori, S. F., Roland, E. H., and Teska, T. M. 1965, *Rev. of Sci. Inst.,* **36**, 611.

No. 109 THE POLARISCOPE BALLOON-BORNE SERVO SYSTEM

by Jack E. Frecker

February 18, 1968

ABSTRACT

This paper describes the stable platform for the Polariscope 71-cm Cassegrain telescope that is mounted in a box-like aluminum gondola (Fig. 1). It is designed to "lock on" certain stars or planets during balloon flights at 36 km altitude and measure the polarization at 2250 and 2850 Angstroms (Coyne and Gehrels 1968).

1. Stabilization Systems

The Polariscope telescope is to be pointed in a fixed direction in space but the base, or gondola, is free to move about. The gondola weighs 740 kg at launch — this includes 181 kg of ballast, but not the parachute — and is suspended from 52m long nylon shroud lines (see Fig. 2). The gondola acts as a mass bobbing on an underdamped spring, on a simple pendulum, on a compound pendulum; usually there is a combination of all three. As the gondola moves about it must not drag the telescope with it. This absolutely rules out the use of viscous coupling, such as tachometer feedback, between the gondola and the telescope.

Every movement of the telescope causes a counter-movement of the gondola. If the telescope is moved in elevation the gondola is excited in compound pendulum motion with a decay time of 2 or 3 mins. This oscillation must be damped out. The only damping available is the flexing of the nylon suspension system. If the telescope is moved in azimuth the gondola tries to rotate in the opposite direction. It is then necessary to torque against the balloon through the suspension system to counteract the azimuth motion of the gondola.

There are three natural resonant frequencies in the suspension system. Simple pendulum has a frequency of about 1/20 cps. Torsional pendulum motion is roughly the same. Compound pendulum is close to 1/2 cps. Cross-over frequencies of the servo system must be above these resonant frequencies and below any of the mechanical resonant frequencies of the instrument itself.

2. Choice of Gimbals

Three gimbals are used on Polariscope. One gimbal ring is movable in elevation. The axis of the inner gimbal, or telescope proper, is normal to the elevation axis and lies in the plane of the gimbal ring (see Fig. 1). This is called the cross-elevation axis, and the telescope is free to move ±10° in this axis. A third axis, in azimuth, is controlled to keep the gondola opening approximately centered about the telescope. For a true orientation system a fourth axis would be necessary, controlling about a line through the center of the telescope, and it would prevent the image plane from rotating during the observations.

The inner gimbal, or telescope proper, weighs about 140 kg. The outer gimbal ring is a boxlike

39
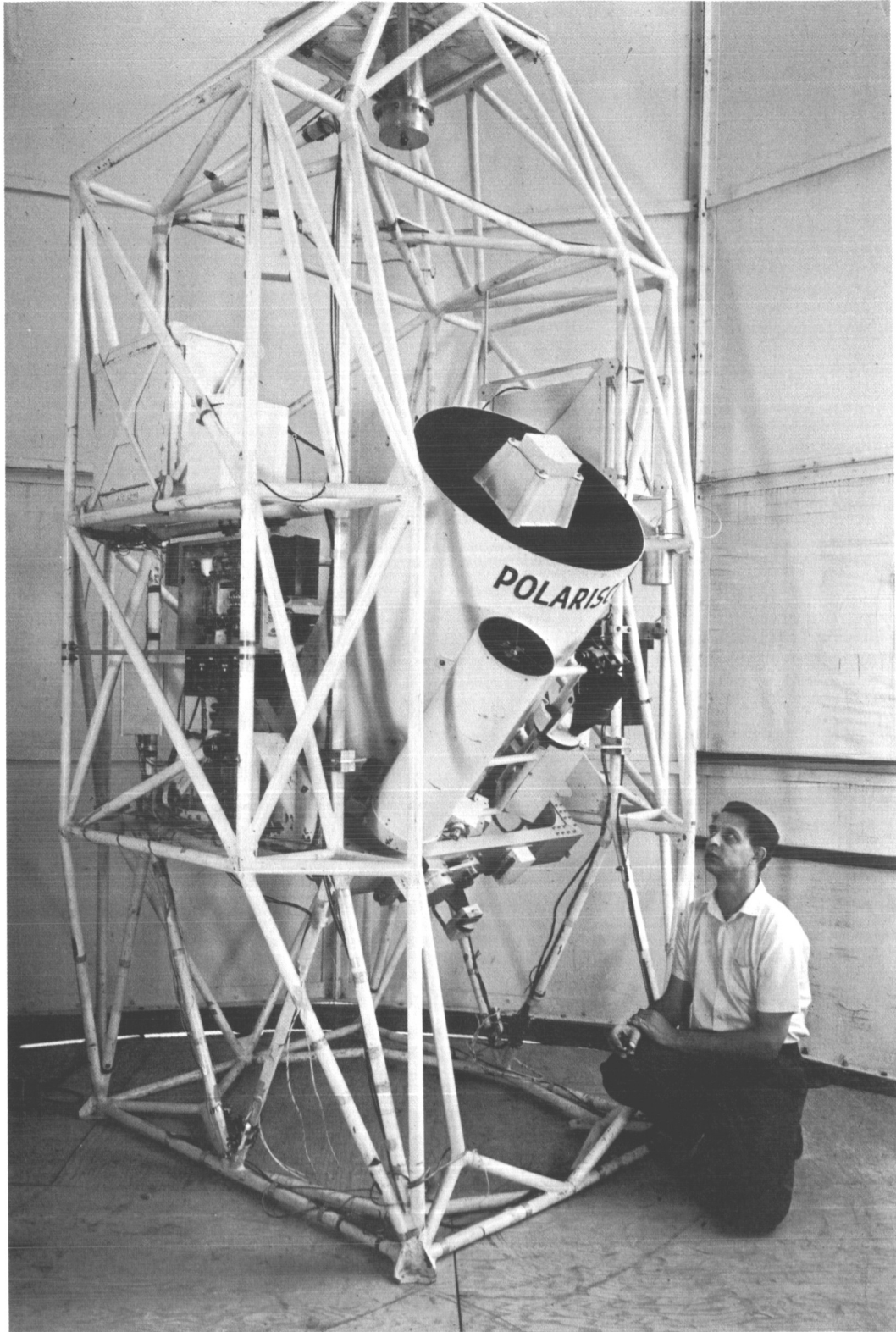
Fig. 1 Polariscope 71-cm telescope, with 20-cm startracker and 7.5 cm vidicon camera lens, within elevation gimbal on gondola frame.
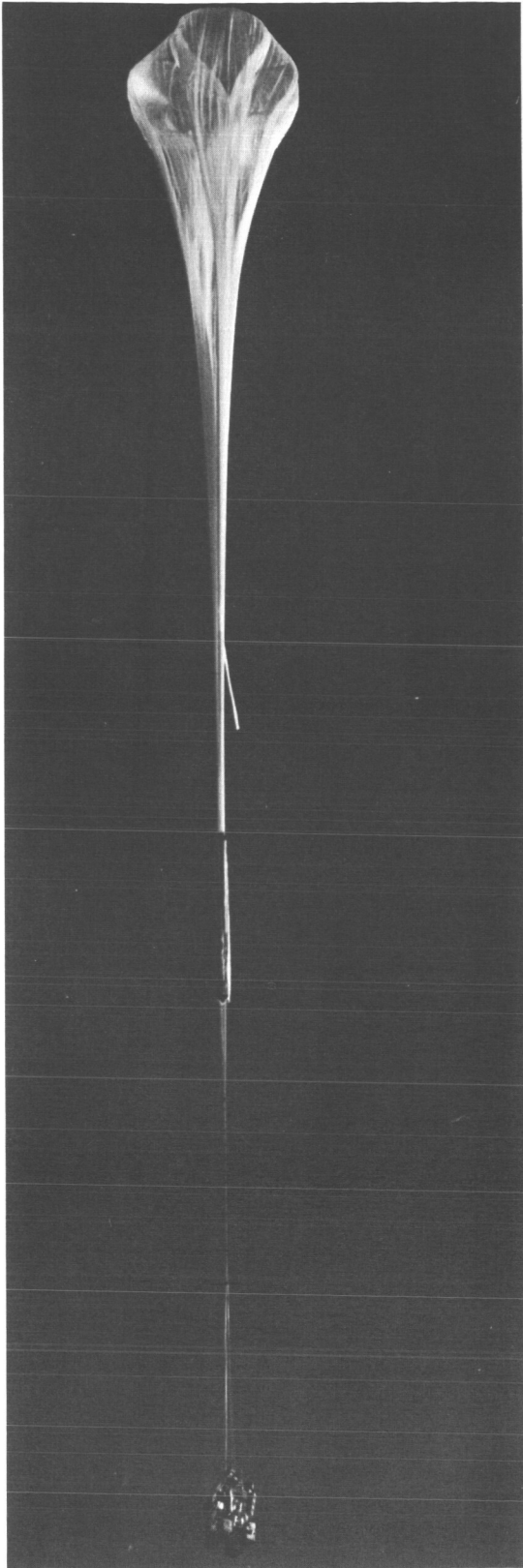
Fig. 2 Polariscope in flight shortly after launch. Photo courtesy D. L. Brumbaugh.

AZIMUTH MOMENT OF INERTIA = 408×10^7 gm cm^2

ELEVATION MOMENT OF INERTIA 40.8×10^7 gm cm^2

CROSS ELEVATION MOMENT OF INERTIA = 21.8×10^7 gm cm^2
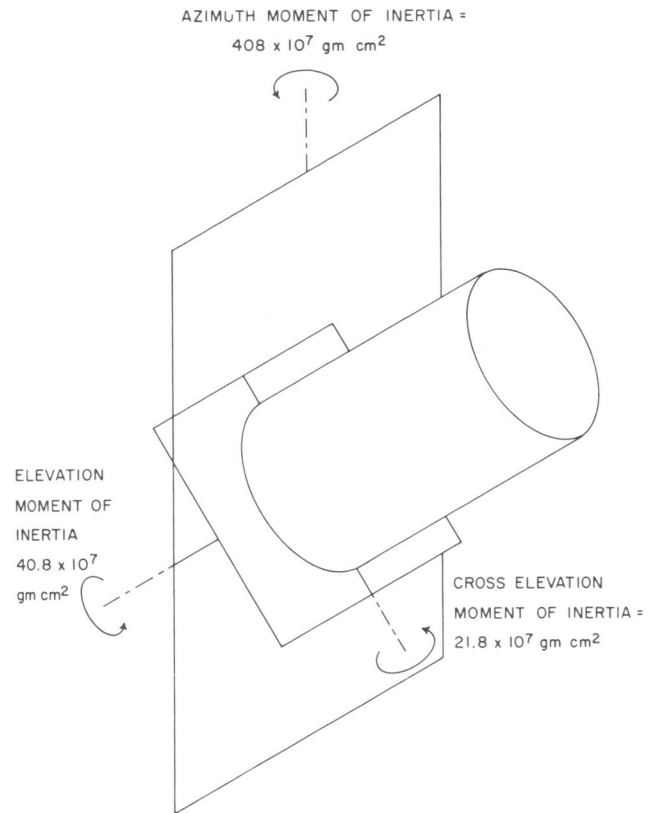
Fig. 3 Gimbal diagram of Polariscope.

structure made of aluminum channel. As such it is quite flexible. To avoid a low resonant frequency between the drive motors and the driven element it was decided to drive the telescope in both axes from two sides rather than from one side of the gimbal ring. This permits a higher servo cross-over frequency than would be possible if the gimbals were driven from one side only. At least 14×10^7 dyne cm (10 foot pounds) of peak torque motors made by Inland Motor Corporation of Virginia were selected to be prime movers. Torque motors normally drive their load directly, with no reduction ratio. The most nearly suitable motor built by Inland would be the model 5730, but, used in pairs, these would have required as much as 510 W of peak electrical power to the motors for 19×10^7 dyne cm of torque. Smaller motors and a reduction ratio are therefore indicated.

It is difficult to build a servo system that will point to within a few seconds of arc using gear trains with several minutes of arc backlash. We therefore adopted a technique, pioneered for balloon telescopes by G. A. Newkirk of the High Altitude Observatory, that uses gearless reduction ratios involving smooth discs or shafts driving each other, relying
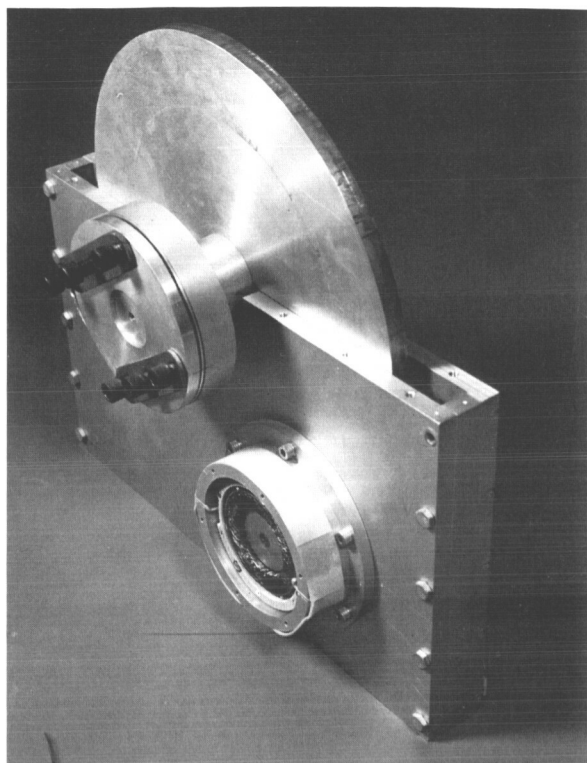
Fig. 4   Elevation motor mount. Idler bearing shaft is concealed by elevation trunnion. Gimbal ring bolts to trunnion with the six Allen head screws. Thrust bearings (not shown) prevent drive disc from touching sides of box.
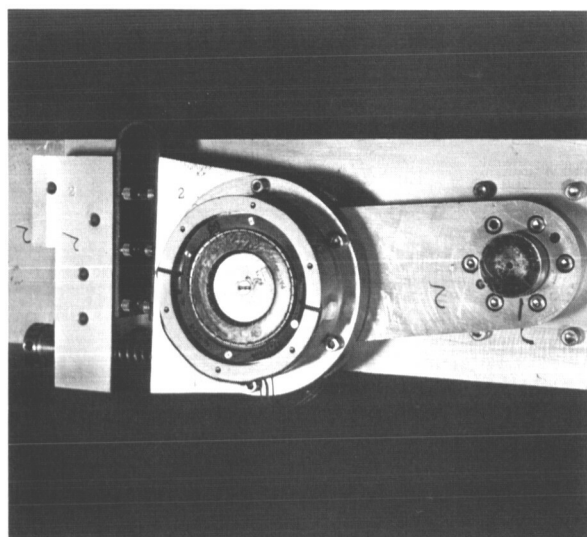
Fig. 5   Cross Elevation motor mount installed on gimbal ring. Hairpin-like steel spring is a flexure bearing; coil spring forces motor shaft against drive disc sector.
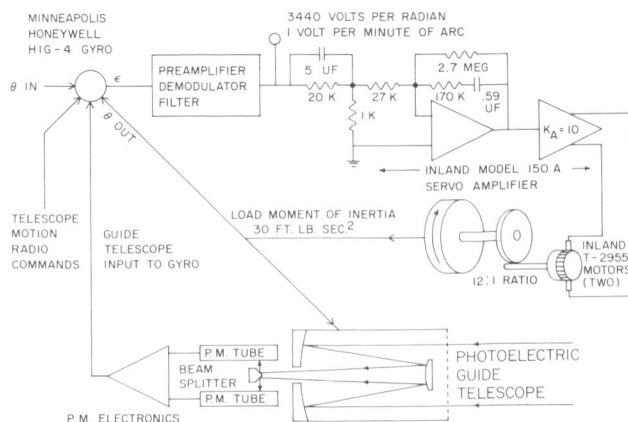
Fig. 6   Block diagram of elevation servo. Photoelectric guide telescope contains a tetrahedral beam splitter at the focal plane of the telescope, and four photomultiplier tubes. If the optical beam is centered on the beam splitter the outputs of the photomultiplier tubes are equal and the precession current to the gyro is zero. If the optical beam is off-axis the outputs of the photomultiplier tubes are unequal and a precession current to the gyro causes the telescope to move toward the star until it is optically centered in the guide telescope.

only on pressure of one member against another to avoid slippage (Hull 1964; as a general reference we used Nidey 1962). Our prime mover (see Figs. 3, 4, 5, and 6) consists of two Inland model 2955 motors per axis; they drive smooth shafts, 2.5 cm in diameter. These in turn drive 32-cm diameter by 1.3-cm thick aluminum discs affixed to the load. The discs are gravity loaded against the motor shafts in elevation. In cross elevation the motor mount is spring loaded against the drive disc sector. This system requires only 150 W of peak electrical power per axis for 27×10^7 dyne cm of torque. It has low friction and zero backlash.

A block diagram of the elevation servo electrical system appears in Fig. 6. A Minneapolis-Honeywell HIG-4 gyro is used as the inertial reference element. A good gyro of this type will cause a servo system to point in a fixed direction in space with a small (less than one earth-rate unit) drift caused by the rotation of the earth, which can be trimmed out. Its null position can be changed by electrical precession signals from outside. Its output is a 1600 HZ phase-sensitive error signal. This signal is amplified, demodulated and filtered, being raised to a level where $K_\theta = 1$ V per min of arc, or 3440 V/rad. This is followed by an Inland model 150A servo amplifier consisting of an operational preamplifier whose transfer function is set by external components, feeding a 150 W output power amplifier with a volt-

age gain of 10. The amplifier drives two Inland model 2955 motors, each driving the load moment of inertia of 41×10^7 gm cm^2 through 12:1 gearless reduction ratios.
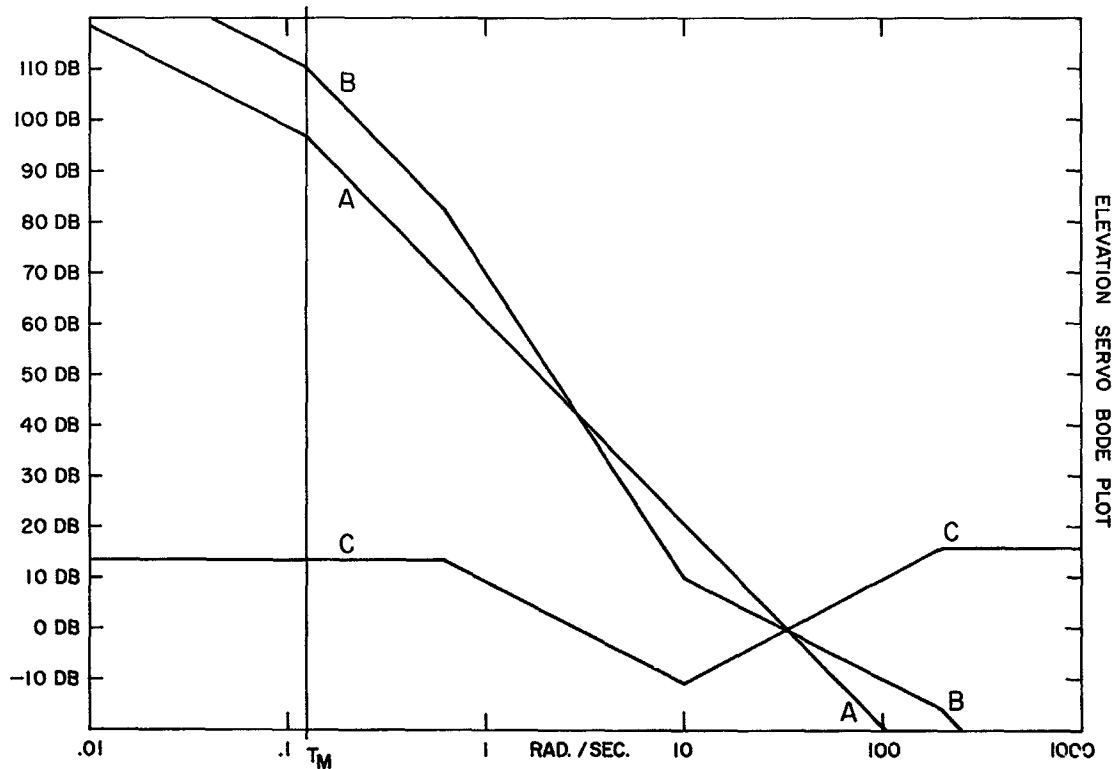
Radio commands for telescope motion are applied as precession currents to the HIG-4 gyros. These signals can control the telescope at rates from 1°/min to 50°/min.

When the telescope is brought to within 5 mins of arc of the desired star the photoelectric guide telescope "sees" the star and generates precession currents with its photomultiplier tubes to correct the gyros constantly, holding the telescope "locked on."

Figure 7 is a Bode plot of the elevation servo (*Inland Handbook* 1964). Curve A is the uncompensated servo open loop gain assuming that K_θ equals 3440 volts per radian, times the power amplifier gain of 10, times the operational amplifier gain arbitrarily assumed set at unity, times the transfer function of the motor and load. Specifically it a plot of:

$$\text{Open loop gain} = \frac{K_\theta K_A}{K_B} \cdot \frac{1}{S(1+T_M S)},$$

where $T_M = \dfrac{J_T}{K_B K_T / R_M}$ and

K_θ is Transducer sensitivity,	3440 V/rad;
K_A is power amplifier gain,	10 V/V;
J_T is combined motor-load moment of inertia,	41×10^7 gm cm^2;
K_B is motor winding back EMF constant,	4.08 V/(rad/sec);
K_T is motor winding torque sensitivity constant,	4×10^7 dyne cm/A;
R_M is motor resistance,	3.35 ohms;
T_M is system mechanical time constant,	8.22 secs.

Curve B is a Bode plot of the compensated servo with a zero decibel cross-over frequency of 5 HZ or 31.5 rad./sec. and $K_\theta K_A/K_{\mu} = 40,000$. This cross-over frequency was chosen as the geometric mean between the compound pendulum frequency and a mechanical resonant frequency that exists in the telescope. Curve C is the difference between curve A and B and is the desired gain-frequency response curve of the operational preamplifier in the Inland servo amplifier. The network values to accomplish this end are shown in Fig. 5. Actually, the 27K resistor is made 33K to compensate for increased servo gain due to cooling off of the torque motors at altitude.

The cross elevation servo is similar to the elevation servo, differing only in moment of inertia and network gain. Pointing accuracy of the elevation and cross-elevation servo is ±6 arc sec peak error, or ±2 arc sec RMS error.

3. Azimuth Servo

The purpose of the azimuth servo is to keep the gondola opening approximately centered about the telescope. The prime mover is a shaft directly driven by a 7 ft. lb. torque motor. It receives its error signal from a precision potentiometer on the cross-elevation axis. Unlike a conventional servo system which torques against a solid mass, this servo system torques against a spring, namely the parachute shroud lines. With 52 m suspension length and 740 kg gondola weight they have a spring function of approximately 9.5×10^7 dyne cm for 30° deflection. The electronic network for the system was designed empirically rather than scientifically and will not be discussed here.

4. Flight Results

Polariscope flew for the first time with this servo system in March 1967. Performance of the elevation and cross-elevation servo was impeccable throughout the flight. The azimuth shaft bound up once at the beginning of the flight but freed itself and operated properly during the remainder of the flight. This momentary failure has since resulted in the expenditure of considerable effort to improve the azimuth shaft structure and to select the best possible bearing and lubricant. Bearing and motor friction is now 0.54×10^7 dyne cm with 726 kg loading the bearing. The second flight with this system occurred in January 1968 and the performance in azimuth was faultless as well as that in elevation and cross-elevation.

REFERENCES

Direct-Drive Servo Design Handbook, Inland Motor Corp., Radford, Virg. 1964.

Coyne, G. V., and Gehrels, T. 1968, *LPL Comm.* 7, 33.

Hull, H. 1964, Engineering Report of Coronascope II-α (High Altitude Obs., Boulder, Colo.).

Nidey, R. A. 1962, Stabilization and Orientation of the Payload, Space Division Report 010-62 (Kitt Peak National Obs., Tucson, Ariz.).

No. 110 A MECHANICAL COORDINATE CONVERTER

by G. Van Biesbroeck and T. Gehrels

February 18, 1968

ABSTRACT

A simple device is described for mechanically converting spherical coordinates from one system to another.

A coordinate converter was made for use in the Polariscope balloon program to allow quick transformations of spherical coordinates. By setting positional data in one coordinate system, the operator can easily see the correspondig coordinates in another system. This makes possible, for instance, the immediate translation from the equatorial system to an altazimuth system.

Each system of coordinates is represented by two circles at right angles to each other. The horizontal system has a stationary base supporting a horizontal circle divided by 360° in azimuth. A stationary vertical circle graduated from 0° to 90° corresponds to the geographic latitude. In its plane slides a non-graduated circle, inscribed with a single white arrow. This circle holds the pivots of the second system of coordinates, which define hour-angle and declination, also in degrees. Over the whole arches the altitude circle whose base ring slides over the stationary azimuth circle. The altitude circle carries a sliding pointer that reaches inward to the declination circle.

In the figure the balloon latitude is set at 31°0 and the pointer at an object low (elevation 26°4) in the northwest sky (azimuth 311°); the corresponding local hour angle of 83° west, and northern declination of 47° can now be read from the inner coordinates. Another example, not shown here, is for an observation of Mars at 3:00 a.m. on 9 March 1967 Mountain Standard Time, for which the Air Almanac lists Greenwich hour-angle 104°6 and southern declination 10°2. At the time of the observation, made by the Polariscope 71-cm telescope, the balloon was located high over the Grand Canyon, at northern latitude 36°3 and longitude 112°9 west of Greenwich. To determine the elevation and azimuth, the latitude circle is first moved so that the arrow indicates 36°3. Next, the inner coordinate system is pivoted to read the "Grand Canyon hour-angle" of 112°9 − 104°6 = 8°3 east. The pointer is moved to indicate 10°2 south on the declination circle. One then reads the elevation (42°8) and the azimuth (168°8).

The converter's precision is about ±0°2. This requires careful machining of divided circles and precise alignment of the perpendicularity of the circles and of the location of the pivots.

45

Fig. 1   A Mechanical Coordinate Converter.

No. 111 THE DESIGN OF LOW-COST PHOTOMETRIC TELESCOPES*

by HAROLD L. JOHNSON

1. Introduction

The design and construction of astronomical telescopes intended specifically for photometric work has never been discussed in great detail. It is usually assumed that telescopes designed for general astronomical work also are suitable for photometry. To a considerable extent this is true, and much good photometry has been done with telescopes whose designers had other applications in mind. On the other hand, no general-purpose telescope I have used is capable of providing maximum efficiency for all types of photometric work. For example, no telescopes of moderate or large aperture (except those to be discussed in this article) are capable of slewing rapidly from one part of the sky to another.

A further limitation of the general-purpose telescope, imposed not by the design of the telescope itself but by the fact that it is used for general purposes by many astronomers, is the relatively small amount of telescope time that is available; and even this limited time usually is broken into many short runs of a few days, making it difficult to establish and to maintain proper photometric systems.

Our recent work in the far infrared has brought to light a number of serious problems, such as the very large long-wavelength background radiation from the telescope itself, whose solutions dictate telescope designs not normally considered.

We have found it necessary to design and build our own photometric telescopes, so that we can satisfy our requirements for special telescope designs and for large amounts of uninterrupted observing time. Since we want special purpose telescopes that will not be available for general use, it is difficult to justify the large budgets needed for modern general-purpose telescope designs. As a result, there is an additional design requirement; namely, that our telescopes must be built at relatively low cost, while meeting our other requirements.

2. Design Requirements for a Photometric Telescope

The performance specifications for an astronomical telescope that will be used exclusively for photoelectric photometry differ in certain important respects from those for telescopes that will be used for general astronomical work. Since we deal, so far as the photometer is concerned, with essentially on-

axis images, rapid deterioration of the images with distance from the optical axis is unimportant; therefore, cassegrain systems with easily produced primary mirror figures, such as ellipsoids or spheres, are acceptable. Furthermore, it is permissable that the quality of the on-axis images be significantly poorer than is needed for many other applications.

On the other hand, the rigidity of the entire telescope and the precision of the right ascension and declination drives should be at least equal to those expected from the best telescopes. We have found that, for the maximum observing efficiency, the photometric telescope should be included as a component in the measuring and data-recording system, with control of the telescope slow motions for moving back and forth between star and sky regions vested in the data-recording system, rather than under the direct control of the observer. Provision for offset guiding is essential, both for measuring stars too faint to be set on visually and for making long exposures in infrared wavelengths.

The design of a low-cost photometric telescope represents a compromise between cost and precision. If we are to minimize the cost and at the same time satisfy the requirements of the photometry, we must be very clear about the degree of precision needed at every point in the telescope design. Every specification must be examined thoroughly to be sure that the minimum precision that will accomplish the job actually is specified.

The first requirement of the design is that the telescope shall be capable of very rapid slewing from one part of the sky to another. We shall specify that the telescope can be slewed from four hours east hour angle to four hours west hour angle, or from declination −30° to +60°, in less than 30 seconds of time. In a low-cost telescope, this requirement necessarily implies that the telescope is hand-slewed, with hand-operated clamps; the cost of electro-mechanical drives capable of driving and stopping the telescope safely at these rates is incompatible with our budgets. Thus, our first specification is that the photometric telescope is to be hand-slewed, with hand-operated clamps.

As is often the case, further specifications follow from the first one. Since we wish to make photometric telescopes of apertures as great as 60 inches, we must keep the moving mass of the telescope as low as possible; if we do not, the observers will not be able to slew it by hand. Telescope mountings of the symmetri l equatorial class, such as fork or English yoke types, do not require counterweights

and, therefore, have minimum mass and inertia for a given telescope aperture.

The requirement of low telescope-cost restricts our choice of polar-axle bearings to standard self-aligning roller or ball bearings (i.e., costly oil-pad bearings, etc., are prohibited). These two bearings should be as far apart as possible in order to minimize bearing loads and the effects of inaccuracies in bearing construction.

Thus, our choice of telescope mounting has been narrowed down to the English yoke type. This mounting has the disadvantage that, as is the case of Mount Wilson 100-inch telescope, the region of the North (or South) celestial pole is not accessible. The area of the sky north of declination +65° or +70° (or south of −65 or −70°) is not large, however, and in our experience this restriction seems not to be serious. The complete symmetry of the English yoke makes for a rigid structure that minimizes gravitational deflections and their effects upon the observations. It is especially important that a photometric telescope be rigidly constructed and that it be as free as possible of the lightly damped oscillations that are excited, in most large telescopes, by high-speed setting and guiding motions. A photometric observer makes many setting and guiding motions during a night's observations and rapid, accurate, setting and guiding is essential for efficient work.

The overall length of the telescope tube should be short, in order to minimize inertia and cost. A short tube also is more rigid than a long one. On the other hand, a short telescope tube means a small primary focal-ratio and, consequently, more difficulty for the optician who must figure the mirrors. We can, however, reduce the optician's problems by relaxing the specification on image size; images two or three seconds in diameter are satisfactory for almost all photometric work. The use of an ellipsoidal or spherical figure on the primary mirror makes the optician's work much simpler; this is particularly true for the spherical primary, even though the secondary mirror must then have a strongly aspheric surface. The resultant small field of good image definition does not restrict significantly the use of the telescope for photometry.

While it is possible to relax the specifications on image quality and field of view of a photometric telescope, the specifications on setting, guiding and sidereal tracking motions cannot be greatly different from those for general-purpose telescopes; in fact, as mentioned earlier, the setting and guiding motions should be more precise in some respects than many such

telescopes exhibit. Not only should the motions be rapid (15 seconds of arc per second of time for guiding; ten times this rate for setting) but the telescope must stop immediately upon release of the push button, with no significant coast or oscillation. Since we wish to move the telescope back and forth between star and sky regions, under the control of the data-recording system, the backlash in the drive system must be very small, less than about one second of arc. Most astronomical telescopes can meet this requirement in the right ascension drive (because the gears are pre-loaded and driven continuously in one direction), but very few have declination drives of the necessary precision. We have found a tangent arm assembly for the declination drive coupled with a relatively fine-pitch screw to be good, low-cost, means of obtaining the required precision.

While the precision required of the right-ascension tracking drive is about the same as that required from a standard optical telescope (periodic and random errors less than about ± 1 second of arc, if possible), our budgets do not permit us to buy the expensive, precision, worm and gear sets that are installed on high-precision general-purpose telescopes. We have found, however, that standard-precision worms and gears will produce the required drive accuracy (periodic errors of one or two second amplitude), provided that very careful attention is paid to the concentricity of the worm and its shaft, and to the design of the end-thrust bearings for the worm shaft. The worm teeth must be concentric with the shaft ± 0.0002 inch and the runout of the end-thrust bearings must be less than 0.0001 inch, for a 30-inch diameter worm gear.

In order to keep the total cost as low as possible, all other specifications must be examined to be certain that no greater precision than is absolutely necessary is specified. For example, the absolute pointing accuracy should not be specified to be better than about ± 6 minutes of arc (but note that the English yoke is the best mounting for minimum pointing error). This precision is quite satisfactory for use with a finding telescope of $1°$ field. We use right-ascension and declination circles attached to the telescope, instead of shaft encoders and readout dials, not only because they are cheaper but also because they are simpler and, therefore, less likely to get out of order. The requirement of low cost means that no frills, such as filling and grinding of weldments, can be included. No machine work can be done that does not contribute directly to the performance of the telescope for its intended purpose.

The type of building in which the telescope is installed must also be considered as part of the problem. Most rotating domes, especially those of the larger sizes, move quite slowly compared with our specifications. Thus a roll-off roof structure, which leaves the telescope open to the sky, is indicated for a photometric telescope. Such buildings also meet the requirement of minimum cost. The only significant problem posed by this design is the effect of wind upon the relatively unshielded telescope; our experience indicates, however, that simple wind screens can provide a satisfactory solution to this problem.

3. The 28-inch Photometric Telescope

The result of our first attempt to apply the design principles outlined above is the 28-inch telescope at the Catalina Station of the Lunar and Planetary Laboratory. The telescope is shown in Fig. 1 and the roll-off-roof building is shown in Fig. 2. The primary mirror focal ratio is 2.7, and the cassegrain focal-ratio is 15. The primary mirror is ellipsoidal; the secondary, spherical. The mirrors are Pyrex and the mirror supporting mechanisms are conventional.

The right-ascension and declination drives are powered by Superior Electric Company Slo-Syn stepping motors. The very large range of synchronous speeds provided by these motors makes it unnecessary to change gears between setting, guiding and sidereal tracking motions; all speeds are provided by these motors, in conjunction with the electronic drive circuits. These same motors are coupled to the photometric data-recording system, so that the telescope "wobbles" automatically between the star and sky regions, under the control of the photometer. With this system it is convenient to make photoelectric exposures as long as several hours while "wobbling" at 15 second intervals back and forth between star and sky. Very frequent comparison of star and sky regions is essential in long-wavelength (5μ, 10μ, 20μ) photometry, because of the very bright, variable background.

The 28-inch telescope was put into operation in July 1963; the total cost of the installation, telescope and roll-off building, was approximately forty thousand dollars. Since its installation, the telescope has been used continuously for photometric observations in ultraviolet, visible and infrared wavelengths. The first stellar and planetary observations at 20 μ were made with the 28-inch telescope by Dr. F. J. Low. Almost all of the published JKL observations of the bright stars, and many of the UBVRI observations
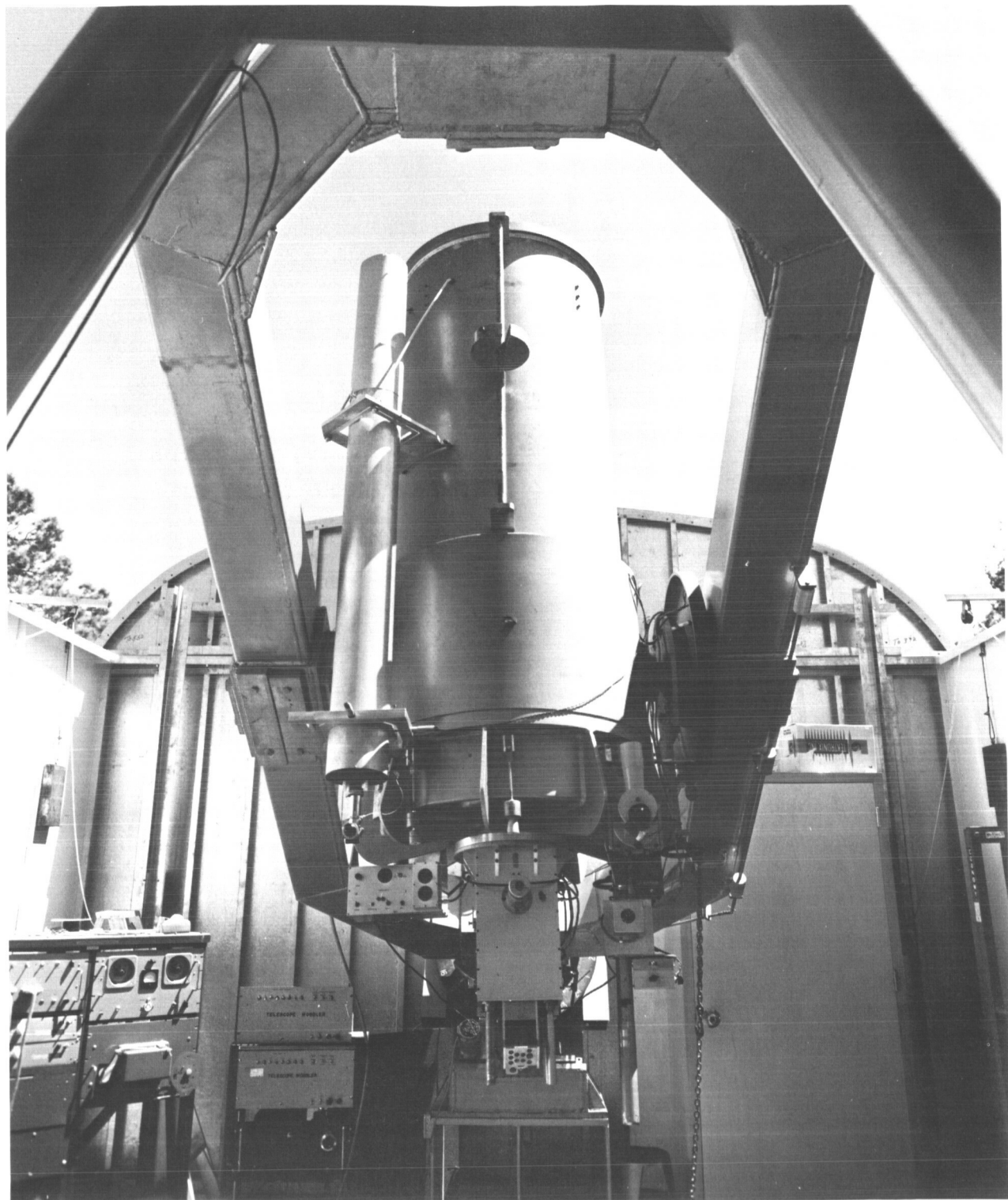
Fig. 1   The 28-inch photometric telescope from the north, inside the building. The JKL photometer is shown attached to the telescope. The 6-inch finder, mounted on the left side of the main telescope tube, can be offset ±1° from the main telescope and has high-power eyepieces for guiding long exposures. The photometric data recording and automatic telescope-"wobble" systems are housed in the cabinets in the lower left corner of this photograph. The telescope was constructed by Astro Mechanics, Inc., of Austin Texas. The optics were figured by Mr. Don Loomis, of Tucson, Arizona.

Fig. 2   The roll-off-roof building which houses the 28-inch telescope. The south wall of the building (at left) is hinged and folds down for observations of southern stars.
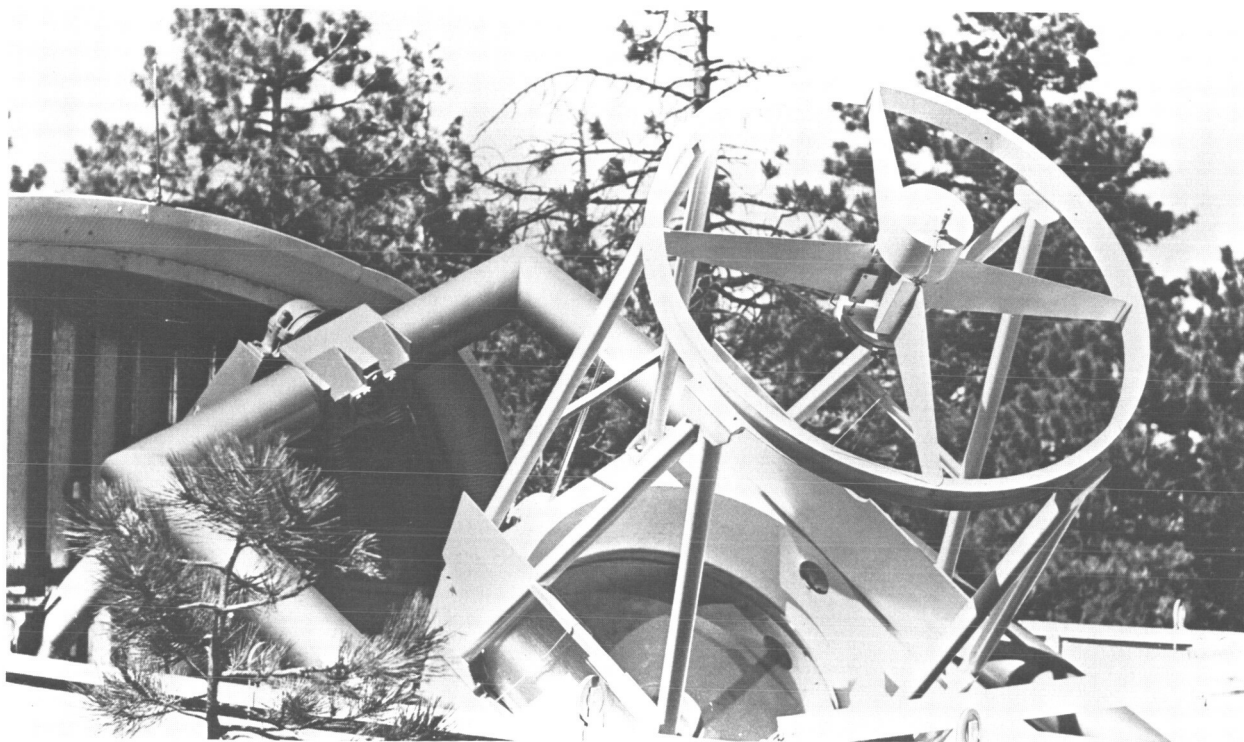
Fig. 3   The 60-inch telescope from the west. The details of the north end of the yoke and polar-axle are visible in this photograph, which was taken before the finders and sky baffler had been installed. The telescope was constructed by Astro Mechanics, Inc., of Austin, Texas. The mirrors were figured by Mr. Robert L. Waland of the Lunar and Planetary Laboratory.
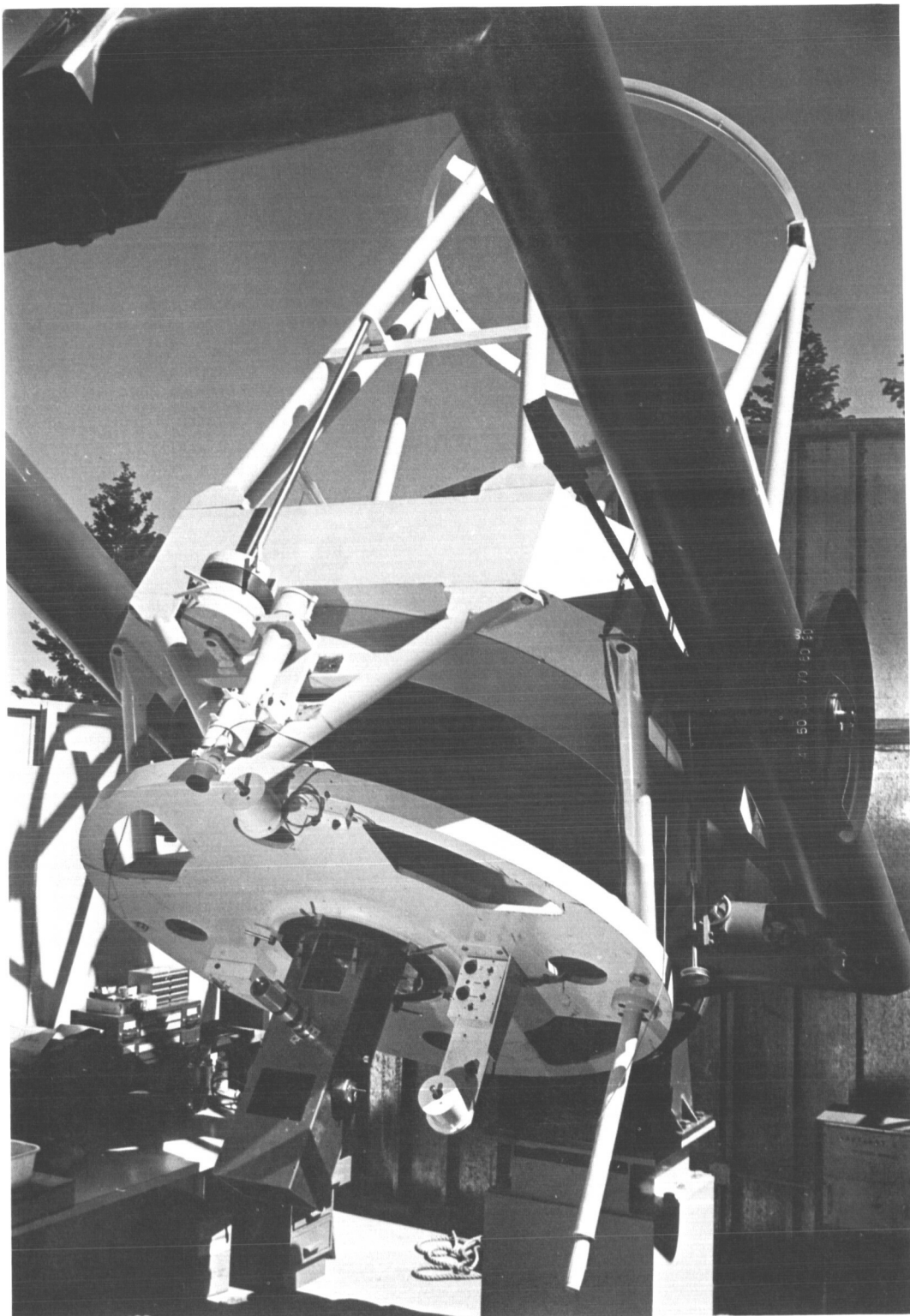
Fig. 4 The 60-inch telescope from the north, inside the roll-off-roof building. The back of the all-aluminum primary mirror is visible in this photograph, which was taken before the 6-inch finder (shown in Fig. 7) was installed. All photographs for this article are by Dennis Milon or Fred Forbes, Lunar and Planetary Laboratory.
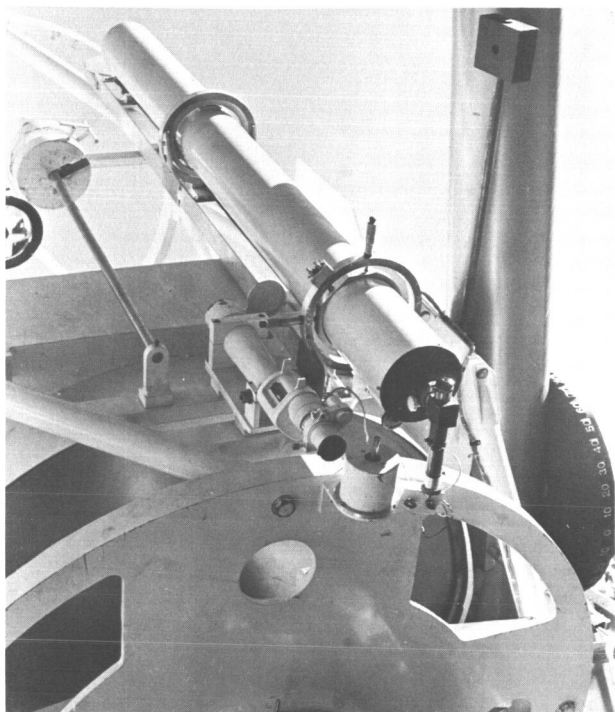
Fig. 5 The 3-inch and 6-inch finders, mounted on the 60-inch telescope. The 6-inch finder can be offset +1° from the main telescope and has high-power eyepieces for guiding long exposures.

(Johnson, Mitchell, Iriarte and Wisniewski 1966), were made by this telescope. It has shown itself to be an excellent photometric instrument, fully capable of satisfactory performance for the most critical applications.

4. The 60-inch Photometric Telescope

Our next step was to design and construct a 60-inch photometric telescope, based upon the design principles we have outlined, and the experience with the 28-inch. Views of this telescope are shown in Fig. 3, 4, 5, 6 and 7; the roll-off building, which is quite similar to that of the 28-inch, is shown in Fig. 8.

This telescope differs from the 28-inch in that the primary mirror is an all-aluminum casting (following a design by the Kitt Peak National Observatory). The primary mirror is about nine inches thick in the center, tapering to a thickness of one-fourth inch at the edge. It is bolted firmly into the telescope, with no other support mechanism. The figure of the primary mirror is spherical, with a focal-ratio of 2. The Pyrex secondary mirror produces a focal-ratio of 14 at the Cassegrain focus. The image produced by the 60-inch telescope is approximately 4 seconds
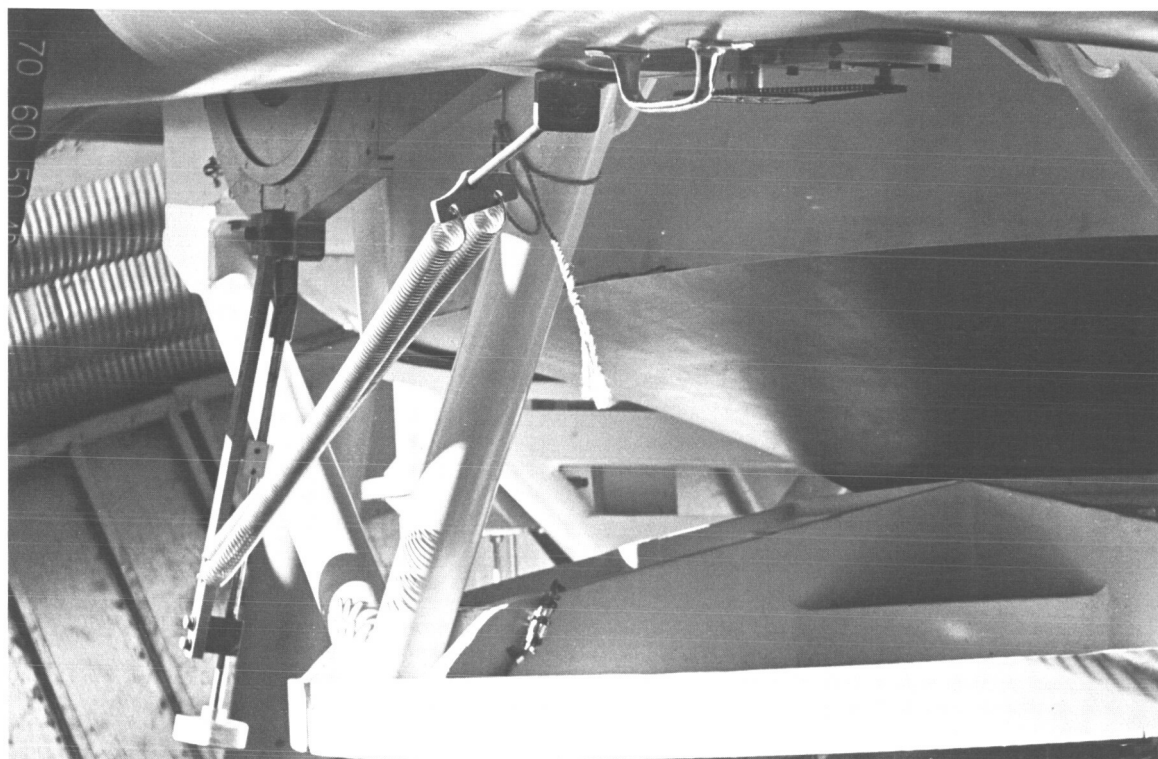

Fig. 6 A view from the side of the 60-inch telescope, showing the conical back of the primary mirror. This all-aluminum mirror is bolted solidly to the backing plate.
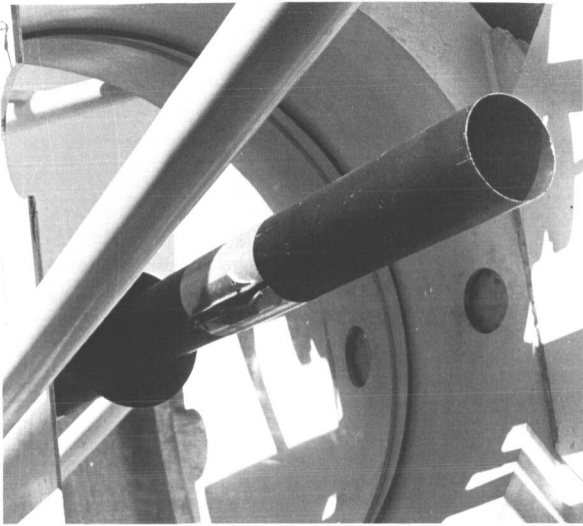
Fig. 7   A view of the front surface of the 60-inch all-aluminum primary mirror. The long tube protruding from the center of the mirror is part of the sky-baffling system.

of arc in diameter and its size and shape are not noticeably dependent upon the direction in which the telescope is pointed, indicating that the radically different concept of mirror support is sound.

The all-aluminum mirror has demonstrated another advantage, due to the high thermal conductivity of the metal. The 28-inch and 60-inch telescopes are located about 100 yards apart on the same ridge at the Catalina Station and the ambient temperatures at the two sites are practically identical. The 28-inch telescope exhibits the usual changes in focus and image quality caused by changes in the ambient temperature. Because of the low temperature-conductivity of Pyrex, the 28-inch primary mirror warps appreciably with changes in air temperature. On the other hand, the 60-inch telescope's image and focus remain almost constant with temperature changes, even over the extreme range from daytime to nightime temperatures.

Fig. 8   The roll-off-roof building which houses the 60-inch photometric telescope. The telescope is shown in its rest position. The south wall of the building (at left) is hinged and folds down for observations of southern stars. The hanging weights counterbalance the wind screens.

Following the practice at the Kitt Peak National Observatory, the 60-inch primary mirror was Kanigen coated prior to the optical figuring. Unfortunately, the Kanigen coat was not entirely satisfactory, and we were not able to reduce the telescope images below about 3 or 4 seconds in diameter. With a good Kanigen coating, however, it is possible to make a 60-inch aluminum-mirror telescope which produces images one or two seconds in diameter. We are, in fact, now making a second telescope of the same design from which we expect images about one second in diameter. The primary mirror of the first 60-inch telescope will be reworked after the completion of the second one.

The construction of the setting, guiding and sidereal-tracking motions was copied from those developed for the 28-inch telescope. Thus, the 60-inch also is integrated with the data recording apparatus and it wobbles automatically between star and sky regions.

The 60-inch photometric telescope was put into operation in September 1965; the total cost of the project (telescope, roll-off roof building, and the necessary experimental and developmental work) was approximately $130,000.

It has not been in use as long as the 28-inch, but the 60-inch has already produced significant observational contribution to astronomical knowledge. For example, UBVRIJK observations on two 13th magnitude giant star members of the globular cluster M3 have been obtained with this telescope, thus making possible the first observational determination of the bolometric corrections and effective temperatures of individual globular cluster stars.

REFERENCES

Johnson, H. L., Mitchell, R. I., Iriarte, B. and Wiśniewski, W. Z. (1966) *Comm. LPL*, 4, 99.